IDENTIFICATION OF NEUROINFLAMMATORY MARKERS IN A MOUSE MODEL WITH A DEFICIENCY OF NEU1

A Thesis Submitted to
the Graduate School of
Izmir Institute of Technology
in Partial Fulfillment of the Requirements for the Degree of

MASTER OF SCIENCE

in Molecular Biology and Genetics

by
Ebru ADA

July 2024
IZMIR

We approve the thesis of **Ebru ADA**

Examining Committee Members:

Prof. Dr. Volkan SEYRANTEPE
Department of Molecular Biology and Genetics, Izmir Institute of Technology

Assoc. Prof. Dr. Gülistan MEŞE ÖZÇİVİCİ
Department of Molecular Biology and Genetics, Izmir Institute of Technology

Assoc. Prof. Dr. Kemal Uğur TÜFEKÇİ
Vocational School of Health Services, Izmir Democracy University

8 July 2024

Prof. Dr. Volkan SEYRANTEPE
Supervisor, Department of Molecular Biology and Genetics
Izmir Institute of Technology

Prof. Dr. Özden YALÇIN ÖZUYSAL
Head of Department of Molecular Biology and Genetics

Prof. Dr. Mehtap EANES
Dean of Graduate School

ACKNOWLEDGEMENTS

First of all, I would like to express my deepest regards and respect to my supervisor Prof. Dr. Volkan SEYRANTEPE for his patient, support, guidance and extensive knowledge in my research and thesis studies.

I would like to thank The Scientific and Technological Research Council of Turkey (TUBITAK) (121Z099) for the financial support of the Project and for providing me scholarship.

I would like to extend my sincere thanks to my colleagues as family members of SEYRANTEPE Laboratory. I am grateful to my supportive friends, Hatice Hande BASIRLI, Melike CAN ÖZGÜR, Beyza KAYA, Orhan Kerim İNCİ, Selman YANBUL, Tufan Utku ÇALIŞKAN, Nurselin ATEŞ, Tuğçe ŞENGÜL, İlker GÜMÜŞ for their mentoring, belief, support and kindness during my research and thesis work. I especially want to thank Seçil AKYILDIZ DEMİR for her assistance and help during my undergraduate and graduate studies. I am also appreciative of all undergraduate members of SEYRANTEPE Laboratory for their sincere kindness, and infinite help.

At last, but not least, I am thankful to my family members, my father Saim ADA, my mother Cemile ADA, my brother Emre ADA for their infinite love and infinite trust for my entire career, and their infinite belief, motivation, patient, and support during my thesis.

ABSTRACT

IDENTIFICATION OF NEUROINFLAMMATORY MARKERS IN A MOUSE MODEL WITH A DEFICIENCY OF NEU1

Lysosomal neuraminidase 1 is responsible for sialic acid removal from oligosaccharides and glycoconjugates. Neu1 sialidase forms enzyme complex with protective protein cathepsin A, and glycosidase β-galactosidase. Mutations in Neu1 sialidase cause sialidosis, and *Neu1-/-* mice show symptoms of sialidosis patients. GM3 ganglioside is defined as substrate of lysosomal sialidase in vitro, and marked increase in GM3, GD3, and GM4 ganglioside levels in brain, spleen and liver autopsy tissues of sialidosis patients. Additionally, it was monitored that Neu1 has regulatory roles in immune response; expression of interleukins, activation of Toll-like receptor, and production of NF-kB in immune cells. However, relationship between inflammatory pathways and secondary lipid metabolisms in Neu1 sialidase deficiency remains unclear. Here, we aimed to investigate secondary lipid alterations and inflammatory response in tissues of *Neu1-/-* mice. In this study, lipidomic, molecular, histological and immunohistochemical analyses were performed in brain, spleen and kidney tissues of 2- and 5-month-old *Neu1-/-* mice. Decreasing levels of secondary lipids (phosphotidylcholine, phosphatidylethanolamine, and phosphotidylinositol) and elevated levels of pro-inflammatory cytokines, glycoconjugate accumulations, morphological degenerations, oligodendrocyte and neuronal loss, astrogliosis, and microgliosis were observed in brain, spleen and kidney of 2- and 5-month-old *Neu1-/-* mice. In the light of our findings, reduced levels of glycerophospholipids may be considered as biomarkers of activated inflammatory response in Type II sialidosis mice model. In the future studies, novel therapeutic strategies can target these altered glycerophospholipids, and their regulation can be crucial for alleviation of pathogenesis in sialidosis patients.

ÖZET

NEU1 EKSİKLİĞİ BULUNAN FARE MODELİNDE NÖROENFLAMASYON BELİRTEÇLERİNİN ARAŞTIRILMASI

Lizozomal nöraminidaz 1, oligosakaritlerden ve glikokonjugatlardan sialik asidin uzaklaştırılmasında sorumludur. Neu1 sialidaz, koruyucu protein katepsin A ve glikosidaz β-galaktosidaz ile enzim kompleksi oluşturmaktadır. Neu1 sialidazdaki mutasyonlar sialidoza neden olur ve *Neu1-/-* fareleri sialidoz hastalarının semptomlarını gösterir. In vitro çalışmalarda, GM3 gangliosidinin lizozomal sialidazın substratı olduğu gösterilmiştir ve sialidoz hastalarına ait otopsi dokularında GM3, GD3 ve GM4 gangliosid düzeylerinde belirgin bir artış gözlenmiştir. Ayrıca Neu1 enziminin interlökinlerin ekspresyonu, Toll benzeri reseptörün aktivasyonu ve bağışıklık hücrelerinde NF-kB üretimi gibi bağışıklık yanıtında düzenleyici rollere sahip olduğu bulunmuştur. Ancak Neu1 sialidaz eksikliğinde enflamatuar yollar ile sekonder lipit metabolizmaları arasındaki ilişki belirsizliğini korumaktadır. Burada *Neu1-/-* faresine ait dokulardaki sekonder lipit değişikliklerini ve enflamatuar yanıtı araştırmayı amaçladık. Bu çalışmada 2 ve 5 aylık *Neu1-/-* farelerine ait beyin, dalak ve böbrek dokularında lipidomik, moleküler, histolojik ve immünohistokimyasal analizler gerçekleştirildi. 2 ve 5 aylık *Neu1-/-* faresine ait beyin, dalak ve böbreklerinde ikincil lipitlerin (fosfotidilkolin, fosfatidiletanolamin ve fosfotidilinositol) seviyelerinde azalma gözlemlenirken ve pro-inflamatuar sitokin seviyelerinin arttığı, glikokonjugat birikimleri, morfolojik dejenerasyonlar, oligodendrosit ve nöron kaybı, astroglioz ve mikroglioz olduğu bulunmuştur. Bulgularımızın ışığında, Tip II sialidoz fare modelinde azalmış gliserofosfolipid düzeyleri, aktif inflamatuar yanıtının biyobelirteçleri olarak düşünülebilir. Gelecekteki çalışmalarda, yeni terapötik stratejilerin belirlenmesinde ekspresyonları değişen gliserofosfolipidlerin hedef alınması ve bunların düzenlenmesi, sialidoz hastalarında hastalığın seyrini hafifletmek için çok önemli bir role sahip olabilir.

Dedicated to my precious family…

TABLE OF CONTENTS

LIST OF FIGURES

LIST OF THE TABLES

CHAPTER 1

INTRODUCTION

1.1. Sialidases

Sialidases which are also named as neuraminidases are responsible for removal of alpha-glycosidically linked sialic acid residues from glycoconjugates (glycoproteins, glycolipids), oligosaccharides and gangliosides (Monti & Miyagi, 2012). Sialidases carry distinct important biological functions such as cellular differentiation, intercellular communication, cellular growth, apoptosis, and neuronal plasticity (Minami et al., 2021; Miyagi & Yamaguchi, 2012).

Mammalian sialidases are including four different groups, and these sialidases are expressed by a variety of genes such as Neu1, Neu2, Neu3, and Neu4 (Table 1.1). The classification of these neuraminidases are linked to their subcellular localization; Neu1 is found in lysosomes (Miyagi & Tsuiki, 1984). Neu2 is localized into cytosol (Miyagi & Tsuiki, 1985; Monti et al., 1999). Neu3 is placed as associated with plasma membrane (Miyagi et al., 1990). Neu4 is localized to mitochondria, ER and lysosomes (Seyrantepe et al., 2004; Yamaguchi et al., 2005). Neuraminidases also differ from each other in enzymatic environment (optimal pH variable), and specificity of their substrates (Mahadevan et al., 1967; Saito et al., 1996; J. Wang et al., 2009).

Neuraminidase 1 (Neu1 sialidase) has the highest expression level among the sialidases that is found in lysosomes and have an important biological role in sialic acid removal from oligosaccharides and sialylated glycoconjugates degradation in lysosomes (Bonten et al., 1996; Magesh et al., 2006).

Neuraminidase 2 (Neu2 sialidase) is located in cytoplasm of the cells, and its responsible for the hydrolyzation of oligosaccharides, glycoproteins, and degradation of gangliosides (GM3) (Funakoshi & Suzuki, 2009; Tokuyama et al., 1997).

Neuraminidase 3 (Neu3 sialidase) is found in cell surface as a component of peripheral membrane protein, and it has an active role in ganglioside degradation pathway, specifically GM3, GD3, GD1a, and GD1b are the ideal substrates of Neu3 enzyme (LI et al., 2001; Yamaguchi et al., 2006). Neu3 is also responsible for the

modulation of gangliosides' oligosaccharide chains, and this modulation is effective on the cell signaling, insulin signaling, cellular differentiation, and apoptosis (Miyagi & Yamaguchi, 2012).

Neuraminidase 4 (Neu4 sialidase) is localized into lysosomal lumen, endoplasmic reticulum, and mitochondrial inner and outer membranes (Seyrantepe et al., 2004; Yamaguchi et al., 2005). Neu4 sialidase is specifically active on the oligosaccharides, glycoproteins, and gangliosides; significantly GD1a and GM2 activity is shown (Seyrantepe et al., 2008).

Table 1.1. Mammalian sialidase properties (Monti & Miyagi, 2012)

	NEU1	**NEU2**	**NEU3**	**NEU4**
Major Subcellular Localization	Lysosome	Cytosol Nucleus	Plasma Membrane	Lysosomes Mitochondria Endoplasmic Reticulum
Substrate Preference	Oligosaccharides Glycopeptides 4MU-Neu5Ac[1]	Glycoproteins Oligosaccharides Gangliosides	Gangliosides	Glycoproteins Gangliosides Oligosaccharides
Optimal pH	4.4-4.6	6.0-6.5	4.5-4.7	4.5-4.7
Cellular Functions/ Involved Pathways	Catabolism in lysosomes Exocytosis Immune response	Myoblast differentiation	Neuronal differentiation Tumorigenesis	Neuronal differentiation Apoptosis Adhesion
Localization in Genome	6p21.31	2q37.1	11q13.5	2q37.3

1.1.1. Neuraminidase 1

Sialidase 1 is located into the lysosomes of the cell, and additionally it was shown that Neu1 enzyme can be localized to plasma membranes in the case of distinctive cellular stimulants (Cross et al., 2003; Liang et al., 2006; Lukong et al., 2001). The first study which defined the human Neu1 gene is responsible for the expression of Neu1 enzyme, was published by Pshezhetsky et.al. in 1997. Neu1 gene was located on the 6p21.3 chromosomal location in humans, and Neu1 enzyme consist of 145 amino acids in its structure and it was located on 17th chromosome in mice genome (Oohira et al., 1985;

Pshezhetsky et al., 1997; Womack et al., 1981). Neu1 gene expression is identified all tissues in the body of humans, but expression levels are different from each other; highest expression is shown in pancreas, and less expression is seen in the brain (Bonten et al., 1996). In mice, Neu1 expression is also varied in tissue-specific manner, such as highest levels of Neu1 expression is defined in kidney and pancreas tissues, and less expression is observed in brain, and spinal cord, and lowest expression is showed in liver, spleen and lung tissues (Igdoura et al., 1998).

Neu1 enzyme is responsible for the catalyzation of sialic acid removal from the oligosaccharides, sialoglycoconjugates (glycolipids, gangliosides and glycoproteins) in lysosomes of the cells (Frisch & Neufeld, 1979; Scheneider-Jkob- & Cantz, 1991).

Neuraminidase 1 enzyme is a part of an active and stable protein complex which additionally contains the glycosidase β-galactosidase. β-GAL enzyme that is responsible for the β-D-galactose removal from the β-D-galactosides. (Pshezhetsky & Ashmarina, 2001; Verheijen et al., 1982). The protective protein cathepsin A is one of the chaperone proteins, and PPCA interaction with β-galactosidase enzyme maintains the stabilization of β-GAL. Additionally PPCA is significantly important for Neu1 sialidase because Cathepsin A provides the lysosomal localization, active state of catalyzation, and stability of Neu1 enzyme in lysosomes(D'Azzo et al., 1982). The deficiency of protective protein cathepsin A enzyme causes impairment in glycosidase β-galactosidase and Neuraminidase 1 activity, and results with galactosialidosis that is one of the lysosomal storage diseases (D'Azzo et al., 1982; Zhou, 1996).

Neuraminidase 1 enzyme has regulatory roles in immune response additionally the sialic acid removal from the glycoconjugates. In previous studies, it was shown that the Neu1 sialidase deficiency is related with decreased expression of IFN- γ in CD4+ and CD8+ T cells (Nan et al., 2007; Pshezhetsky & Hinek, 2011). Neu1 enzyme is also crucial for the expression of Th2 cytokines, interleukins and its activity are related with the activation of Toll like receptors (Abdulkhalek et al., 2011; G.-Y. Chen et al., 2014; X. P. Chen et al., 1997). Neu1 sialidase activity is also correlated with the phagocytic processes of dendritic cells, and macrophages with removal of sialic acids of surface receptors in both PPCA deficient, and PPCA/Neu1 deficient mice models (Seyrantepe et al., 2010). Therefore; Neu1 activity can be crucial for activation of innate immune related receptors, and production of NF-kB proteins in macrophages and dendritic cells (Amith et al., 2010). In another study, it was shown that PPCA and Neu1 enzymes are found in cell-membrane complex with elastin-binding protein (EBP) which has the same structure with spliced

variant form of β-galactosidase enzyme, and Neuraminidase 1 has an important role in tropoelastin secretion, and release of tropoelastin (Hinek et al., 2006). In a previous cancer research, activity of Neu1 sialidase and metastasis of cancer cells are negatively correlated with each other (Miyagi et al., 1994; Uemura et al., 2009). Decreased expression of Neuraminidase 1 was observed and increased GM3 ganglioside levels were detected in decreased Neu1 sialidase activity in mouse B16 melanoma cells (Sawada et al., 2002). In early research, it was shown that GM3 ganglioside is one of the substrates of lysosomal sialidase in vitro, but later studies demonstrated that in all Neu1 deficient fibroblasts have not resulted with accumulation of GM3 ganglioside (Aerts et al., 2019; Fingerhut et al., 1992). In decreased levels of Neu1 activity showed marked increase in GM3, GD3, GM4 and LM1 ganglioside levels in spleen, liver, and kidney of human autopsy tissues (Ulrich-Bott et al., 1987).

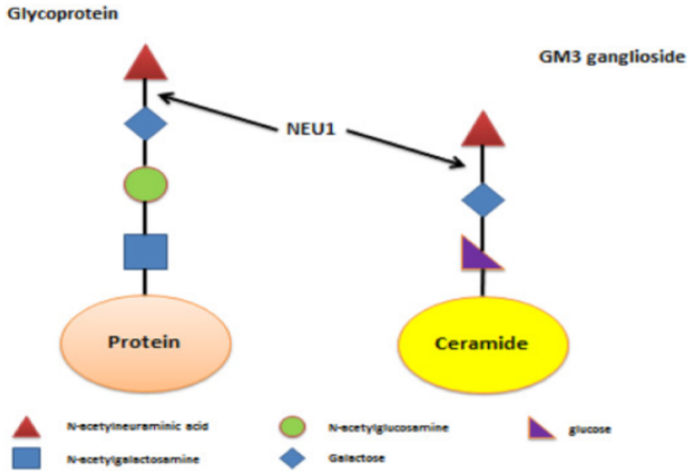

Figure 1.1. Conversion of Glycoprotein and Glycolipid (GM3 ganglioside) molecules by Neuraminidase 1 enzyme (Mohammad et al., 2018).

1.2. Lysosomal Storage Diseases

Lysosomes have significant roles in cells such as degradation of biological molecules which maintains cellular homeostasis, intercellular interactions, and autophagy (Ballabio & Bonifacino, 2020; Gros & Muller, 2023; Zhang et al., 2021). Lysosomal storage disorders are inheritable single-gene defects which are seen very rare in populations. Lysosomal storage diseases belong to metabolic disorders due to accumulation of various molecules (oligosaccharides, glycoproteins, glycolipids) in

lysosomes of visceral organs and central nervous systems because of mutations in enzyme encoding genes, and the deficient activator or transport proteins that are specifically necessary for functional enzyme activity (Platt et al., 2012, 2018a). Lysosomal storage diseases are transferred to next generations as autosomal recessive and X-linked inheritance. These deficient enzymes may be responsible for hydrolyze activity, post-translational modification, or transporter proteins of lysosomal proteins (Neufeld, 1991; Tardy et al., 2004). Presence of non-functional enzymes in lysosomes of cells causes the insufficient degradation of biological molecules such as glycoconjugates, and oligo/polysaccharides in lysosomes, therefore; these biomolecules excessively accumulate, and results in disruption in cellular homeostasis (Breiden & Sandhoff, 2020a; Ferreira & Gahl, 2017).

Progressive accumulation and storage of biomolecules occurs in visceral organs (kidney, liver, spleen), central nervous system, muscle, eye etc. (Boustany, 2013). The symptoms and disease phenotypes (less, mild and severe onsets) of LSD patients are depending to the type of stored biological molecules, and residual activity of the deficient activator protein or mutated enzyme; delay on developmental stages, pathology in central nervous system, and enlarged visceral organs can be observable (Platt et al., 2012, 2018a; Tardy et al., 2004). According to the residual activity and location of gene mutation, severity and onset of the disease are separated from each other (Boustany, 2013; Ferreira & Gahl, 2017). Age of the disease decreases with decreased activity of the mutant enzyme and symptoms of the disease become more severe. Histopathological conditions are shown in different LSD patients, such as vacuolization in affected tissues due to the storage of unmetabolized substrates (Conzelmann & Sandhoff, 1983; Tourtellotte et al., 1965). LSD diagnosis is done with detection of accumulated materials, and disease specific biomarkers from patient samples (Bobillo Lobato et al., 2016).

1.2.1. Sialidosis

Sialidosis is a glycoprotein disease which belongs to lysosomal storage diseases, and its inheritance occurs in autosomal recessive manner. Sialidosis is caused from the Neuraminiadase 1 enzyme deficiency, and oligosaccharides with sialic acid residues, glycoconjugates such as glycosphingolipids, and glycoproteins accumulates gradually in lysosomes of the cells (Seyrantepe et al., 2003). Sialidosis patients are diagnosed with the

undefined oligosaccharides which are compatible with galactosialidosis in urine and body fluid samples (Van Pelt et al., 1988). Sialidosis have two variant onsets in classification of severity of disease symptoms, and onset of the age; Type I Sialiodosis (late, mild, nonneuropathic form) and Type II (early, dysmorphic) Sialidosis (Seyrantepe et al., 2003; Van Pelt et al., 1988).

Type I sialidosis, is also called as cherry red spot myoclonus syndrome, is the mild form of the Sialidosis which symptoms of the patients are seen later twenty or thirty ages. Type I Sialidosis patients have the myoclonus syndrome (uncontrolled muscle movement), and impairment in their vision (Caciotti et al., 2020; D'Azzo et al., 2015). Intelligence of Type I Sialidosis patients is either not affected or slightly affected, gradually loss in vision, challenges in voluntary movements, and tremors/seizures can be monitored, and may wheelchair be necessary. In histopathological findings, vacuolization in immune cells, and swollen lysosomes are observed in liver and bone marrow cells. Diagnosis is performed with the sialic acid containing oligosaccharide detections in urine samples of patients (D'Azzo et al., 2015), and accumulated oligosaccharides are also identified in neuronal tissues in the biopsy samples of patients of Type I sialidosis (Sekijima et al., 2013).

Type II sialidosis is the severe, neuropathic form and early onset the disease which has three substypes; congenital (before birth), infantile (birth and 12 months) and juvenile onset (age 2). Type II sialidosis patients share similar phenotypic features such as visceromegaly, deformations in vertebrae, serious mental retardation, and facial edema (D'Azzo et al., 2015). In sialidosis, various clinical phenotypes can be identified due to the various mutations in Neu1 gene (34 nonsense, missense mutations, insertions, or deletions (Seyrantepe et al., 2003). Accumulation of different gangliosides (GD3, GM3, GM4 and LM1) in patients' visceral organs is defined, but not seen in the patients' brains (Breiden & Sandhoff, 2020a). Type I and Type II sialidosis patients have similar characteristic features such as enlarged visceral organs, mental retardation (none or severe), deformed vertebrae, loss in hearing, visual loss, and life expectancy of patients are depending on the onset of disease and appearance of the symptoms (Caciotti et al., 2020; Sekijima et al., 2013).

1.2.2. Neu1 (Neuraminidase 1) deficient Mice Model

Neuraminidase 1 deficient mice model was firstly created in 2002 by d'Azzo et.al. with null knock out in Neu1 gene locus to understand the significance of Neu1 enzyme in cellular pathways. In Figure 1.2., created Neu1 mice model is representing the Type II sialidosis patient characteristics, and d'Azzo et.al. showed that this mice model has enlarged visceral organs such as spleen and liver (hepatosplenomegaly), severe defects in kidney histology, impairments in neurological status, defects in spinal cord, and accumulation of oligosaccharides in urine samples (de Geest, 2002). In this study, highest expression of Neu1 gene and activity of Neu1 enzyme is seen in the kidney, and intestines in wild type mice models, and Neu1 expression and enzymatic activities are shown in the lowest levels in homozygous null mice models (de Geest, 2002). *Neu1-/-* mice model which are 1-month old have significantly smaller size nearly 25% than *WT* mice. Additionally, ballooned cell structures in epithelial and liver tissues, and vacuolation in glomeruli regions of kidney tissues and ballooned structure of epithelial cells of intestine tissues of 5-month-old Neu1 knock out mice model are identified with hematoxylin & eosin staining of fixed and paraffin-embedded tissues (de Geest, 2002). Neu1 knock mice models is able to breed until 10 weeks old, and they can live until 12 months (8-12 months old lifespan); but in later onset of their age, gait abnormalities, decreasing in weight, and increased tremors was monitored (de Geest, 2002).

In the brain of 5-month-old Neu1 knock out mice model (*Neu1-/-)*, vacuolization in microglial cells and macrophages are observed due to the storage materials (related with neuroinflammation), severe affected cells is observed in dentate gyrus, Purkinje cell layer in cerebellum is nearly not affected in hematoxylin & eosin staining of fixed and paraffin-embedded tissues (de Geest, 2002).

In the Neuraminidase 1 deficiency, it is found that Neu1 causes heightened levels of lysosomal exocytosis by regulating the localization of Lysosomal Associated Membrane Protein (LAMP1) to cellular membrane (Holt et al., 2006; Yogalingam et al., 2008). LAMP1 protein has an active role in lysosomal exocytosis with localization of lysosomes into the cellular membrane, and in *Neu1-/-* mice model, sialic acid residues cannot be removed from the LAMP1 protein, and oversialylated lysosomes is engaged to plasma membrane in a long period of time (Kima et al., 2000; Rodríguez et al., 1997). In previous studies, the function of LAMP1 in lysosomes is identified with silenced LAMP1

gene in the cells with deficiency of Neu1, and it was shown number of lysosomes that is associated into cellular membrane, and lysosomal exocytosis is decreased (Schwake et al., 2013; Yogalingam et al., 2008). Therefore, the significant effect of Neu1 sialidase in lysosomal exocytosis is demonstrated in earlier studies, and release of lysosomal content is highly elevated in visceral organs, and pathological conditions can be monitored in these tissues which are also characteristic phenotypes of sialidosis (Wu et al., 2010). *Neu1-/-* mice models are mimicking the Type II Sialidosis phenotype with splenomegaly, increasing in the erythrocyte, and hematopoietic progenitor cell counts; according to these alterations, extramedullary hematopoiesis is indicated in *Neu1-/-* mice models (de Geest, 2002).

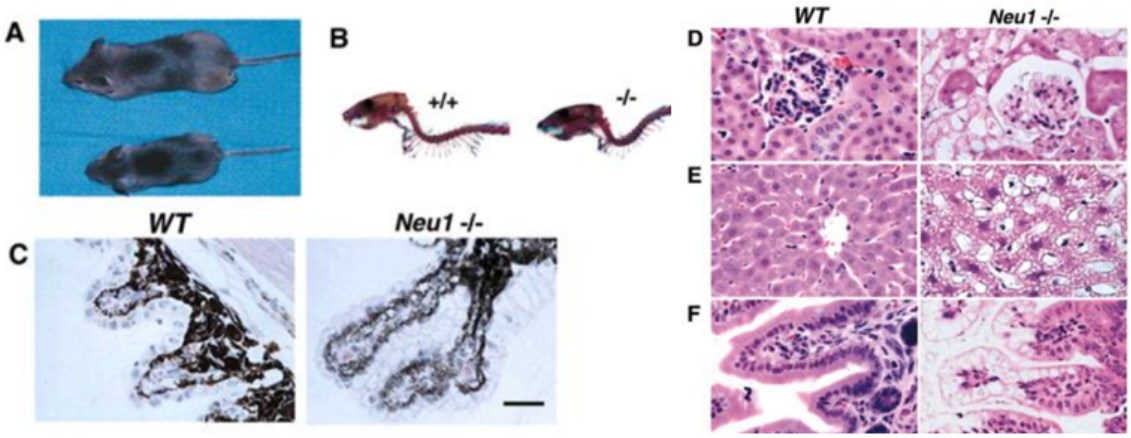

Figure 1.2. Clinical and histopathological phenotype of *Neu1-/-* mice. 1-month-old *Neu1-/-* mice in smaller size according to the *WT* mice models (A). Increasing curvature of the spinal cord of 5-month-old *Neu1-/-* mice is defined with staining of spine, 5-month-old wild type mice is observed without any curvature in their spine (B). Histopathological analysis of *Neu1-/-* mice tissues and comparison to *WT* mice tissues with hematoxylin& eosin staining (C-F). Severe ballooned structure of epithelial cells in eyes of 5-months of *Neu1-/-* mice (C). Considerable vacuolation of epithelial cells in glomeruli and tubuli of 5-month-old *Neu1-/-* kidney tissues (D). Kupffer cells with significant ballooned pathology, and hepatocytes with microvaculation is shown in the liver tissues of 5-month-old *Neu1-/-* mice (E). Epithelial cells of intestinal villi of 3-weeks-old *Neu1-/-* is defined with excessive vacuolation (F).

Type II sialidosis patients also have muscle atrophy which is also related with the hypotonia, and degeneration in the muscle structure was observed. Also, deformed skeletal structure in *Neu1-/-* mice model was shown (Zanoteli et al., 2010). Previous studies demonstrated that there is a relationship between the muscle atrophy and highly sialylated LAMP1. High number of sialylated LAMP1 causes the increased lysosomal exocytosis, and increasing infiltration of connective tissue which results in the degeneration of muscle fibers in vitro (primary myofibroblast cells), and in vivo studies of 4 months old *Neu1-/-* mice models (Zanoteli et al., 2010). Additionally, the hearing loss of *Neu1-/-* mice model is one the sialidosis phenotypic features (Wu et al., 2010). Previously, it was indicated that increased number of Lamp1 and Lamp2 that shows the lysosomal localization into the plasma membrane, and increased lysosomal exocytosis can be resulted in alteration in sound transduction, and progression of hearing loss in *Neu1-/-* mice models (Wu et al., 2010). In previous studies, there is early aging phenotype in *Neu1-/-*; but it was very interesting to observe amyloid deposits which is the characteristic feature of the Alzheimer's Disease in the *Neu1-/-* mice models (Bellettato & Scarpa, 2010). In lysosomes, it was demonstrated that oversialylated amyloid precursor protein is accumulated, and due to the excessive lysosomal exocytosis, accumulated Aβ peptides was released from the cellular membrane to extracellular matrix (Ohmi et al., 2009; Sidransky & Lopez, 2012). In further investigations, Neu1 gene deletion in Alzheimer's Disease mice model shows that amyloid precursor protein levels are increasing, and plaque formation is observed (Annunziata et al., 2013). Another study proved that cerebral injection of Neuraminidase I in AD mice model brain, decreased the plaque formation, and this treatment strategy can be useful to prevent progression of the severe phenotype of the sialidosis and AD (Annunziata et al., 2013; Bellettato & Scarpa, 2010). As a result, the deficiency in Neu1 sialidase in *Neu1-/-* mice is linked to AD phenotype, and disease development (Annunziata et al., 2013). In various studies, the link between the activity of Neu1 sialidase and cellular pathways were described (Dridi et al., 2013; Seyrantepe et al., 2010). There is oversialylated cellular proteins in the macrophages of CathAS190A-Neo mice model which leads to secondary deficiency of Neu1 sialidase by decreased activity of Neu1 sialidase in nearly all tissues, and treatment of CathAS190A-Neo mice with exogenous Neu1 sialidase decreased the number of sialylated cellular membrane proteins, and macrophages can have the normal phagocytosis processes (Seyrantepe et al., 2010).

In previous studies, glucose intolerance, and insulin resistance is demonstrated in CathAS190A-Neo mice model which leads to secondary deficiency of Neu1 sialidase (de Geest, 2002). Therefore, high fat diet was administered to CathAS190A-Neo mice, even though insulin production were normal, insulin sensitivity was reduced that can results with hyperglycemia in CathAS190A-Neo mice models (Dridi et al., 2013). In this study, deficiency in Neu1 sialidase in sialidosis patients' fibroblasts demonstrated impairment in insulin signaling. According to this study, it was concluded insulin receptor kinase (IRK) can be one of the targets of Neu1 sialidase, and Neu1 is responsible for the desialylation of IRK by binding of insulin, and stimulation of IRK activation (Dridi et al., 2013).

1.3. Neuroinflammation

Neuroinflammation is the inflammatory response that is produced by brain or spinal cord. Neuroinflammation is regulated with the release of cytokines (IL-6, IL-1β, and TNF-α), chemokines (CCL2, CCL5), secondary messengers (nitric oxide), and reactive oxygen species (ROS) (DiSabato et al., 2016). Neuroinflammatory response is depending on the source of inflammation, duration of the inflammatory condition, and primary stimulus. Astroglia and microglia cells are responsible for production, release, and localization of peripheral inflammatory molecules into central nervous system (Figure 1.3.). Acute neuroinflammation in infectious diseases and traumatic injuries in CNS is an advantageous situation in organisms, and results with Il1 and Il4 cytokine mediated neuroprotection, immune surveillance and injury induced remodeling of macrophages (Figure 1.3.) (Y. Sun et al., 2022). In high degree of neuroinflammation, elevated levels of cytokine & chemokine expression and release, and impairment of blood brain barrier integrity was demonstrated due to peripheral immune cells infiltration into CNS. Traumatic brain injuries, aging, neurodegenerative diseases can cause chronic inflammation in CNS (Bosch & Kielian, 2015)

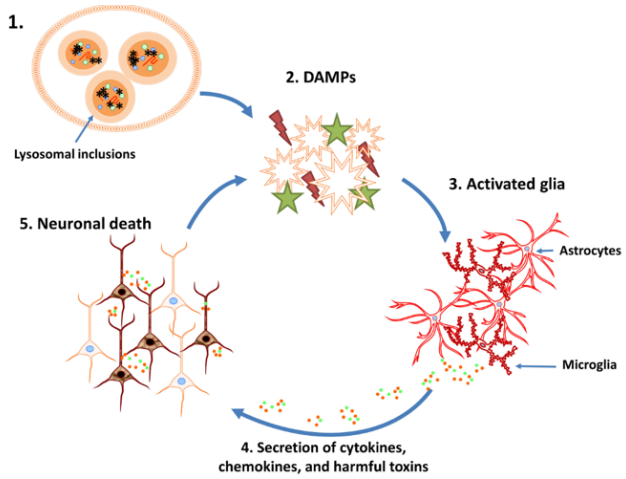

Figure 1.3. Potential neuroinflammation and neuronal cell death cycle in Lysosomal Storage Diseases (Bosch & Kielian, 2015).

1.3.1. Microgliosis

Microglial cells are the local immune cells which are positioned in brain and spinal cord. Microglial cells are important for neurotropic and growth factor release, repairment of the CNS tissues by communicating with astrocytes and oligodendrocytes, elimination of the myelin debris, cytokine- chemokine expression and release, synaptic pruning, and avoidance of neuronal death (Bachiller et al., 2018). Microglial activation in the central nervous system (CNS) can take place in two different and functional types: M1 microglia shows the proinflammatory phenotype, and M2 provides immunosuppressive/anti-inflammatory phenotype. Depending on localization of signals and factors that are stimulated, microglial cells can be reactive by classical and alternative activation pathways. Classical activation, M1 phenotype, is regulated by toll-like receptors and IFN- γ signaling pathways. M1 microglia can encode and produce tumor necrosis factor-α (TNF-α), interleukin-1β (IL-1β), superoxide, nitric oxide (NO), and reactive oxygen species (ROS), and M1 microglial cells can result with neuroinflammation, neurotoxic environment, and neuronal apoptosis. Alternative activation, M2 phenotype, is closely associated with release of Il4, Il13 and Il10 cytokines. M2 microglial cells have cellular functions such as promoting anti-inflammation, tissue repair, regeneration of nerve and axons. Also, M2 microglial cells are responsible for extracellular matrix (ECM) reconstruction (Colonna & Butovsky, 2017; Guo et al., 2022). Additionally, M2 microglia are driven by the coordinated

regulation of various anti-inflammatory factors and provide immunosuppression and neuroprotection by antagonizing M1 pro-inflammatory responses (Tang & Le, 2016). M1 and M2 microglia phenotypes are a concept shared by various neurodegenerative diseases. Microglial activation or dysfunctional microglial cells are associated with the progression of cognitive deficits in neurodegenerative diseases. The release of pro-inflammatory cytokines and the increase in phagocytic activity is triggered by increased microglial cell activation, and cause decrease in synaptic plasticity and learning/memory capacity (Elmore et al., 2018; Tichauer et al., 2014; Zöller et al., 2018).

1.3.2. Astrogliosis

Astrocytes are the neuroglial cells which are abundantly found in central nervous system. Astrocytes have an active role in energy supplying for neurons, homeostasis of blood brain barrier and its integrity, removal of the excess neurotransmitters from synapses, ensuring the neurotropic environment by reactive oxygen species by detoxification and clearance of reactive oxygen species from CNS, and regulation of microglial cells (Jäkel & Dimou, 2017; Valles et al., 2023). Reactive astrocytes can be classified as A1 presents the neurotoxic properties, and A2 shows neuroprotective characteristics; according to healthy and pathological conditions of CNS (Khodadadei et al., 2022). A2 astrocyte phenotype is regulated by release of IL-1β, and IL-6 cytokines, and A2 astrocytes maintain the neuroprotection with expression of anti-inflammatory cytokines-chemokines, degradation and removal of free radicals, growth factors secretion and synaptogenesis regulation. A1 astrocytes are activated with TNF-α, and IL-1α in inflammatory conditions by NF-κB pathway with activated M1 microglial cells. A1 astrocytes express and release high amounts of pro-inflammatory cytokines, chemokines, and reactive oxygen species and causes impairment in synaptic dysfunction, neuronal homeostasis, and neuronal death (Y. Chen et al., 2020; Ding et al., 2021). Astrogliosis is elevated number of highly activated astrocytes which resulted from traumatic brain injuries, neurodegenerative disorders, and neuroinflammatory conditions (Pekny & Pekna, 2014; Verkhratsky et al., 2014).

1.3.4. Lysosomal Storage Diseases and Neuroinflammation

Lysosomal Storage Diseases (LSDs) are one of the rare genetic diseases which are seen in a small group of a population (1:5000), and generally inherited with autosomal recessive manner; only three of them is inherited as X-linked pattern (Platt et al., 2018b; Poswar et al., 2019). Up to present, more than 70 different lysosomal storage diseases have been identified; they are observed because of the lysosomal enzyme or membrane encoding gene deficiencies and resulted with dysfunctional biosynthesis and degradation of macromolecules and accumulation of undegraded metabolites in intra-lysosomal locations (Futerman & van Meer, 2004). Many lysosomal diseases show elevated levels of neuroinflammatory markers and activated microgliosis and astrogliosis due to the impairment of lysosomal degradation (Bosch & Kielian, 2015).

In Neimann Pick disease type C, a type of LSDs, resulted from the deficient NPC proteins, which is encoded by NPC1/NPC2 genes, and maintains the uptake and movement of cholesterol lipids in neuronal and glial cells in myelination process, and functionality of neurons (Vruchte et al., 2004). In Neimann Pick disease type C mouse models, it was demonstrated that activated microglial cells and neurodegenerative phenotypes in the brain regions. In various regions of the brain, high expression levels of TNF-α and IL-1β cytokines and decreased neuronal cell counts were identified.

Gaucher disease belongs to sphingolipidoses subgroups of LSDs, it is defined from the deficient lysosomal glucosylceramidase enzyme that is encoded by the GBA1 gene (Wong et al., 2004). Gaucher diseases is identified with accumulation of the glucosylceramides, and glucosylsphingosine in brain (Farfel-Becker et al., 2014). In Gaucher disease type II and III, expression of IL-1α, IL-1β, TNF-α, IL-6 which are proinflammatory cytokines, are increased in both Gaucher disease mouse model, and Gaucher disease patients' blood (Wong et al., 2004).

Tay-Sachs disease, which is a GM2 gangliosidosis, and one of the LSDs, resulted from the deficiency of lysosomal β-hexosaminidase α (HEXA) enzyme, that is encoded by the Hexa gene, α subunit of HEXA enzyme (Yamanaka et al., 1994). Mutations in the Hexa gene causes the impaired conversion of GM2 ganglioside into GM3 ganglioside; therefore, aggregation of GM2 ganglioside is defined in the central nervous tissues in both Tay-Sachs patients, and mouse models (Hexa−/−Neu3−/−) (Demir et al., 2020a). In Tay-Sachs mice model, expression levels of proinflammatory cytokines (Ccl2, Ccl3,

CCl4, and Cxcl10) is identified in the cortex region, and Ccl4, Cxcl13 cytokines levels are also highly expressed in cerebellar region of the brain. Also, decreasing expression levels of anti-inflammatory cytokines such as Il10, Il2, and Il11 were identified in both cortical and cerebellar regions of the brain. Besides these findings, microglial activation was demonstrated with the Moma2 that is a specific microglial marker, elevated levels of Moma2-positive cells were monitored in cortex, thalamus and cerebellum regions of Tay-Sachs mice model (Demir et al., 2020a).

1.4. Lipids

Lipids are one of the essential biomolecules which are responsible for the distinct functions such as structural components of plasma membranes, storage of energy, acting as a messenger molecule in intercellular processes, blood clotting, enzyme cofactors, and cellular differentiation and growth (Roy & Tedeschi, 2021; Stephenson et al., 2017). In addition to these various functions of lipids, they may have also important roles in synaptogenesis, transmission of the impulses, and protection of myelin sheath in central nervous systems (Fuller & Futerman, 2018; Liu et al., 2021). Classification of lipids can be identified into eight different subgroups: fatty acids, glycerolipids, glycerophospholipids, sphingolipids, sterols, prenols, saccharolipids, and polyketides (Cermenati et al., 2015; Stephenson et al., 2017). In these lipid subgroups, glycerophospholipids, sphingolipids and cholesterols are significantly important in homeostasis, structural components of neuronal membranes, and neuronal development and functions (Breiden & Sandhoff, 2020). In previous studies, secondary accumulation of these major lipid subtypes is linked to neuroinflammation and neurodegenerative conditions in various lysosomal storage diseases (Walkley & Vanier, 2009).

1.4.1. Glycolipids

Glycolipids are found in the cellular membranes, and their structure has an amphiphilic nature (D'Angelo et al., 2013) . Glycolipids is composed of sugar head groups which has a hydrophilic feature, and hydrophobic parts are consist of different lipids subclasses such as ceramides, sphingolipids, acyl glycerol, and phenyl phosphate

which is attached to the plasma membrane of cells (Cheng-Sánchez & Sarabia, 2018; Slotte, 2013). Glycolipids are responsible for the cellular communication/recognition, signaling pathways, fluidity of the cellular membrane, and formation of the lipid rafts of the cellular membranes, and these glycolipids may be involved in distinct cellular pathways which are linked to inflammatory response and tumorigenesis (D'Angelo et al., 2013; Jala et al., 2022).

1.4.2. Glycosphingolipids

Glycosphingolipids are one of the types of glycolipids, and sphingolipids which is containing amino alcohol sphingosine, fatty acyl chain and a sugar molecule (mono/disaccharide) in its structure, and these sphingolipids' synthesis is processed in endoplasmic reticulum, and they are found in central nervous system tissues (brain) in higher concentrations (Iqbal et al., 2017; Olsen & Færgeman, 2017). Ceramides are the core structure of the glycosphingolipids which consist of long hydrocarbon tail (fatty acids), and sphingosine. Ceramides are found in elevated levels in cellular membranes especially in nervous system (Coet et al., 1998). Glycosphingolipids can be synthesized from glucosylceramide or galactosyl ceramides, and they may play important roles in cellular environment such as involvement in signaling pathways, developmental and differentiation processes in tissues of nervous system (Borodzicz et al., 2015; D'Angelo et al., 2013; Slotte, 2013).

1.4.3. Glycerophospholipids

Glycerophospholipids are one of the main constituents of plasma membranes which is also named as glycerophosphatides, and they are composed of glycerol backbone, two fatty acid chains, and polar head group, phosphoryl groups such as ethanolamine (PE), inositol (PI), choline (PC), serine (PS) etc (Holub & Kuksis, 1978; van Meer et al., 2008). Remodeling of glycerophospholipids is identified in former studies which is named as Land's cycle and describing the production of major glycerophospholipids (Shindou et al., 2009; A. Yamashita et al., 2014). In glycerophospholipid synthesis and lipid mediators' production pathways (Figure 1.4.), phospholipase A, acyl-CoA synthase, lysophospholipid acyltransferases, and transacylase

enzymes have significant roles, and different studies also demonstrated that distinct LPLAT and AGPAT enzymes were also responsible for these glycerophosphotidates synthesis (Murakami et al., 2011; Shindou et al., 2009; A. Yamashita et al., 2014). Glycerophospholipids in the mammalian cells can differ in quantities and compositions in types of cells, organelles, plasma membranes of tissues (van Meer et al., 2008). Glycerophospholipids may have significant roles in cellular signaling, trafficking of the vesicles, respiratory and visual pathways, membrane protein activity and stability, and fluidity of the cellular membranes (Pietzner et al., 2017); additionally, metabolism of the glycerophospholipids can be a part of the generation and may be a potential mediator of the immunological responses (Shimizu, 2009; Yu et al., 2021; Zhu et al., 2022).

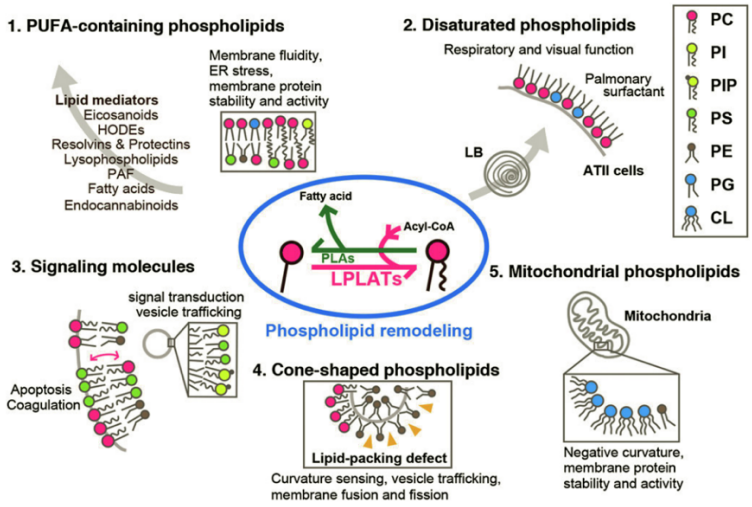

Figure 1.4. Remodeling of the glycerophospholipids, and their diverse function in cellular pathways (Hishikawa et al., 2014).

1.4.4. Secondary Lipid Alterations in Lysosomal Storage Diseases

Previously, it was defined that specific groups of the lipids such as sphingolipids, glycerophospholipids and cholesterol are significant components of the cellular membrane of central nervous system, and responsible for the maintenance of neuronal development, and proper functioning of neurons (Fuller & Futerman, 2018b). In the lysosomal storage diseases, deficiency/mutation in certain enzymes or their activator/transporter proteins result in the accumulation of specific biomolecules which are the targets of these defined enzymes and leading to impairment in the lipid metabolism and accumulation of the secondary lipids due to the breakdown of the lysosomal integrity

(Samie & Xu, 2014). Impairment in the specifically targeted lipid molecules results with the primary disorder in lipidomics, and additionally alterations in secondary lipids is defined in lysosomal storage diseases (primary disorders) (Samie & Xu, 2014; Vruchte et al., 2004).

Neimann-Pick C disease, one of the LSDs, has resulted from the deficient NPC proteins, which is encoded by NPC1/NPC2 genes, and maintains the uptake and movement of cholesterol lipids in neuronal and glial cells in myelination process, and functionality of neurons (Vruchte et al., 2004). In the Neimann-Pick C disease, due to the presence of defective NPC1/NPC2 proteins that was shown the sphingosine and cholesterol accumulation as a primary disorder condition. Additionally, elevated levels of lactosylceramide, glucosylceramide, GM2 and GM3 gangliosides is observed in the Niemann-Pick disease type C mice models as alterations of secondary lipid metabolisms (Lloyd-Evans et al., 2008; Vruchte et al., 2004).

Gaucher disease belongs to sphingolipidoses subgroup of LSDs, it is defined from the deficient lysosomal glucosylceramidase enzyme that is encoded by the GBA1 gene (Wong et al., 2004). Gaucher diseases is identified with the primary accumulation of the glucosylceramides, and glucosylsphingosine in nervous system tissues specifically brain (Farfel-Becker et al., 2014). In the neuronopathic mice model of Gaucher disease, accumulation of glycosylceramides is detected in the neurons with higher levels. Besides the primary accumulation of glycosylceramides, the elevated levels of GM2 and GM3 gangliosides were detected in the Gaucher patient brains, increased levels in secondary lipids (Farfel-Becker et al., 2014; Nilsson & Svennerholm, 1982; Wong et al., 2004).

In Krabbe disease, a type of lysosomal storage diseases, which is inherited in autosomal recessive manner. Krabbe disease is identified as a result of mutations in GALC gene that encodes the β-galactocerebrosidase enzyme (Vanier & Svennerholm, 1975). β-galactocerebrosidase is responsible for the maintenance of galactocerebroside degradation into ceramide and galactose, and the deficiency of β-GALC enzyme causes the galactocsylceramide accumulation in Krabbe disease patients' central and peripheral nervous system tissues (Vargiami et al., 2016; White et al., 2009). In addition to galactocsylceramide accumulation, alterations in secondary lipid metabolism are defined such as decreased levels of GD1a, GM1, and increased levels of GD2, GD3, and GM3 gangliosides (Fu et al., 1999).

Tay-Sachs disease, which is a GM2 gangliosidosis, and one of the LSDs, has resulted from the deficiency of lysosomal β-hexosaminidase α (HEXA) enzyme, that is

encoded by the Hexa gene, α subunit of HEXA enzyme (Yamanaka et al., 1994). Mutations in the Hexa gene causes the impairment in conversion of GM2 ganglioside into GM3 ganglioside. Aggregation of GM2 ganglioside is defined in the central nervous tissues in both Tay-Sachs patients, and mouse models (Hexa−/−Neu3−/−) (Demir et al., 2020a). Secondary lipid alterations are monitored in Tay-Sachs mice models, glycerophospholipid levels such as PE, PE-O, PC, PI, and PS were decreased in the cortex region of the brain (Can et al., 2022). In hippocampal region of brain in Tay-Sachs mice model, reduced levels of sphingomyelin, and sterol lipids, and significantly higher expression levels of TAG is observed (Can et al., 2022).

1.5. Aim of the Study

In this thesis study, we proposed that understanding the biological importance of lysosomal sialidase Neu1 in different tissues such as brain, kidney, spleen and age groups of *Neu1-/-* mice models. Previously generated *Neu1-/-* mice model is compared to the different age groups 2, and 5-month-old *Neu1-/-* mice models, and the wild type mice models in order to identify inflammatory conditions, and secondary lipid alterations. According to these purposes, molecular, histopathological, and immunohistochemical analyses were performed. Upon the whole, these analyses enlighten the significant roles of Neu1 sialidase in inflammatory pathways, and secondary lipid metabolism. Finding out the relationship between the inflammation and alterations in secondary lipid metabolisms is significant to determine the biomarkers in Neuraminidase I deficiency and specify the new therapeutic approaches in sialidosis.

CHAPTER 2

MATERIALS & METHODS

2.1. *Neu1-/-* and *WT* Mice

Neu1-/- knock out mice models were donated from Prof. Dr. Alessandro d'Azzo (St. Jude Children's Research Hospital Genetic Department, Tennesse, USA), female and male Neu1+/- heterozygote mice models were placed from USA to our faculty animal facility in Izmir Institute of Technology Animal Research Center in Turkey. *WT* and knock out Neu1 mice were maintained under constant humidity, temperature and 12 hours consecutive light/dark cycle, and their feeding was ad-libitum. Each experiment of Neu1 mice models were performed accordingly Turkish Institute of Animal Health guide for the care and use of laboratory animals, and ethical permissions were received from the Institutional Animal Care and Use Committee of the Izmir Institute of Technology.

In order to handle 2- and 5-month-old wild type and *Neu1-/-* mice models, 1 months old heterozygote 2 female *Neu1+/-* and 1 male *Neu1+/-* mice were placed and crossed in each breeding cage because *Neu1-/-* mice models were infertile after 10 weeks. The life expectancy of *Neu1-/-* mice were 8-12 months; therefore, 2-, and 5-months old age periods were chosen in investigation of neuroinflammation and secondary lipid alterations in sialidosis mice models.

2.2. Mice Genotyping

2.2.1. DNA Isolation

Mice offspring were separated to two different cages as females and males from breeding cages after they were 1 month old. To distinguish mice from each other and carry out DNA isolation, ears and tails were cut. 0,5 cm tails were taken from mice and incubated with 250 ul tissue lysis buffer (10% 1M Tris pH 7.6, 2.5% 0.2M EDTA, 20% SDS, 4% 5M NaCl) and 6 ul proteinase K solution at 55°C for 16 hours. Tails were

centrifuged for 10 minutes at 13000 rpm, and supernatant was taken, and mixed with 250 ul 100% isopropanol by upside& down. Then, 1 minute centrifuge at 15000 rpm was performed, and DNA pellet was visible. Supernatant were discarded, and 250 ul 70% ethanol was added and 1 minute centrifuge at 15000 rpm was performed. Ethanol was discarded and air-dry were performed at 55°C for 10 minutes. After that, 100 ul distilled water was mixed with DNA pellet, and incubated at 55°C for 1 hour. Lastly, dissolved DNA pellets were stored at -20°C for further polymerase chain reaction.

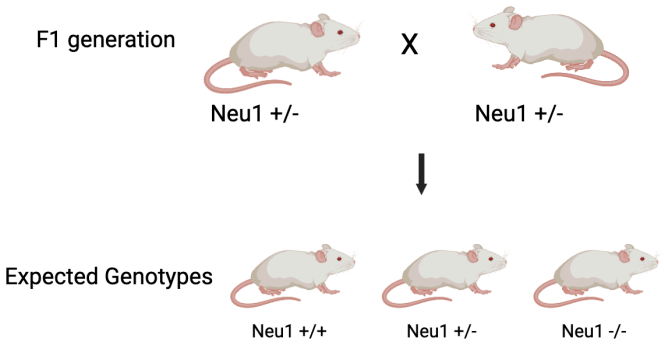

Figure 2.1. Representative scheme of Neu1 mice breeding.

2.2.2. Polymerase Chain Reaction for Neu1, WT and Mutant Alleles

To analyze *Neu1-/-* and *WT* mice, genotyping was carried out with isolated DNA samples by using Neu1 specific mutant and wild-type allele primers. In Neu1 PCR conditions for each DNA samples, 5 ul PCR buffer, 1 ul 400 uM dNTP, 1 ul MNTG-1 forward, 1 ul MNTG-2 (0.4 uM), forward (0.4 uM), 1 ul LacZ reverse primers (0.4 uM), 0.25 ul Taq Polymerase (GeneDirex), and 39.25 ul distilled water were mixed as total 48.5 ul PCR mixture, and 1.5 ul isolated DNA were added. Neu1 PCR conditions were consisting of initial denaturation 94°C for 3 minutes, 30 cycles of denaturation at 94°C for 30 seconds, annealing at 58.1°C for 30 seconds and extension at 72°C for 1 minute, and final extension at 72°C for 10 minutes. After PCR process, DNA samples were loaded onto 1% agarose gel mixture, and gel running was carried out at 100V for 30 minutes. Mice genotypes were identified with band lengths under UV light by Fusion SL.

Table 2.1. Neu1 gene wild type and knock out allele primers in mice genotyping

Gene	Primers	Primer Sequence	Product size
Neu1	MNTG-1	GACAGGGATCGCCGGGAGCTATGG	WT allele: 180 bp KO allele: 400 bp
	MNTG-2	CACCAGGCTGAAGTCATCCTCTGC	
	LacZ	GATAGGTTACGTTGGTGTAGATGGGCG	

2.3. Mice Tissue Preparation

To achieve lipidome analysis, RT-PCR, western blotting, histopathological and immunopathological investigations; soft and fixed mice brain, spleen, and kidney tissues were handled.

2.3.1. Soft Mice Tissues

Wild type and *Neu1-/-* mice were sacrificed inside CO_2 cabinet when they were at the age of 2- and 5-month-old. Brain, spleen, kidney, and liver tissues were immediately removed and froze on dry ice. Brain tissue was dissected into cortex, thalamus, and cerebellum regions. Obtained mice tissues were stored at -80°C until further biochemical experiments.

2.3.2. Fixation of Mice Tissues

2- and 5-month-old wild type and *Neu1-/-* mice were anaesthetized with ketamine (75-100 mg/kg) and xylazine (5-10 mg/kg). Then, trans cardiac perfusion was performed with brain, spleen, and kidney tissues by 10-12 ml NaCl and 10 ml %4 paraformaldehydes in PBS (PFA). Fixed tissues were waited overnight at 4°C. On other day, PFA was removed, and 10% and %20 sucrose in PBS were poured onto fixed tissues and placed at 4°C for 2 hours respectively. After that, %30 sucrose in PBS were added onto tissues, placed at 4°C for overnight and waited until tissues were sank. Fixed tissues were embedded into freezing blocks with OCT (Tissue-Tek, Sakura) on dry ice. Mice tissues

were sectioned as 10-micron thickness onto poly-L-lysine covered microscope slides, and slide storage was done at -80°C until histopathological and immunopathological protocols.

2.4. Lipidomic Analysis

2.4.1. Preparation of Mice Tissues for Lipidome Analysis

Previously, cortex, and cerebellum tissues of 2- and 5-month-old wild type and *Neu1-/-* mice were stored at -80°C. For lipidomics, 30 mg from cortex, and cerebellum were measured, and these tissues were homogenized in 1X D-PBS (without Mg&Ca) with metal beads by tissue homogenizator (Retsch MM400). Cortex and cerebellum homogenization were performed with 20 s^{-1} frequency during 40 seconds for three times. According to the protocol of Lipotype company, homogenized tissues were diluted in 1X D-PBS (without Mg&Ca) as the final concentration will be 5 mg/ml. Prepared cortex and cerebellum tissues were stored at -80°C until sent away and samples were forwarded to Lipotype company (Dresden, Germany) on dry ice.

2.5. RT-PCR

Soft cortex, cerebellum, kidney, and spleen tissues of 2- and 5-month-old wild type and *Neu1-/-* mice were kept at -80°C, and gene expression analysis of these tissues were carried out for Ccl2, Ccl3, Ccl5, Cxcl10, and GFAP chemokine and astrocyte-related genes.

2.5.1. RNA Isolation

50 mg tissues were measured from 2- and 5-month-old wild type and *Neu1-/-* mice cortex, cerebellum, kidney, and spleen tissues, and they were homogenized with metal beads in 1 ml RiboEx reagent by tissue homogenizator (Retsch MM400) with 20 s^{-1} frequency during 60 seconds for four times. Homogenized tissues were incubated at room

temperature for 5 minutes: Then, 200 ul choloroform were added onto homogenizates and waited for 2 minutes at room temperature. After incubation, samples were centrifuged at 12000 g at 4°C for 15 minutes, and upper phase were taken. Then, 500 ul 100% isopropanol were put, and mixed with samples by up& down, and kept for 10 minutes at room temperature. After that, samples were centrifuged at 12000 g for 10 minutes at 4°C, and supernatant were discarded. 1 ml 70% ethanol were added onto RNA pellets, and centrifuged at 7500 g for 5 minutes at 4°C. After centrifugation, ethanol was discarded, and samples were put onto air-dry process. When RNA pellets were invisible in air-dry process, 50 ul RNase-free distilled water were added, and RNA concentrations of each sample, were measured with Implen Nanophotometer N50.

2.5.2. cDNA synthesis

20 ul cDNA synthesis reaction mix were prepared with 4 ul 5x iScript reaction mix, 1 ul iScript Reverse Transcriptase, and total 15 ul nuclease free-water and RNA template (1000 ng total RNA) from 2- and 5-month-old wild type and *Neu1-/-* mice cortex, cerebellum, kidney, and spleen RNA samples. cDNA synthesis reaction protocol was followed by priming step at 25°C for 5 minutes, reverse transcription process for 20 minutes at 46°C, and reverse transcriptase inactivation for 1 minute at 95°C. After cDNA conversion of RNA samples, GAPDH (housekeeping gene) PCR were carried out for conformation of successful cDNA synthesis. In GAPDH PCR, 2.5 ul 10X reaction buffer, 1.5 ul $MgCl_2$, 1 ul 10 mM for each dNTP, 1 ul forward primer, 1 ul reverse primer, 0.5 ul Taq polymerase, and 16 ul distilled water was added, and cDNA reaction mixture was completed to 25 ul by addition of 1.5 ul cDNA. GAPDH PCR conditions were followed respectively, initial denaturation for 2 minutes at 95°C, 30 cycles of denaturation for 20 seconds at 95°C, annealing for 15 seconds at 65°C, and extension for 20 seconds at 72°C, and final extension at 72°C for 3 minutes. In order to obtain GAPDH PCR, cDNA samples were loaded onto 1% agarose gel mixture, and gel running was performed at 100V for 25 minutes. Visualization of GAPDH bands were done under UV light by Fusion SL.

2.5.3. RT-PCR Analysis

In SYBR Green qPCR mixture, 5 ul SYBR Green mix, 0.2 ul forward primer, and 0.2 ul reverse primer, 3.6 ul distilled water and 1 ul 100 ng cDNA was added for each 2- and 5-month-old wild type and *Neu1-/-* mice cortex, cerebellum, kidney, and spleen samples. RT-PCR was carried out with Roche LightCycler 96 and was followed by Taq polymerase activation in 1 cycle at 95°C, then 45 cycles of 15 seconds at 95°C,1 minute at 57°C and 1 minute at 72°C. GAPDH were used in analysis as housekeeping gene to normalize inflammation-related gene expressions.

Table 2.2. Inflammation related mice primers in RT-PCR

Gene	Primer Sequences	PCR product size
Ccl2	F: 5'-ATGCAGTTAATGCCCCACTC-3' R: 5'-TTCCTTATTGGGGTCAGCAC-3'	167 bp
Ccl3	F: 5'-TCTGTACCATGACACTCTGC-3' R: 5'-AATTGGCGTGGAATCTTCCG-3'	103 bp
Ccl5	F: 5'-AGTGCTCCAATCTTGCAGTC-3' R: 5'-AGCTCATCTCCAAATAGTTG-3'	108 bp
Cxcl10	F: 5'-ACCATGAACCCAAGTGCTGCCGT-3' R: 5'-AGGAGCCCTTTTAGACCTTTTTTG-3'	298 bp
GFAP	F: 5'-AGTAACATGCAAGAGACAGAG-3' R: 5'-TAGTCGTTAGCTTCGTGCTTG-3'	113 bp
GAPDH	F: 5'-CCCCTTCATTGACCTCAACTAC-3' R: 5'-ATGCATTGCTGACAATCTTGAG-3'	347 bp

2.6. PCR Array

Soft cortex, cerebellum and kidney tissues of 2 and 5-month-old *WT* and *Neu1-/-* mice stored at -80°C, and gene expression analysis of these tissues were performed for 84 different cytokines, chemokine, interleukin, and their receptor genes with Qiagen RT² Profiler™ PCR Array Mouse Cytokines & Chemokines (PAMM-150ZF-12).

2.6.1. RNA Isolation

30 mg of 2- and 5-month-old *WT* and *Neu1-/-* cortex, cerebellum and kidney tissues were measured, then 600 ul Buffer RLT Plus with B-mercaptoethanol was added onto each sample, and these tissues were homogenized by tissue homogenizator (Retsch MM400) at 25 s^{-1} frequency during 30 seconds for 2 times. Homogenized samples were centrifuged at 15000 rpm for 3 minutes at room temperature. Then, supernatants were put onto gDNA eliminator column, and centrifuged for 30 seconds at room tempature. After that, 600 ul 70% ethanol were put onto liquid part and mixed. 600 ul from samples were added onto Rneasy spin column, and centrifugation were performed at 11000 rpm for 15 seconds at room temperature. Flow-through was discarded, and 500 ul Buffer RPE was added onto spin column and centrifuged for 15 minutes at 11000 rpm at room temperature, and this step was carried out twice. After that, flow-thorugh was discarded, and 40 ul RNase-free distilled water were added onto spin column, and centrifugation was done at 11000 rpm for 1 minute at room temperature. Lastly, RNA concentrations of each sample, were measured with Implen Nanophotometer N50.

2.6.2. cDNA synthesis

20 ul cDNA synthesis reaction mix were prepared with 4 ul 5x iScript reaction mix, 1 ul iScript Reverse Transcriptase, and total 15 ul nuclease free-water and RNA template (1000 ng total RNA) from 2 and 5-month-old wild type and *Neu1-/-* mice cortex, cerebellum, and kidney RNA samples. cDNA synthesis reaction protocol was performed by priming step at 25°C for 5 minutes, reverse transcription process for 20 minutes at 46°C, and reverse transcriptase inactivation for 1 minute at 95°C. After cDNA conversion of RNA samples, GAPDH (housekeeping gene) PCR were done for conformation of successful cDNA synthesis. In GAPDH PCR, 2.5 ul 10X reaction buffer, 1.5 ul $MgCl_2$, 1 ul 10 mM for each dNTP, 1 ul forward primer, 1 ul reverse primer, 0.5 ul Taq polymerase, and 16 ul distilled water was mixed, and cDNA reaction mixture was completed to 25 ul by addition of 1.5 ul cDNA. GAPDH PCR conditions were carried out respectively, initial denaturation for 2 minutes at 95°C, 30 cycles of denaturation for 20 seconds at 95°C, annealing for 15 seconds at 65°C, and extension for 20 seconds at 72°C, and final

extension at 72°C for 3 minutes. In order to obtain GAPDH PCR, cDNA samples were loaded onto 1% agarose gel mixture, and gel running was performed at 100V for 25 minutes. GAPDH bands were visualized under UV light by Fusion SL.

2.6.3. PCR Array Analysis

RT^2 Profiler PCR Array mixture was prepared 1350 ul iTaq Universal SYBR Green Supermix, 102 ul 500 ng cDNA synthesis reaction, and 1248 ul nuclease-free water as total volume of master mix 2700 ul. 25 ul PCR components were added to each column of 96-well plate by multichannel pipettes using 4 tips only. RT^2 Profiler PCR Array was performed with Roche LightCycler 96 and was followed by Taq polymerase activation in 1 cycle at 95°C, then 45 cycles of 15 seconds at 95°C, 1 minute at 60°C and 1 minute at 72°C. Actb, B2m, Gapdh, Gusb, and Hsp90ab1 were analyzed as housekeeping genes to normalize inflammation-related gene expressions.

2.7. Western Blotting

Cortex, cerebellum, kidney, and spleen tissues of 2- and 5-month-old *WT* and *Neu1-/-* mice were homogenized in RIPA protein lysis buffer (1% TritonX100, 50mMHepes, 150mM NaCl, 10%Glycerol, 50mM Tris-Base, 1%PMSF, 1% protease inhibitor). 300 ul RIPA buffer were added onto cortex, and cerebellum tissues, and these tissues were homogenized with mini homogenizator. 500 ul RIPA solution was put onto 30 mg kidney and spleen tissues and these tissues were homogenized with the help of metal beads at 20 s^{-1} frequency during 60 seconds for 2 times by tissue homogenizator (Retsch MM400). For 1 hour, protein samples were waited on ice, and vortex was carried out in each 10 minutes. After that, protein samples were centrifuged at 14000 rpm for 10 minutes at 4°C. Supernatants of protein samples were taken. Cortex and cerebellum tissues were diluted 1:20 (38 ul water+ 2 ul protein), and kidney, and spleen samples were diluted 1:30 (58 ul water+ 2 ul protein) with distilled water to identify protein concentrations with Bradford measurement. In order to obtain a standard curve for protein concentration, stock 1 mg/ml BSA (Bovine Serum Albumin) was diluted to 0.8, 0.4, 0.2, and 0.1 mg/ml. Diluted protein samples were loaded onto 96 well plate as 10 ul, and 200

ul Bradford reagent (SERVA Electrophoresis Gmbh, Heidelberg,Germany) were added and mixed. Protein samples and Bradford solution were incubated for 10 minutes at dark. Absorbance of protein samples were performed at 595 nm with iMark microplate reader (iMark microplate absorbance reader, Biorad Laboratories, California,USA). By using BSA standard curve, R^2 and equation from the graph was achieved. According to standard curve equation, protein concentration of samples was calculated. Cortex and cerebellum samples' protein concentrations were adjusted as 20 ug/ml, and spleen, and kidney protein concentrations were adjusted as 50 ug/ml.

After calculation of protein concentrations, protein stocks were prepared with 9 ul protein+ distilled water, and 3 ul 4X loading dye (40% Glycerol, 240mM Tris-HCl pH 6.8,8%SDS, 0.04%Bromophenol Blue, 5% β-mercaptoethanol), and protein stocks were boiled at 95°C for 10 minutes. SDS-PAGE gel preparations were carried out with 10% resolving gel (3.8 ml distilled water, 2 ml 30% Acrylamide, 2 ml pH=8.8 Tris Buffer, 80 ul 10% SDS, 80 ul 10% APS, and 8 ul TEMED), and 5% stacking gel (3.1 ml distilled water, 30% Acrylamide, 1.25 ml pH=6.8 Tris Buffer, 50 ul 10% SDS, 50 ul 10% APS, and 5 ul TEMED) and gel polymerization occurred. After SDS-PAGE polymerization, protein samples were loaded as 12 ul into wells, and gel running were performed at constant 80V for 30 minutes, then at constant 120V for 60 minutes with running buffer (0.25M TrisBase, 1.92 M glycine, 1% SDS at 8.3 pH). After that, transfer of protein samples from SDS-PAGE to nitrocellulose membrane (BioRad) were performed. In transfer step, nitrocellulose membrane and SDS-PAGE were placed between whatman papers by sandwich theory, and transfer was performed with transfer buffer (48 mM TrisBase, 39 mM Glycine, 20% methanol at pH=9.2) at constant 250 mA for 75 minutes. Then, nitrocellulose membranes with protein samples were blocked by 5% non-fat dry milk in PBS-T for 60 minutes at room temperature on shaker. After blocking process, nitrocellulose membranes were washed with 1X PBS-T buffer for 5 minutes and three times. Primary antibody dilutions were done as 1:1000 in red solutions (5 g BSA, 20 mg sodium azide, 4 mg phenol red at 7.5 pH). Primary antibodies: anti-IkB-α (9242, Cell Signalling), anti-NF-kB (ab32536, Abcam), and anti-B-actin (13E5, Cell Signalling) were incubated at overnight at 4°C on shaker. On the other day, nitrocellulose membranes were washed three times for 5 minutes with 1X PBS-T solutions. Then, HRP-conjugated secondary antibodies (Jackson ImmunoResearch Lab) were diluted as 1:10000 in 5% non-fat dry milk in 1X PBS-T. Then, nitrocellulose membrane washing step were done with 1X PBS-T for 5 minutes in three times. In chemiluminescence of nitrocellulose

membranes, enhancer was prepared with 100 mM trisHCl pH=8.5, 22 ul coumaric acid, 50 ul luminol, 2.5 ul H_2O_2, 1 ml enhancer were put onto nitrocellulose membrane, and incubated for 30 seconds at dark. Then, nitrocellulose membrane images were taken by Fusion SL, and protein band intensities were measured with NIH ImageJ. Protein expression intensities were normalized to beta-actin (housekeeping gene), and protein expression graphs were drawn with GraphPad Prism, and analyses were done.

2.8. Histopathological Analysis

Staining of fixed cortex, cerebellum, kidney, and spleen tissues of 2- and 5-month-old *WT* and *Neu1-/-* mice were performed to investigate morphological changes and degeneration in tissues with Hematoxylin- Eosin staining, accumulation of glycoconjugates in tissues by staining Periodic Acid- Schiff method, and Toluidine staining for mast cells detection, and axonal degeneration.

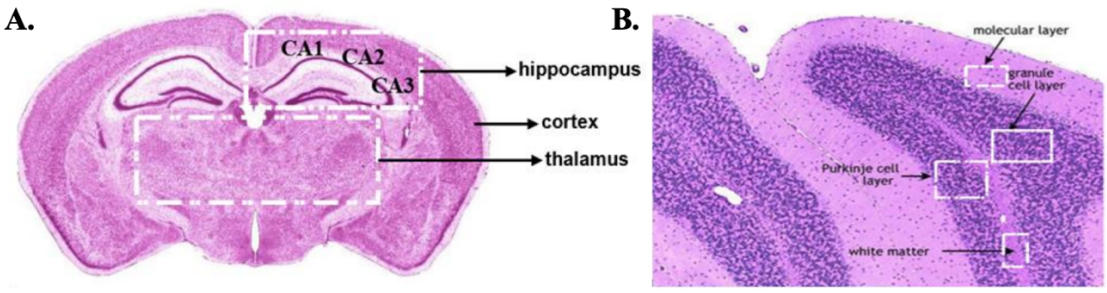

Figure 2.2. Coronal sections of hippocampus, cortex, and thalamus regions of mouse brain (A). Cerebellum region of mouse brain with representation of Purkinje cell layer, white matter, molecular layer, and granule cell layer (B) (Woods et al., 2013).

2.8.1. Hematoxylin- Eosin Staining

Cortex, cerebellum, kidney, and spleen of 2- and 5-month-old *WT* and *Neu1-/-* mice slides were taken from -80°C on ice for 15 minutes and incubated at 55°C for 15 minutes on humidity chamber in incubator. Then, slides were rinsed with distilled water

for 1.5 minutes, and Hematoxylin (Gill's hematoxylin (Merck, Germany)) staining of slides were performed for 3 minutes. After that, slides were rinsed in distilled water for 3 minutes, and under running tap water for 5 minutes. Then, differentiation of slides was carried out in 1% HCl in 70% ethanol for 30 seconds. After differentiation, slides were rinsed in tap water for 5 minutes, and then rinsed in distilled water for 2 minutes. After that, counterstaining with eosin Y solution 0.5% alcoholic (Merck, Germany) was applied for 1 minute. For dehydration of slides, slides were waited in 95% ethanol for 2 minutes twice, then; slides were transferred to 100% ethanol and waited for 2 minutes twice. When the slides dried, they were mounted with cytoseal (Richard-Allan scientificTM cytoseal XYL,Thermofisher,UK). Cortex, cerebellum, thalamus, hippocampus regions of brain, kidney, and spleen tissues photographs were taken with 10x and 20x on light microscopy (Olympus BX53).

2.8.2. Periodic Acid-Schiff Staining

Before staining, cortex, cerebellum, kidney, and spleen of 2- and 5-month-old *WT* and *Neu1-/-* mice slides were taken from -80°C on ice for 30 minutes and incubated at 55°C for 15 minutes on humidity chamber in incubator. Firstly, slides were washed with PBS for 5 minutes, then 10 minutes incubation in Corney's solution (6:3:1 v/v/v ethanol/chloroform/acetic acid). Then, slides were rinsed in distilled water for 2 minutes. After that, Periodic Acid solution 0.5% (Merck,Germany) was applied onto slides for 5 minutes (30 ul for each tissue). Then, running tap water was used to rinse slides for 3 minutes, and then, rinsed with distilled water for 2 minutes. When the slides dried, Schiff's reagent were put onto each tissue as 30 ul for 12 minutes. Then, running tap water was applied to rinse for 5 minutes, and then air-dry waited. After that, slides were stained with Hematoxylin solution (Gill's hematoxylin (Merck, Germany)) for 1.5 minutes. Then, slides were transferred to running tap water for 5 minutes. For dehydration step of slides, slides were incubated for 1 minute in 70%, 96%, and 100% ethanol respectively, and each step were repeated for twice. Dried slides were mounted with cytoseal (Richard-Allan scientificTM cytoseal XYL, Thermofisher,UK). Cortex, cerebellum, thalamus, hippocampus regions of brain, kidney, and spleen tissues photographs were taken with 10x and 20x on light microscopy (Olympus BX53).

2.8.3. Toluidine Blue Staining

Cortex, cerebellum, kidney, and spleen of 2- and 5-month-old *WT* and *Neu1-/-* mice slides were taken from -80°C on ice for 10 minutes and incubated at 42°C for 15 minutes on humidity chamber in incubator. Then, 1X PBS wash were applied for 5 minutes, and slides were transferred into distilled water for 2 minutes. After that, slides were incubated for 15 minutes on humidity chamber at 60°C. Then, slides were stained with Toluidine Blue (0.01 g/10 ml methanol) for 1.5 minutes. After staining, slides were rinsed with distilled water until the water was seen clearly. In dehydration part of staining, slides were dipped for 10 seconds into 96%, and 100% ethanol respectively in twice. Lastly, when the slides dried, they were mounted with cytoseal (Richard-Allan scientificTM cytoseal XYL,Thermofisher,UK). Cortex, cerebellum, thalamus, hippocampus regions of brain, kidney, and spleen tissues photographs were taken with 10x and 20x on light microscopy (Olympus BX53).

2.9. Immunohistochemical Analysis

Staining of fixed cortex, and cerebellum brain regions of 2- and 5-month-old *WT* and *Neu1-/-* mice were performed to investigate active astrocytes with anti-GFAP staining (glial fibrillary acidic protein), neuron number measurement with anti-NeuN staining, anti-CNPase staining for identification of oligodendrocytes and demyelination, and anti-MOMA2 staining for observation of microglial/macrophage activation.

2.9.1. anti-GFAP Staining

Before staining, cortex, and cerebellum of 2 and 5-month-old *WT* and *Neu1-/-* mice slides were taken from -80°C on ice for 30 minutes and incubated at 55°C for 15 minutes on humidity chamber in incubator. Then, slides were dipped and rinsed in 1X PBS for 10 minutes. After that, slides were incubated in ice cold acetone for 15 minutes. Then, edges of cortex and cerebellum tissues were drawn with PAP pen (Sigma-Aldrich), and slides were washed for 5 minutes in three times with 1X PBS. To inhibit nonspecific antibody binding, blocking buffer solution (0.2% Triton X-100, 10% Goat serum in 1X

PBS) was put onto tissues 20 ul for each for 1 hour at room temperature. After blocking process, primary anti-GFAP (Sigma-Aldrich) antibody were diluted 1:200 in blocking solution and incubated at overnight at 4°C on humidity chamber. On the other day, slides were washed in 1X PBS for 5 minutes for three times. Then, secondary antibody anti-rabbit Alexa Fluor®-568 red (Abcam) were diluted in 1:500 in blocking solution, and secondary antibody were added onto cortex and cerebellum tissues; then, incubation with secondary antibody were performed at room temperature for 1 hour at dark. After secondary antibody incubation, slides were rinsed with 1X PBS during 5 minutes for three times. Slides were left to air-dry, and slides were mounted with mounting medium DAPI (ab104139, Abcam). Lastly, slides were photographed with fluorescent microscopy (BX53, Olympus, Germany) with same light intensity. NIH ImageJ were used to analyze immunohistochemical intensities, and graphs were drawn with GraphPad Prism, and analyses were done.

2.9.2. anti-NeuN Staining

Cortex, and cerebellum of 2 and 5-month-old *WT* and *Neu1-/-* mice slides were taken from -80°C on ice for 30 minutes and incubated on humidity chamber at 55°C for 15 minutes in incubator. Then, slides were washed in 1X PBS for 10 minutes. After that, slides were dipped into ice cold acetone for 15 minutes. Then, slides were rinsed in 1X PBS for 5 minutes twice. After that, prevention of nonspecific binding of antibodies, slides were blocked with blocking buffer (0.2% Triton X-100, 10% Goat serum in 1X PBS) for 1 hour at room temperature. After that, anti-NeuN primary antibody (Cell Signaling Technology, The Netherlands) was diluted as 1:50 in blocking solution, and primary antibody was added onto cortex and cerebellum tissues; then, slides were incubated on humidity chamber for overnight at 4°C. On second day, slides were dipped into 1X PBS and washed for 5 minutes in three times. Then, secondary antibody anti-rabbit Alexa Fluor 568 was diluted 1:500 in blocking solutions, and slides were incubated for 1 hour at room temperature at dark. After secondary antibody incubation, slides were rinsed in 1X PBS for 5 minutes in three times. Slides were air-dried, mounted with mounting medium DAPI (ab104139, Abcam). Lastly, photography of slides was taken with fluorescent microscopy (BX53, Olympus, Germany) with same light intensity. NIH

ImageJ were used to analyze, and graphs were drawn with GraphPad Prism, and analyses were done.

2.9.3. anti-CNPase Staining

Before staining, cortex, and cerebellum of 2 and 5-month-old *WT* and *Neu1-/-* mice slides were taken from -80°C on ice for 30 minutes and incubated at 55°C on humidity chamber in incubator until slides were dried. For fixation of tissues on slides were dipped in 4% PFA in 1X PBS for 15 minutes. Then, specimens were rinsed into 1X PBS for 5 minutes in three times. After that, slides were incubated in ice cold 100% methanol for 10 minutes, and slides were washed in 1X PBS for 5 minutes. Slides were incubated with blocking buffer (0.2% Triton X-100, 10% Goat serum in 1X PBS) for 1 hour at room temperature. Then, anti-CNPase primary antibody (Cell Signaling Technology, The Netherlands) was diluted as 1:100 in blocking solution, and primary antibody was added onto cortex and cerebellum tissues; then, overnight incubation of slides on humidity chamber at 4°C was performed. On second day, slides were rinsed 1X PBS for 5 minutes in three times. After that, secondary antibody anti-rabbit Alexa Fluor 488 (green) was diluted as 1:500 in blocking solution, and slides were incubated with secondary antibody on humidity chamber at room temperature for 1 hour at dark. Then, slides were dipped into 1X PBS for 5 minutes in three times in order to remove secondary antibody. In the last step of anti-CNPase staining, slides were mounted with mounting medium DAPI (ab104139, Abcam). Slide photography was taken with fluorescent microscopy (BX53, Olympus, Germany) with same light intensity. NIH ImageJ were used for analyses of demyelination and oligodendrocytes, and graphs were drawn with GraphPad Prism, and analyses were done.

2.9.4. anti-Moma2 Staining

Cortex, and cerebellum of 2 and 5-month-old *WT* and *Neu1-/-* mice slides were taken from -80°C on ice for 30 minutes and incubated on humidity chamber at 55°C for 15 minutes in incubator. Then, specimens were put into 0.1% Triton-X-100 for 15

minutes to enhance permeabilization. After that, Slides were incubated with blocking buffer (0.2% Triton X-100, 10% Goat serum in 1X PBS) for 1 hour at room temperature. Then, anti-Moma2 primary antibody (Cell Signaling Technology, The Netherlands) was diluted as 1:50 in blocking solution, and primary antibody was added onto cortex and cerebellum tissues; then, overnight incubation of slides on humidity chamber at 4°C was performed. On second day, slides were rinsed 1X PBS for 5 minutes in three times. After that, secondary antibody anti-rat Alexa Fluor 568 (red) was diluted as 1:250 in blocking solution, and slides were incubated with secondary antibody on humidity chamber at room temperature for 1 hour at dark. Then, slides were dipped into 1X PBS for 5 minutes in three times in order to remove secondary antibody. In the last step of anti-Moma2 staining, slides were mounted with mounting medium DAPI (ab104139, Abcam). Slide photography was taken with fluorescent microscopy (BX53, Olympus, Germany) with same light intensity. NIH ImageJ were used for analyses of demyelination and oligodendrocytes, and graphs were drawn with GraphPad Prism, and analyses were done.

CHAPTER 3

RESULTS

3.1. Genotyping of Neu1 Mice for Wild-type and knock out alleles

Identification of wild-type and mutant alleles of Neu1 genes were performed with Polymerase Chain Reaction (PCR). According to the band length of Neu1 genes, genotypes of Neu1 mice were defined as wild-type, heterozygote for breeding (Neu1 +/-), and knock out (*Neu1-/-*) (Figure 3.1.)

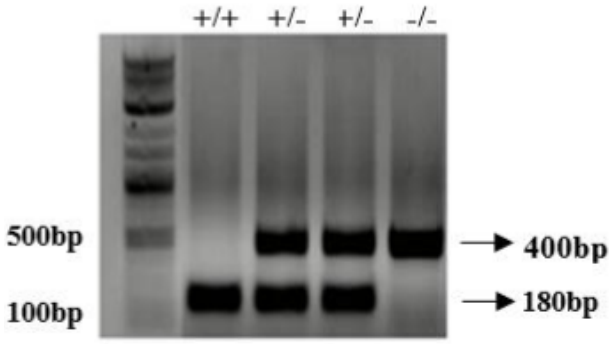

Figure 3.1. Genotyping of wild-type and mutant alleles of Neu1 genes of mice tails with Polymerase Chain reaction. Mutant allele of Neu1 gene is shown with amplified band at 180 bp length, and wild type allele is shown with 400 bp length.

PCR reaction for identification of Neu1 alleles was carried out with specific primers of Neu1 which are MNTG-1, MNTG-2, and LacZ primers, and DNA ladder. Band length of wild-type allele is 180 bp, and mutant allele is 400 bp of Neu1 gene (Figure 3.1).

3.2. Lipidomic Analysis

Lipidome analysis was carried out for the identification of alterations in secondary lipid metabolisms of 2 and 5-month-old *Neu1-/-* mice cortex and cerebellum regions in comparison to *WT*. Alterations in glycerophospholipid and glycolipid levels in 2 and 5-month-old *Neu1-/-* mice cortex tissues were observed (Figure 3.2. and Figure 3.3.), although there is no significant change in glycerophospholipid and glycolipid levels in cerebellum of 2 and 5-month-old *Neu1-/-* mice (Figure 3.4. and Figure 3.5.).

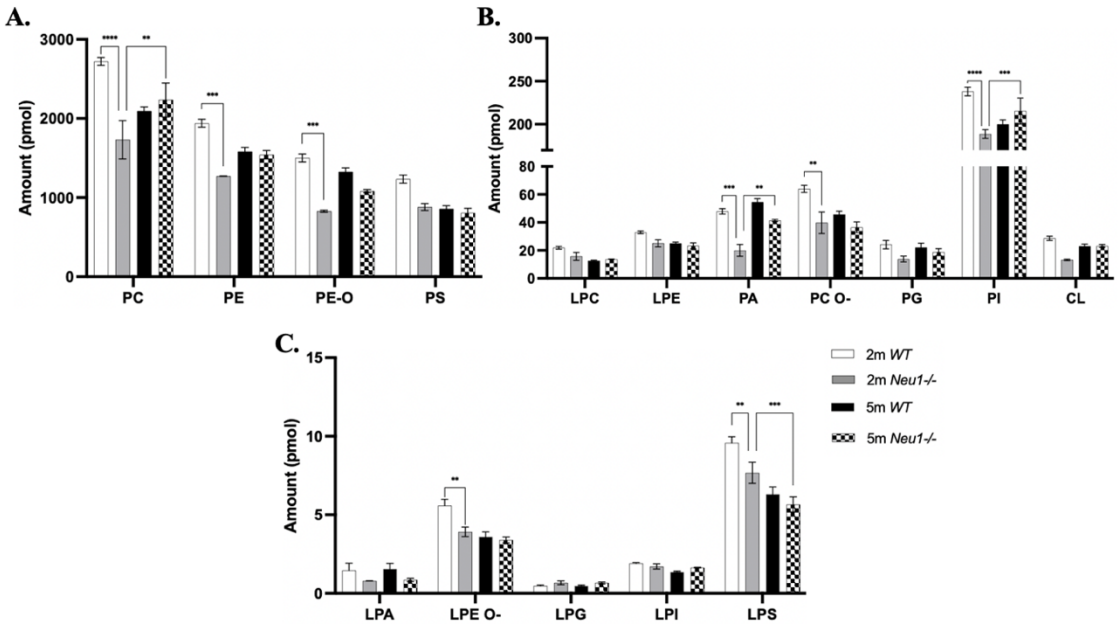

Figure 3.2. Lipidome analysis of major (A), intermediate (B), and minor (C) glycerophospholipids in the cortex of 2-month-old *WT* and *Neu1-/-,* and 5-month-old *WT* and *Neu1-/-* mice. The data are represented as the mean ± SEM, and 2-way-ANOVA analysis was used to determine p-values by using GraphPad. (n = 2, *p < 0.05, **p < 0.01, ***p < 0.005, and *p < 0.001).

In Figure 3.2, significant decrease was monitored in PC, PE, and PE O- major glycerophospholipid levels (Figure 3.2A), in PA, PC O- and PI intermediate glycerophospholipid amounts (Figure 3.2B), in LPE O- and LPS minor glycerophospholipid levels (Figure 3.2C) of 2-month-old *Neu1-/-* mice cortex compared

to the 2-month-old *WT* mice cortex tissue. Additionally, PC, PA and PI glycerophospholipid levels were observed in significantly elevated levels in 5-month-old *Neu1-/-* mice cortex in comparison to the 2-month-old *Neu1-/-* mice cortex tissue; and surprisingly only LPS glycerophospholipid levels were detected in reduced levels in 5-month-old *Neu1-/-* mice cortex according to the 2-month-old *Neu1-/-* mice cortex (Figure 3.2C).

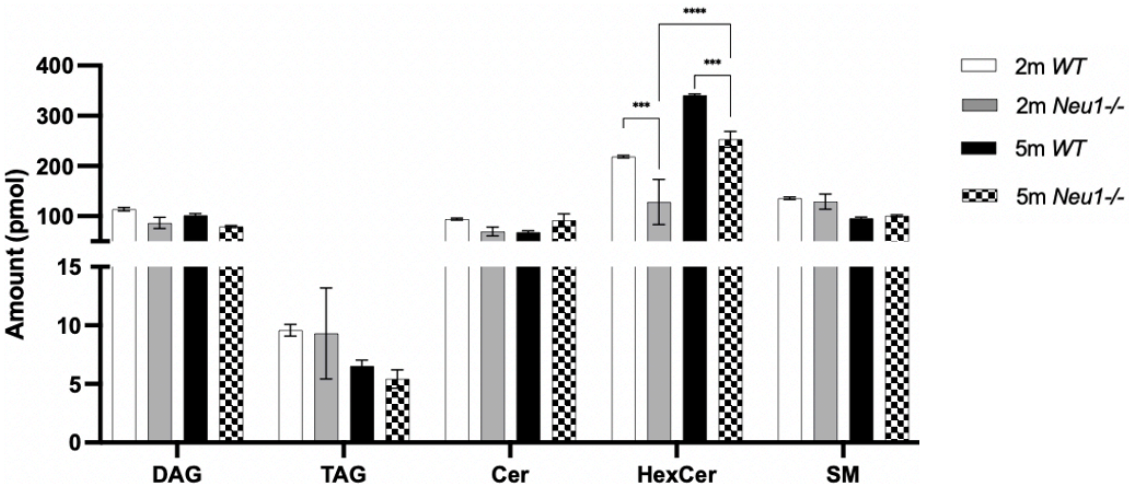

Figure 3.3. Lipidome analysis of glycerolipids (DAG, and TAG), and glycolipids (Cer, HexCer, and SM) in the cortex of 2-month-old *WT* and *Neu1-/-*, and 5-month-old *WT* and *Neu1-/-* mice. The data are represented as the mean ± SEM, and 2-way-ANOVA analysis was used to determine p-values by using GraphPad (n = 2, *p < 0.05, **p < 0.01, ***p < 0.005, and *p < 0.001).

In Figure 3.3., HexCer glycolipid levels were significantly decreased in both 2 and 5-month-old *Neu1-/-* mice cortex tissues that are compared to 2 and 5-month-old *WT* mice cortex, and HexCer glycolipid levels were increased in 5-month-old *Neu1-/-* mice cortex in comparison to 2-month-old *Neu1-/-* mice cortex. There were no significant alterations in glycerolipid (DAG, and TAG), and glycolipid levels (Cer, and SM) in 2 and 5-month-old *WT* mice cortex tissues.

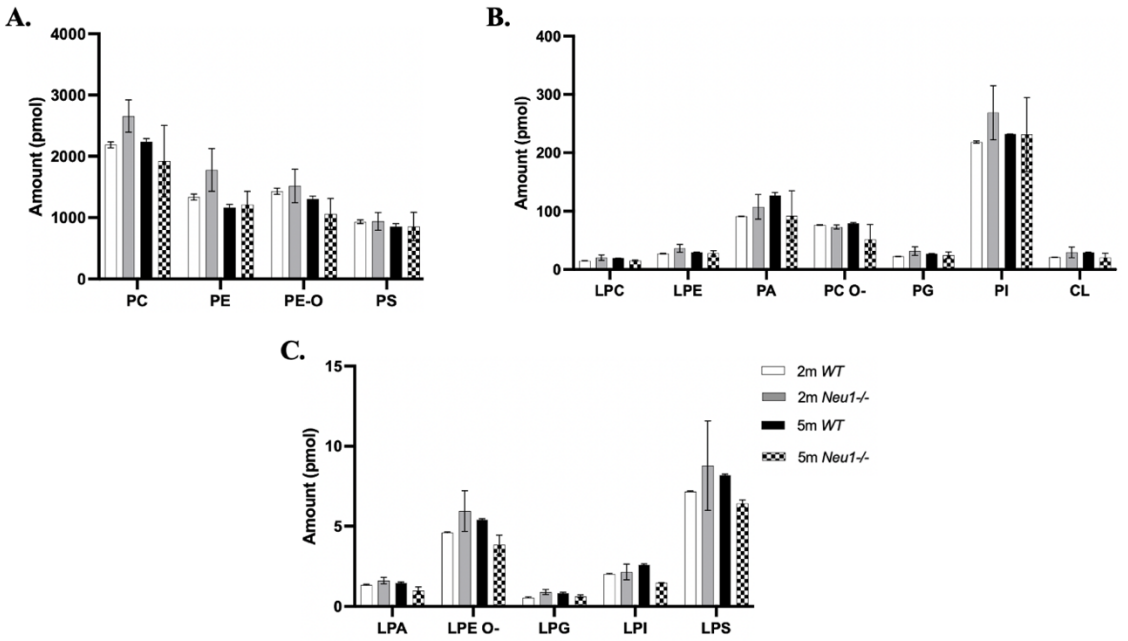

Figure 3.4. Lipidome analysis of major (A), intermediate (B), and minor (C) glycerophospholipids in the cerebellum of 2-month-old *WT* and *Neu1-/-*, and 5-month-old *WT* and *Neu1-/-* mice. The data are represented as the mean ± SEM, and 2-way-ANOVA analysis was used to determine p-values by using GraphPad. (n = 2, *p < 0.05, **p < 0.01, ***p < 0.005, and *p < 0.001).

In Figure 3.4., there were no remarkable increase or decrease in the levels of major, intermediate, and minor glycerophospholipids of both 2 and 5-month-old *Neu1-/-* mice cerebellar regions in comparison to 2 and 5-month-old *WT*.

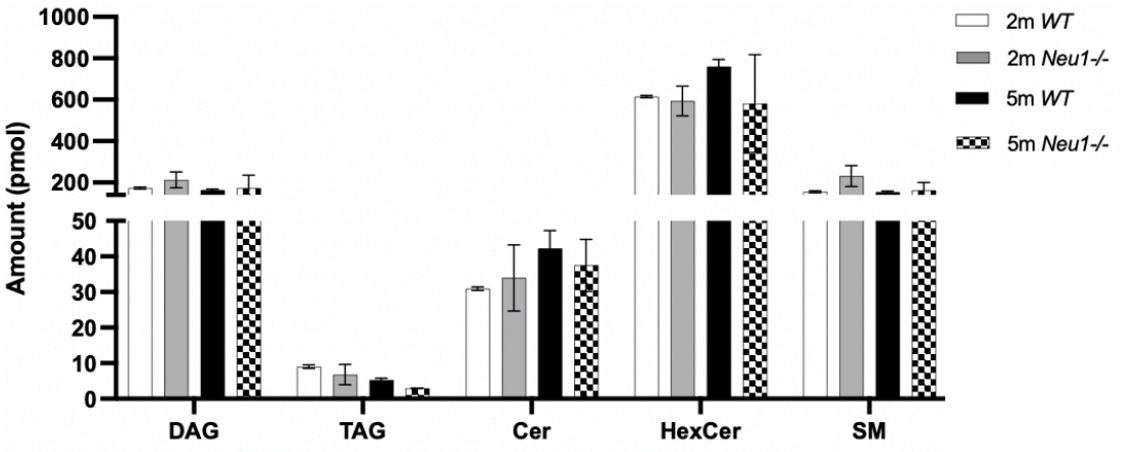

Figure 3.5. Lipidome analysis of glycerolipids (DAG, and TAG), and glycolipids (Cer, HexCer, and SM) in the cerebellum of 2-month-old *WT* and *Neu1-/-*, and 5-month-old *WT* and *Neu1-/-* mice. The data are represented as the mean ± SEM, and 2-way-ANOVA analysis was used to determine p-values by using GraphPad (n = 2, *p < 0.05, **p < 0.01, ***p < 0.005, and *p < 0.001).

In Figure 3.5., no significant change was detected in the levels of glycerolipids, and glycolipids of both 2 and 5-month-old *Neu1-/-* mice cerebellar regions in comparison to 2 and 5-month-old *WT*.

3.3. Real Time PCR (RT-PCR)

Real-Time PCR was performed to investigate the correlation and validation between the Qiagen RT² Profiler™ PCR Array Mouse Cytokines & Chemokines which provides information about gene expression analysis of 84 different cytokines, chemokine, interleukin, and their receptor genes. Inflammation-related genes Ccl2, Ccl3, Ccl5, Cxcl10, and GFAP were analyzed manually in cortex, cerebellum, kidney and spleen tissues of 2- and 5-month-old *WT* and *Neu1-/-* mice, and ΔCT method was used for calculation of expression ratios by GAPDH housekeeping gene.

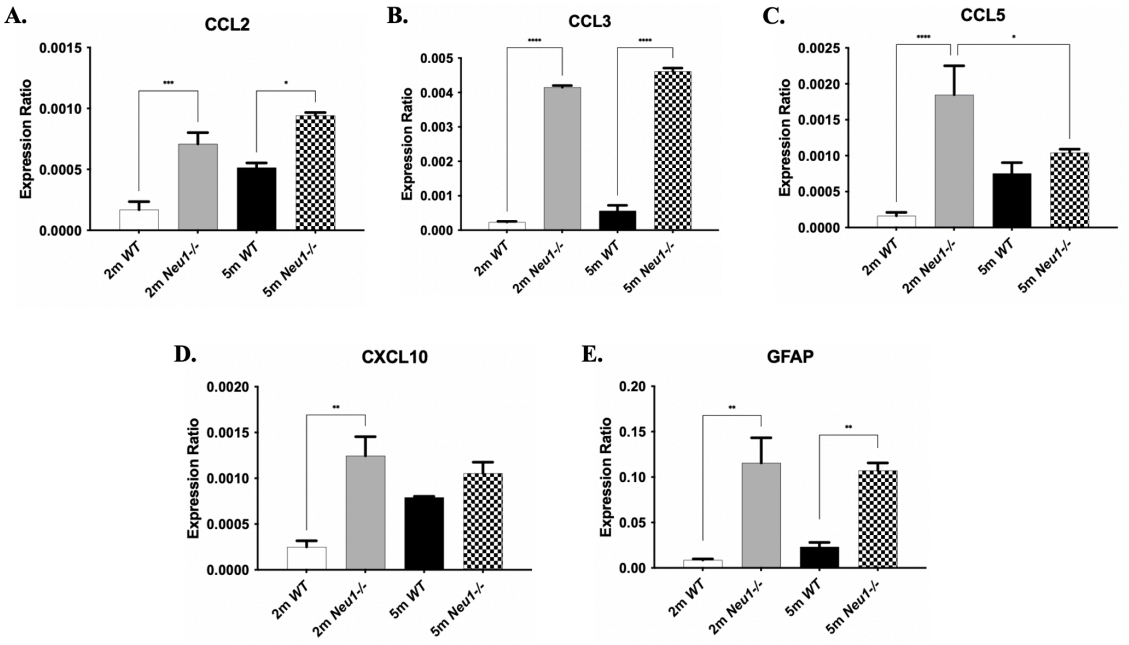

Figure 3.6. Gene expression ratio of inflammation-related genes CCL2 (A), CCL3 (B), CCL5 (C), CXCL10 (D) and GFAP (E) in 2 and 5-month-old *WT* and *Neu1-/-* mouse cortex was shown. Expression ratios were calculated with ΔCT method and one-way-ANOVA analysis was used to determine p-values by using GraphPad. Data were reported as means SEM (n=3, *p<0,05, **p<0,01, ***p<0,001).

In Figure 3.6, remarkable elevated levels of Ccl2, and Ccl3 chemokines in both 2 and 5-month-old *Neu1-/-* cortex tissues in comparison to 2 and 5-month-old *WT* cortex tissues (Figure 3.6A, and Figure 3.6B) were monitored. Increased levels of chemokines including Ccl5, and Cxcl10 were detected in only 2-month-old *Neu1-/-* mice cortex that is compared to 2-month-old *WT*, and surprisingly Ccl5 chemokine expression was decreased in 5-month-old *Neu1-/-* mice cortex in comparison to 2-month-old groups (Figure 3.6C, and 3.6D). Significantly increased GFAP expression levels were monitored in both 2 and 5-month-old *Neu1-/-* cortex tissues in comparison to 2 and 5-month-old *WT* cortex tissues (Figure 3.6E).

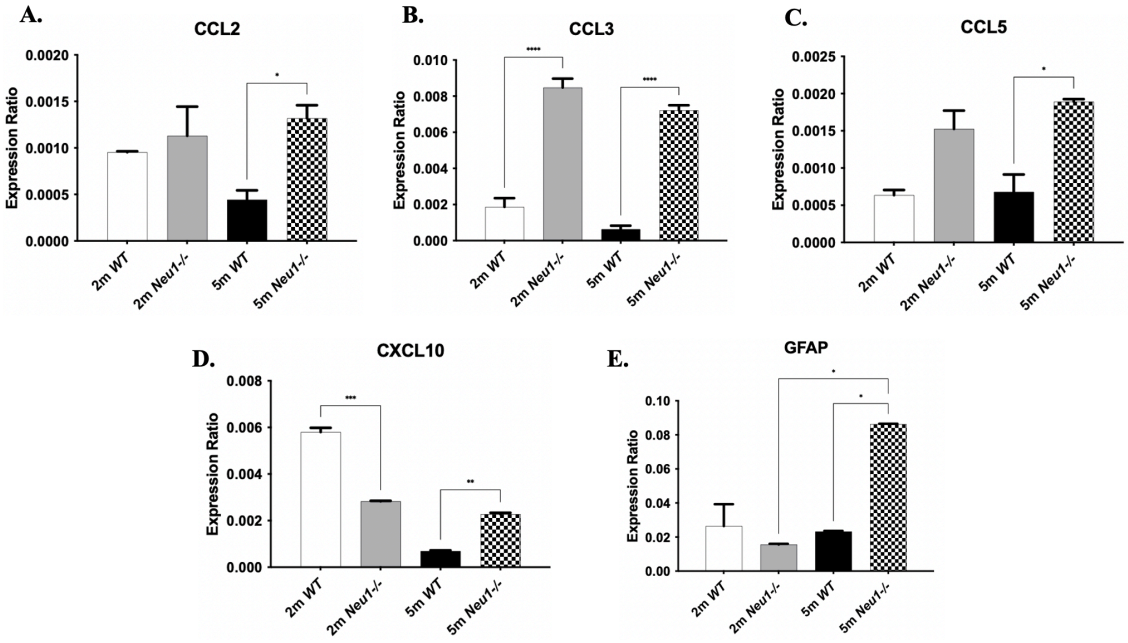

Figure 3.7. Gene expression ratio of inflammation-related genes CCL2 (A), CCL3 (B), CCL5 (C), CXCL10 (D) and GFAP (E) in 2 and 5-month-old *WT* and *Neu1-/-* mouse cerebellum was shown. Expression ratios were calculated with ΔCT method and one-way-ANOVA analysis was used to determine p-values by using GraphPad. Data were reported as means SEM (n=3, *p<0,05, **p<0,01, ***p<0,001).

In Figure 3.7, apparent increasing levels of Ccl2, Ccl3, Ccl5, and Cxcl10 chemokines of 5-month-old *Neu1-/-* mice cerebellum in comparison to 5-month-old *WT* mice cerebellum tissues were observed. Additionally, Ccl3 levels were increased in 2-month-old *Neu1-/-* mice cerebellum in comparison to 2-month-old *WT* cerebellar region (Figure 3.7B), and Cxcl10 chemokine levels were decreased in 2-month-old *Neu1-/-* mice cerebellum in comparison to 2-month-old *WT* cerebellum (Figure 3.7D). Also, GFAP expression levels were increased in 5-month-old *Neu1-/-* mice cerebellum in comparison to 5-month-old *WT*, and 2-month-old group (Figure 3.7E).

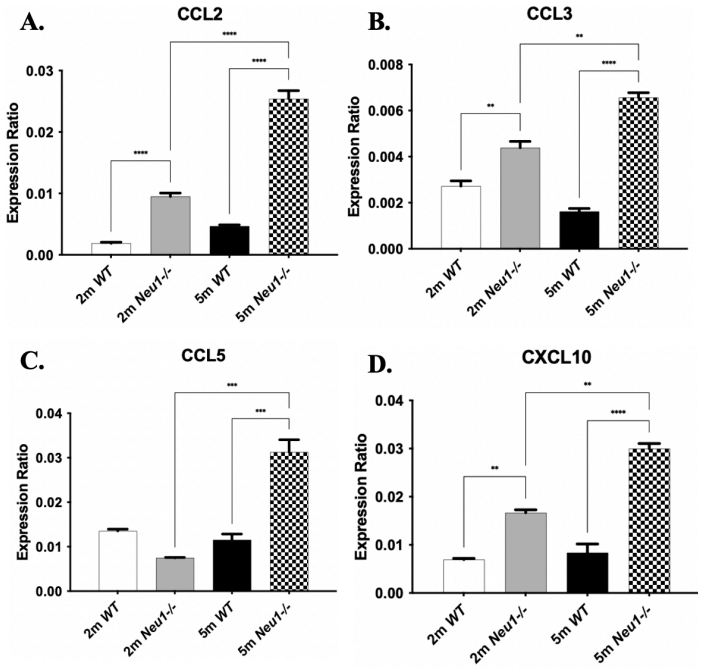

Figure 3.8. Gene expression ratio of inflammation-related genes CCL2 (A), CCL3 (B), CCL5 (C), and CXCL10 (D) in 2 and 5-month-old *WT* and Neu1-/- mouse kidney was shown. Expression ratios were calculated with ΔCT method and one-way-ANOVA analysis was used to determine p-values by using GraphPad. Data were reported as means SEM (n=3, *p<0,05, **p<0,01, ***p<0,001).

In Figure 3.8, remarkable increase of Ccl2, Ccl3, and Cxcl10 chemokines were monitored in both 2 and 5-month-old *Neu1-/-* mice kidney tissues in comparison to 2- and 5-month-old *WT* and younger groups' kidney tissues. Differently, Ccl5 chemokine expression were shown in elevated levels in 5-month-old *Neu1-/-* mice kidney that is compared to 5-month-old *WT*, and 2-month-old *Neu1-/-* kidney tissues (Figure 3.8C).

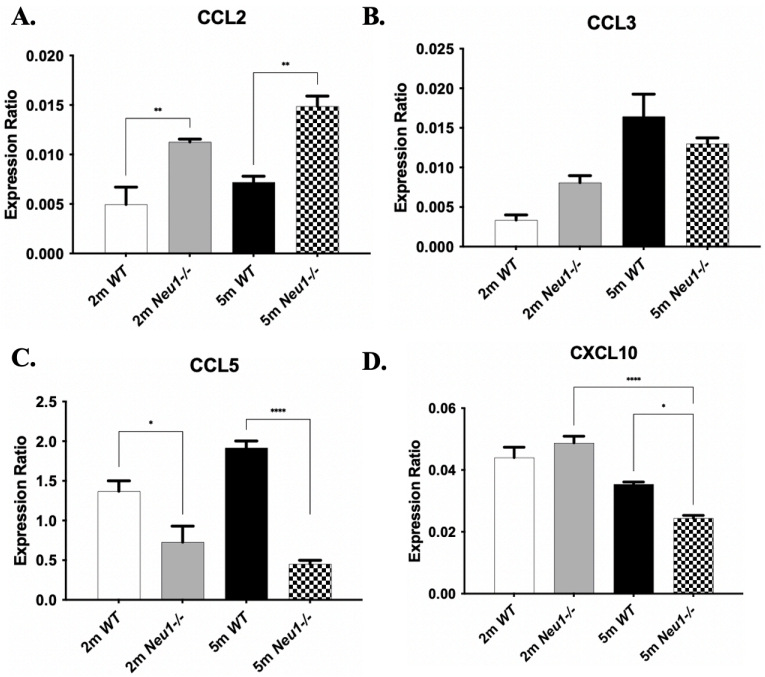

Figure 3.9. Gene expression ratio of inflammation-related genes CCL2 (A), CCL3(B), CCL5 (C), and CXCL10 (D) in 2 and 5-month-old *WT* and *Neu1-/-* mouse spleen was shown. Expression ratios were calculated with ΔCT method and one-way-ANOVA analysis was used to determine p-values by using GraphPad. Data were reported as means SEM (n=3, *p<0,05, **p<0,01, ***p<0,001).

In Figure 3.9A, Ccl2 expression were increased in both 2 and 5-month-old *Neu1-/-* spleen tissues according to the 2 and 5-month-old *WT* spleen. There were no apparent alterations in gene expression of Ccl3 chemokines in spleen tissues of each age groups (Figure 3.9B). In Figure 3.9C, it was observed that Ccl5 gene expressions were decreased in *Neu1-/-* spleen tissues of both age groups in comparison to *WT* spleens. Cxcl10 gene expression was monitored in reduced levels in 5-month-old *Neu1-/-* spleen according to 5-month-old *WT*, and 2-month-old *Neu1-/-* spleen tissues (Figure 3.9D).

3.4. PCR Array Analysis

Real Time PCR analyses were obtained with Qiagen RT² Profiler™ PCR Array Mouse Cytokines & Chemokines which contains 84 different cytokines, chemokine, interleukin, and their receptor genes, and expression ratios of each gene are analyzed with Actb, B2m, Gapdh, Gusb, and Hsp90ab1 as housekeeping genes to normalize inflammation-related gene expressions.

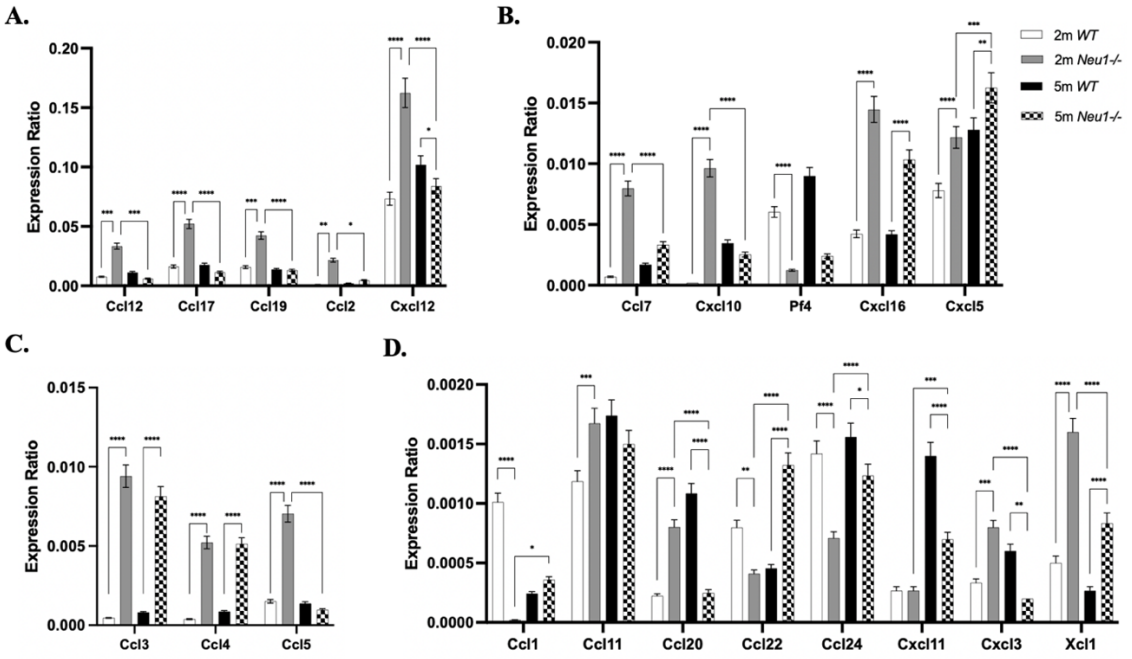

Figure 3.10. Gene expression ratio of chemokines in 2 and 5-month-old *WT* and *Neu1-/-* mouse cortex (A-D). Orderly, 2-month-old *WT* and *Neu1-/-,* and 5-month-old *WT* and *Neu1-/-* cortex tissues. Expression ratios were calculated with ΔCT method and 2-way-ANOVA analysis was used to determine p-values by using GraphPad. Data were reported as means SEM (n=2, *p<0,05, **p<0,01, ***p<0,001).

In Figure 3.10, gene expression of Cxcl16, Cxcl5, Ccl3, Ccl4, and Xcl1 chemokines were shown in elevated levels significantly in both 2 and 5-month-old *Neu1-/-* mice cortex in comparison to 2 and 5-month-old *WT* cortex tissues. Surprisingly, Ccl12, Ccl17, Ccl19, Ccl2, Cxcl12, Ccl7, Cxcl10, Ccl5, Ccl20, Cxcl3, and Xcl1 expression ratios were observed as increasing in 2-month-old *Neu1-/-* mice cortex that is compared to 2-

month-old *WT* cortex tissues; however, their expression was decreased in 5-month-old *Neu1-/-* mice cortex tissues in comparison to 2-month-old *Neu1-/-* groups. Additionally, Pf4, Ccl1, Ccl22, and Ccl24 chemokine gene expressions were decreased in 2-month-old *Neu1-/-* mice cortex in comparison to 2-month-old *WT* cortex; but Ccl1, Ccl22, and Ccl24 levels were increased in elderly *Neu1-/-* mice cortex (Figure 3.10D).

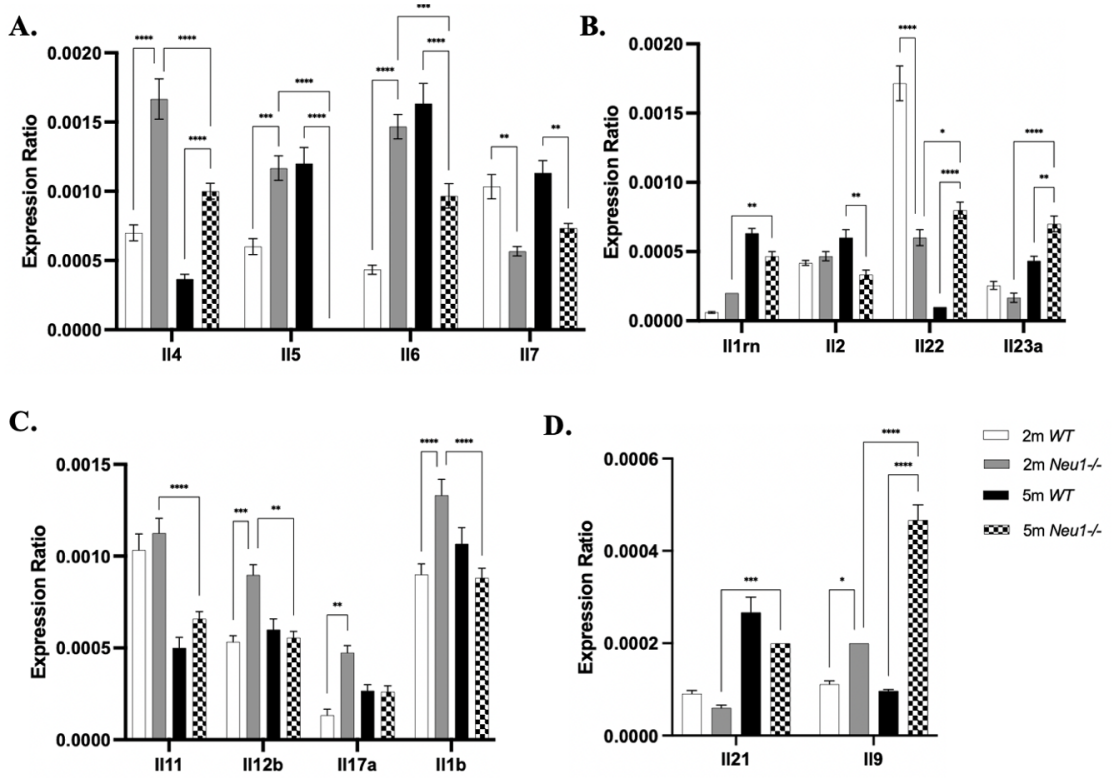

Figure 3.11. Gene expression ratio of interleukins in 2 and 5-month-old *WT* and *Neu1-/-* mouse cortex (A-D). Orderly, 2-month-old *WT* and *Neu1-/-,* and 5-month-old *WT* and *Neu1-/-* cortex tissues. Expression ratios were calculated with ΔCT method and 2-way-ANOVA analysis was used to determine p-values by using GraphPad. Data were reported as means SEM (n=2, *p<0,05, **p<0,01, ***p<0,001).

In Figure 3.11, Il4, and Il9 interleukin expression levels were remarkably increased in both 2- and 5-month-old *Neu1-/-* mice cortex in comparison to 2- and 5-month-old *WT* cortex tissues. Il5, Il6, Il12b, and Il1b interleukins were observed in elevated levels in 2 months-old *Neu1-/-* mice compared to *WT*, however; these interleukin expressions were remarkably reduced in 5-month-old *Neu1-/-* mice. In Figure 3.11A, Il7 interleukin expression was decreased in both 2 and 5-month-old *Neu1-/-* mice cortex in

comparison to *WT*. Il11 interleukin expression was decreased in 5-month-old *Neu1-/-* mice compared to 2-motnh-old *Neu1-/-*, and Il17a interleukin levels were elevated in 2-month-old *Neu1-/-* mice in comparison to *WT* (Figure 3.11C). Il1rn, Il22, Il23a and Il21 interleukin expressions were increased in 5-month-old *Neu1-/-* mice compared to younger age, and Il2 expression were significantly decreased in 5-month-old *Neu1-/-* mice in comparison to *WT* cortex (Figure 3.11B and Figure 3.11D). Il22 interleukin expression was apparently decreased in 2-month-old *Neu1-/-* mice cortex according to *WT* cortex, although its expression was increased in 5-month-old *Neu1-/-* compared to *WT* cortex (Figure 3.11B).

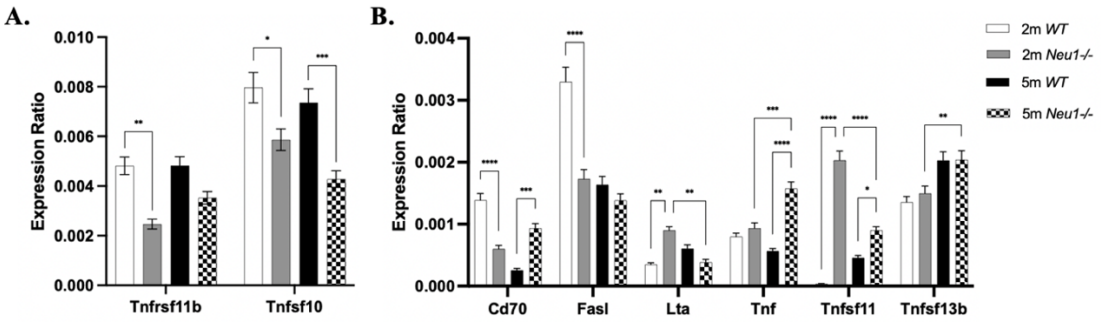

Figure 3.12. Gene expression ratio of TNF-receptor family members (A, B) in 2 and 5-month-old *WT* and *Neu1-/-* mouse cortex. Orderly, 2-month-old *WT* and *Neu1-/-,* and 5-month-old *WT* and *Neu1-/-* cortex tissues. Expression ratios were calculated with ΔCT method and 2-way-ANOVA analysis was used to determine p-values by using GraphPad. Data were reported as means SEM (n=2, *p<0,05, **p<0,01, ***p<0,001).

In Figure 3.12, gene expression of TNF-receptor family members which are Tnfrsf11b, Tnfsf10, Cd70, and FasI was monitored in reduced levels in 2-month-old *Neu1-/-* mice cortex in comparison to *WT*; additionally, Tnfsf10 expression levels were decreased in 5-month-old *Neu1-/-* mice cortex according to 5-month-old *WT*. Lta, and Tnfsf11 gene expression were increased in 2-month-old *Neu1-/-* mice cortex when compared to *WT* (Figure 3.12B). Gene expression levels of Cd70, Tnf, and Tnfsf11 were demonstrated as increased in 5-month-old *Neu1-/-* mice in comparison to 5-month-old *WT*, additionally; Tnf and Tnfsf13b levels were elevated in 5-month-old *Neu1-/-* mice

when compared to younger *Neu1-/-* mice cortex. Lta and Tnfsf11 members' expressions were reduced in 5-month-old *Neu1-/-* mice according to younger groups (Figure 3.12B).

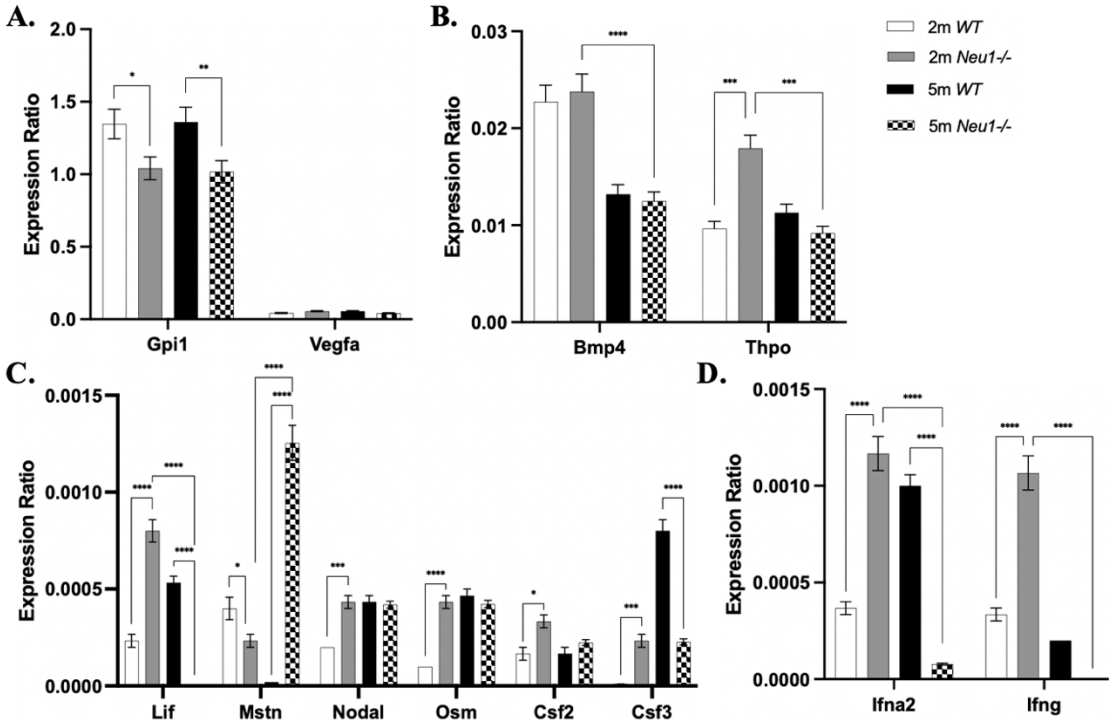

Figure 3.13. Gene expression ratio of growth factors (A-C) and interferons (D) in 2 and 5-month-old *WT* and *Neu1-/-* mouse cortex. Orderly, 2-month-old *WT* and *Neu1-/-,* and 5-month-old *WT* and *Neu1-/-* cortex tissues. Expression ratios were calculated with ΔCT method and 2-way-ANOVA analysis was used to determine p-values by using GraphPad. Data were reported as means SEM (n=2, *p<0,05, **p<0,01, ***p<0,001).

In Figure 3.13A, gene expression of Gpi1 growth factor was reduced in both 2 and 5-month-old *Neu1-/-* mice cortex in comparison to *WT* cortex tissues. In Figure 3.13B, Bmp4 and Thpo gene expressions were decreased in 5-month-old mice cortex when compared to younger Neu-/- cortex tissues, even though Thpo expression was increased in 2-month-old *Neu1-/-* cortex tissues according to 2-month-old *WT*. Expression of Lif, Ifna2, and Ifng was increased in 2 month-old *Neu1-/-* cortex in comparison to *WT*, however; in 5-month-old *Neu1-/-* cortex, their expression levels were decreased when compared to younger *Neu1-/-* mice cortex. Mstn growth factor expression was decreased in 2-month-old *Neu1-/-* mice cortex in comparison to *WT*, but

its expression was increased in 5-month-old *Neu1-/-* mice cortex when compared to 5-month-old *WT*, and younger *Neu1-/-* mice cortex (Figure 3.13C). Nodal, Osm, Csf2 and Csf3 growth factor expression levels were elevated in comparison to 2-month-old *WT* cortex, and additionally; Csf3 gene expression were reduced in 5-month-old *Neu1-/-* cortex according to *WT* cortex tissues (Figure 3.13C).

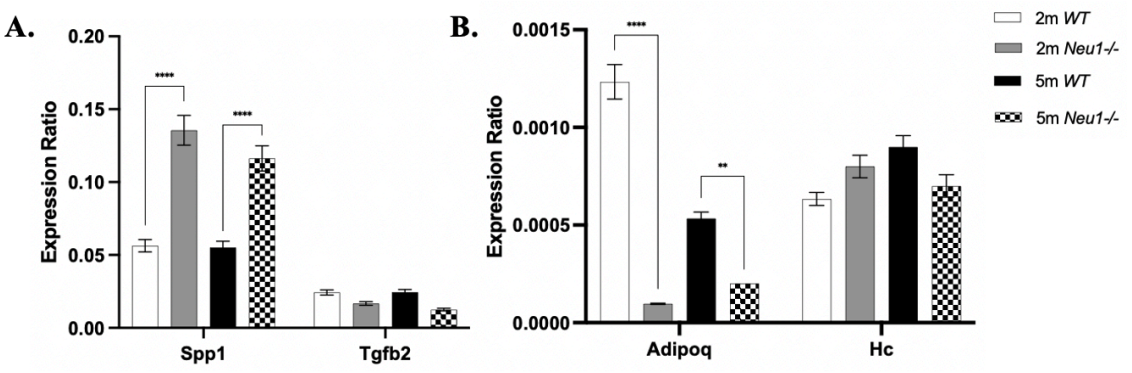

Figure 3.14. Gene expression ratio of other cytokines (A, B) in 2 and 5-month-old *WT* and *Neu1-/-* mouse cortex. Orderly, 2-month-old *WT* and *Neu1-/-,* and 5-month-old *WT* and *Neu1-/-* cortex tissues. Expression ratios were calculated with ΔCT method and 2-way-ANOVA analysis was used to determine p-values by using GraphPad. Data were reported as means SEM (n=2, *p<0,05, **p<0,01, ***p<0,001).

In Figure 3.14A, gene expression level of cytokine Spp1 in mice cortex was remarkably increased in both 2 and 5-month-old *Neu1-/-* mice in comparison to *WT*; but differently, Adipoq cytokine expression was significantly reduced in both 2 and 5-month-old *Neu1-/-* mice when compared to *WT* (Figure 3.14B). There is no significant alteration was observed in both Tgfb2, and Hc cytokine expression levels.

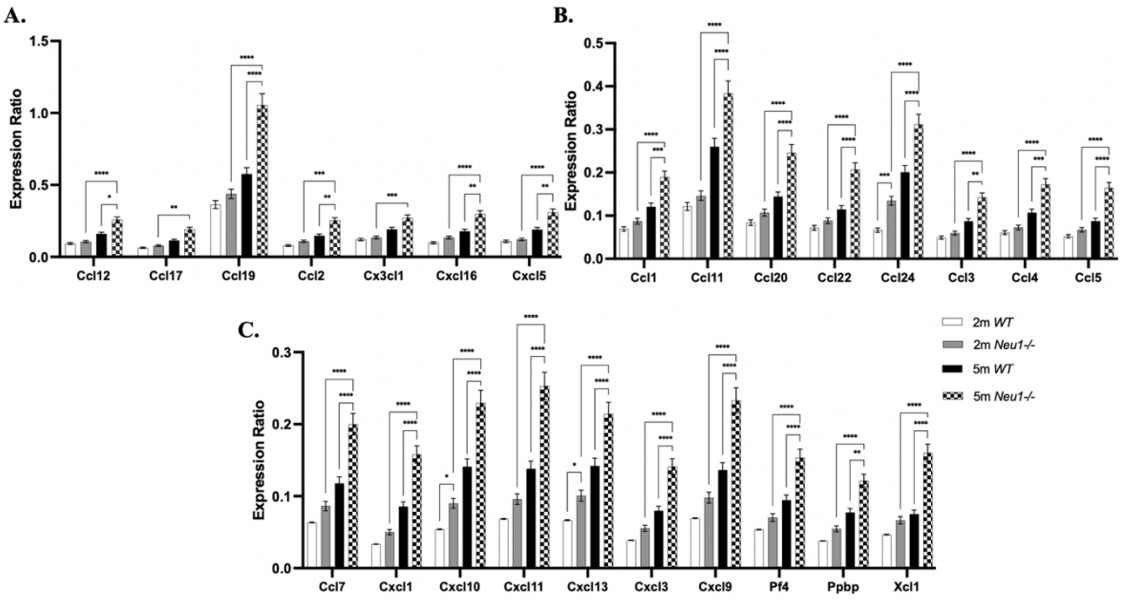

Figure 3.15. Gene expression ratio of chemokines (A, B) in 2 and 5-month-old *WT* and *Neu1-/-* mouse cerebellum. Orderly, 2-month-old *WT* and *Neu1-/-,* and 5-month-old *WT* and *Neu1-/-* cerebellum tissues. Expression ratios were calculated with ΔCT method and 2-way-ANOVA analysis was used to determine p-values by using GraphPad. Data were reported as means SEM (n=2, *p<0,05, **p<0,01, ***p<0,001).

In Figure 3.15A, Ccl12, Ccl19, Ccl2, Cxcl16, and Cxcl5 chemokine expression ratios were apparently increased in 5-month-old cerebellum tissues in comparison to both younger *Neu1-/-* mice and 5-month-old *WT* cerebellum tissues; and, Ccl17 and Cx3cl1 chemokine levels were increased in 5-month-old *Neu1-/-* mice cerebellum when compared to 2-month-old *Neu1-/-* cerebellum. In Figure 3.15B, Ccl1, Ccl11, Ccl20, Ccl22, Ccl24, Ccl3, Ccl4, and Ccl5 chemokine expression levels were significantly elevated in 5-month-old *Neu1-/-* mice cerebellum according to 5-month-old *WT*, and 2-month-old *Neu1-/-* cerebellum. In Figure 3.15C, Ccl7, Cxcl1, Cxcl10, Cxcl11, Cxcl13, Cxcl3, Cxcl9, Pf4, Ppbp, and Xcl1 chemokine expression ratios were increased in 5-month-old *Neu1-/-* mice cerebellum when compared to both younger *Neu1-/-*, and 5-month-old *WT* cerebellum.

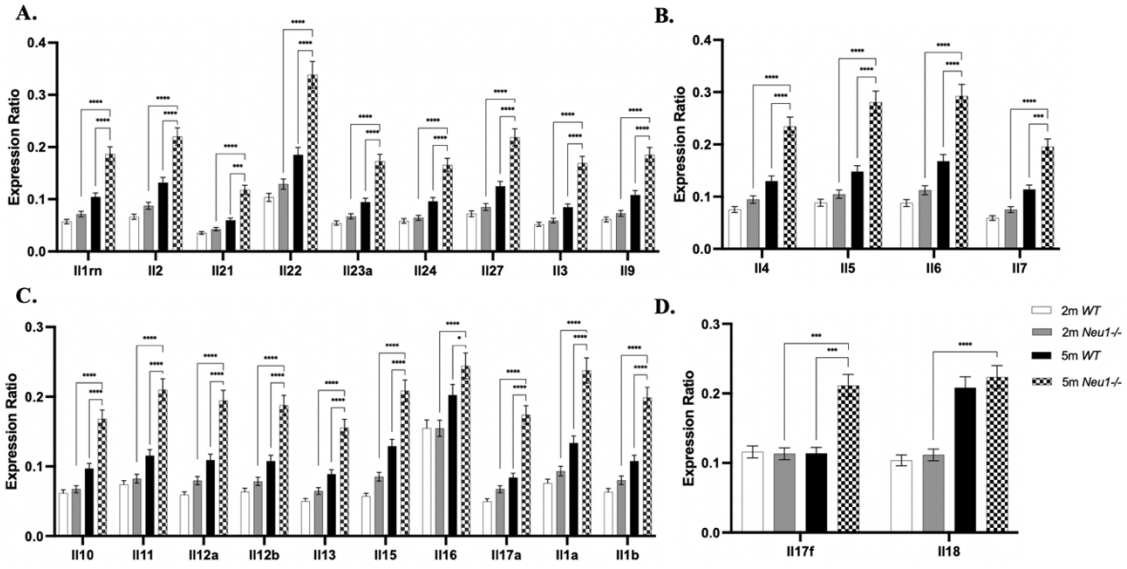

Figure 3.16. Gene expression ratio of interleukins (A, B) in 2 and 5-month-old *WT* and *Neu1-/-* mouse cerebellum. Orderly, 2-month-old *WT* and *Neu1-/-,* and 5-month-old *WT* and *Neu1-/-* cerebellum tissues. Expression ratios were calculated with ΔCT method and 2-way-ANOVA analysis was used to determine p-values by using GraphPad. Data were reported as means SEM (n=2, *p<0,05, **p<0,01, ***p<0,001).

In Figure 3.16A, interleukins Il1rn, Il2, Il21, Il22, Il23a, Il24, Il27, Il3 and Il9 gene expressions were apparently increased in 5-month-old *Neu1-/-* mice cerebellum in comparison to *WT*, and younger *Neu1-/-* mice. In Figure 3.16B, expression levels of Il4, Il5, Il6, and Il7 interleukins were significantly elevated in 5-month-old *Neu1-/-* mice cerebellum when compared to both younger group of *Neu1-/-* and 5-month-old mice cerebellum. In 3.16C, Il10, Il11, Il12a, Il12b, Il13, Il15, Il16, Il17a, Il1a, and Il1b interleukins' gene expression were remarkably increased 5-month-old *Neu1-/-* mice cerebellum in comparison to both younger group of *Neu1-/-* and 5-month-old mice cerebellum. In Figure 3.16D, Il17f and Il16 interleukin expressions were increased in 5-month-old *Neu1-/-* mice cerebellum when compared to younger *Neu1-/-* mice.

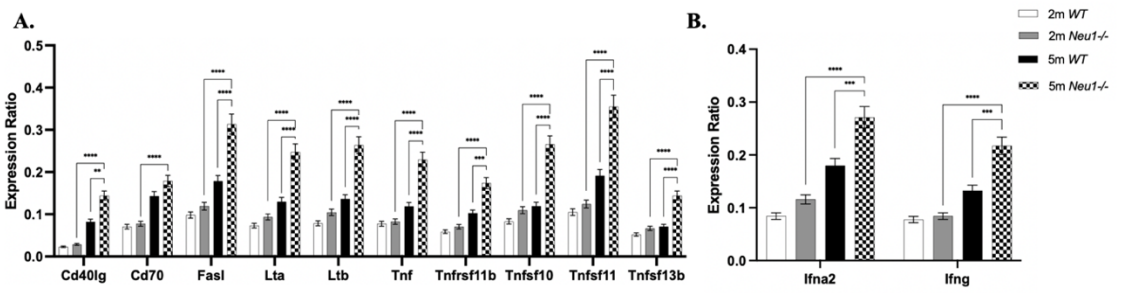

Figure 3.17. Gene expression ratio of TNF-receptor family members (A), and interferons (B) in 2 and 5-month-old *WT* and *Neu1-/-* mouse cerebellum. Orderly, 2-month-old *WT* and *Neu1-/-,* and 5-month-old *WT* and *Neu1-/-* cerebellum tissues. Expression ratios were calculated with ΔCT method and 2-way-ANOVA analysis was used to determine p-values by using GraphPad. Data were reported as means SEM (n=2, *p<0,05, **p<0,01, ***p<0,001).

In Figure 3.17A, TNF-receptor family members including Cd40lg, FasI, Lta, Ltb, Tnf, Tnfrsf11b, Tnfsf10, Tnfsf11, and Tnfsf13b were apparently increased in 5-month-old *Neu1-/-* mice cerebellum in comparison to *WT*, and younger *Neu1-/-* mice cerebellum; and also, Cd70 expression levels were elevated in 5-month-old *Neu1-/-* mice cerebellum when compared to 2-month-old *Neu1-/-* mice cerebellum. In Figure 3.17B, Ifna2 and Ifng TNF-receptor family members gene expression was significantly increased in 5-month-old *Neu1-/-* mice cerebellum in comparison to both younger *Neu1-/-* and *WT* cerebellum tissues.

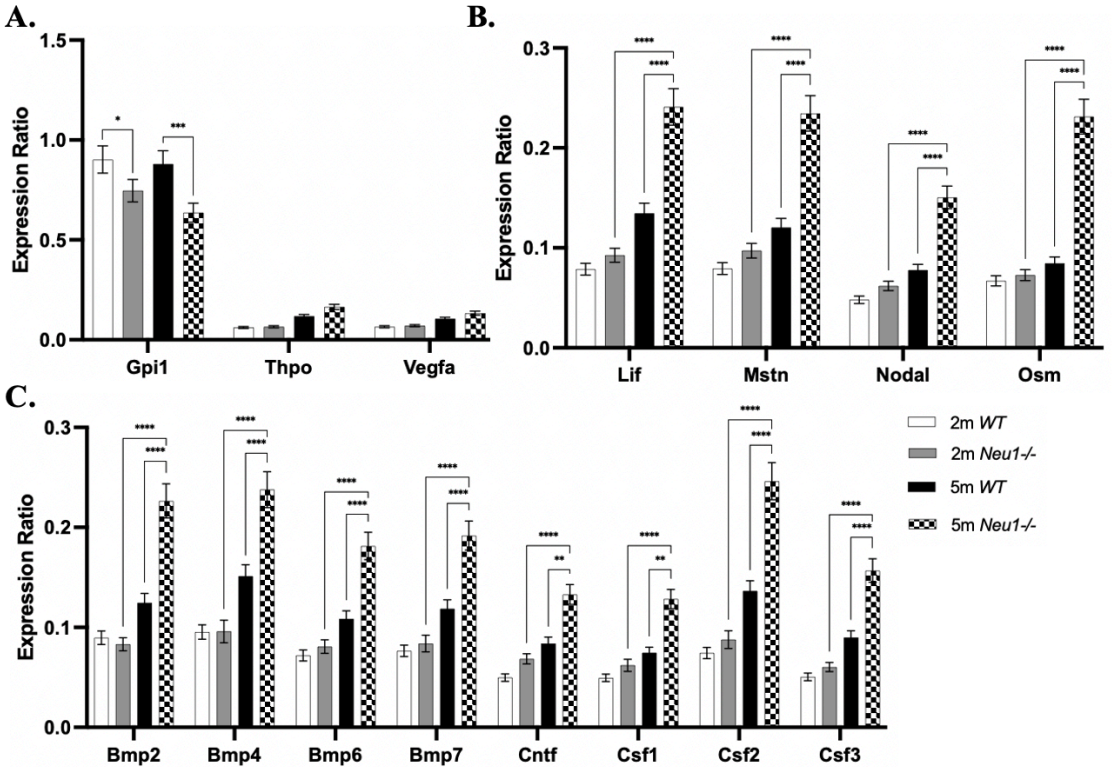

Figure 3.18. Gene expression ratio of growth factors (A-C) in 2 and 5-month-old *WT* and *Neu1-/-* mouse cerebellum. Orderly, 2-month-old *WT* and *Neu1-/-* , and 5-month-old *WT* and *Neu1-/-* cerebellum tissues. Expression ratios were calculated with ΔCT method and 2-way-ANOVA analysis was used to determine p-values by using GraphPad. Data were reported as means SEM (n=2, *p<0,05, **p<0,01, ***p<0,001).

In Figure 3.18A, Gpi growth factor expression ratio was apparently decreased in both 2 and 5-month-old *Neu1-/-* mice cerebellum tissues in comparison to 2 and 5-month-old *WT* cerebellum; but there was no significant change in Thpo, and Vegfa growth factors in both 2 and 5-month-old *Neu1-/-* mice cerebellum tissues. In Figure 3.18B, Lif, Mstn, Nodal, and Osm growth factors' expression ratio was increased significantly in 5-month-old *Neu1-/-* mice cerebellum in comparison to both *WT*, and younger *Neu1-/-* mice cerebellum. In Figure 3.18C, expression of growth factors including Bmp2, Bmp4, Bmp6, Bmp7, Cntf, Csf1, Csf2, and Csf3 was monitored in remarkable increase according to *WT*, and younger *Neu1-/-* mice cerebellum.

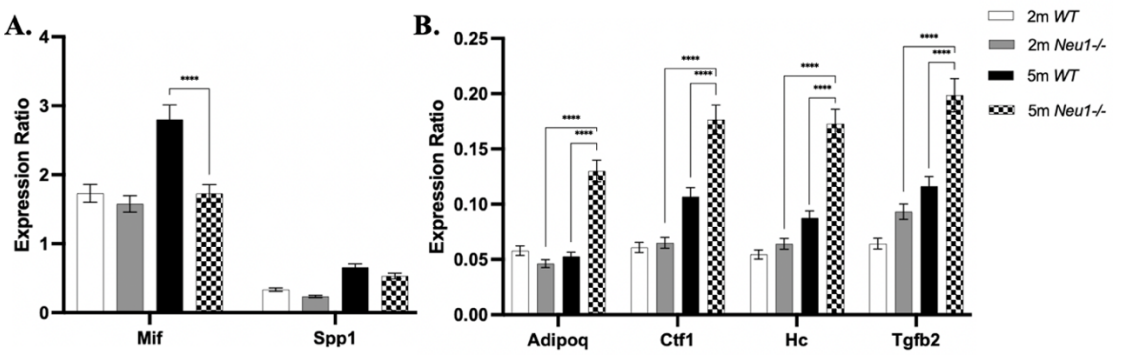

Figure 3.19. Gene expression ratio of other cytokines (A, B) in 2 and 5-month-old *WT* and *Neu1-/-* mouse cerebellum. Orderly, 2-month-old *WT* and *Neu1-/-,* and 5-month-old *WT* and *Neu1-/-* cerebellum tissues. Expression ratios were calculated with ΔCT method and 2-way-ANOVA analysis was used to determine p-values by using GraphPad. Data were reported as means SEM (n=2, *p<0,05, **p<0,01, ***p<0,001).

In Figure 3.19A, Mif cytokine expression was decreased in 5-month-old *Neu1-/-* cerebellum in comparison to 5-month-old *WT* cerebellum tissue, but there was no apparent change in Spp1 cytokine levels. In Figure 3.19B, gene expression of other cytokines that is including Adipoq, Ctf1, Hc and Tgfb2 were significantly elevated in 5-month-old *Neu1-/-* cerebellum when they were compared to 5-month-old *WT*, and 2-month-old *Neu1-/-* mice cerebellum.

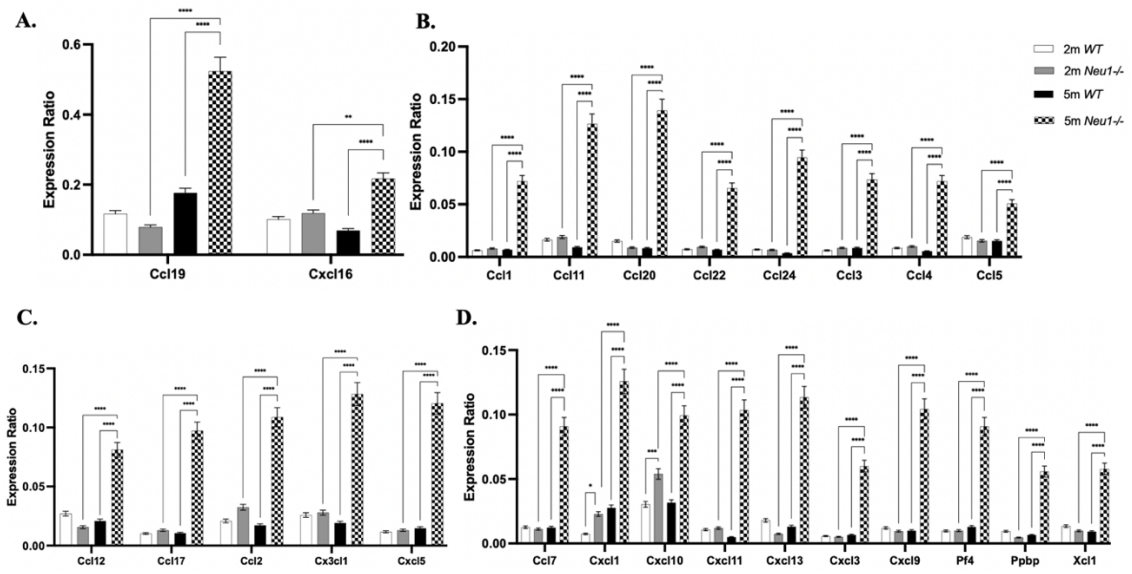

Figure 3.20. Gene expression ratio of chemokines (A-D) in 2 and 5-month-old *WT* and *Neu1-/-* mouse kidney. Orderly, 2-month-old *WT* and *Neu1-/-,* and 5-month-old *WT* and *Neu1-/-* kidney tissues. Expression ratios were calculated with ΔCT method and 2-way-ANOVA analysis was used to determine p-values by using GraphPad. Data were reported as means SEM (n=2, *p<0,05, **p<0,01, ***p<0,001).

In Figure 3.20A, gene expression of Ccl19, and Cxcl16 chemokines were apparently elevated in 5-month-old *Neu1-/-* mice kidney in comparison to both *WT*, and 2-month-old *Neu1-/-* mice kidney. Expression levels of other chemokines such as Ccl1, Ccl11, Ccl20, Ccl22, Ccl24, Ccl3, Ccl4, and Ccl5 were observed in 5-month-old *Neu1-/-* mice kidney when compared to *WT*, and younger *Neu1-/-* mice kidney (Figure 3.20B). In Figure 3.20C, Ccl12, Ccl17, Ccl2, Cx3cl1, and Cxcl5 chemokine levels were remarkably increased in 5-month-old *Neu1-/-* kidney according to younger *Neu1-/-* and 5-month-old *WT* kidney tissues. Ccl7, Cxcl1, Cxcl10, Cxcl11, Cxcl13, Cxcl3, Cxcl9, Pf4, Ppbp and Xcl1 chemokines were highly expressed in 5-month-old *Neu1-/-* mice kidney in comparison to *WT*, and younger Neu1-/- kidney; and additionally, Cxcl1 and Cxcl10 gene expressions were elevated in 2-month-old *Neu1-/-* kidney according to 2-month-old *WT* (Figure 3.20D).

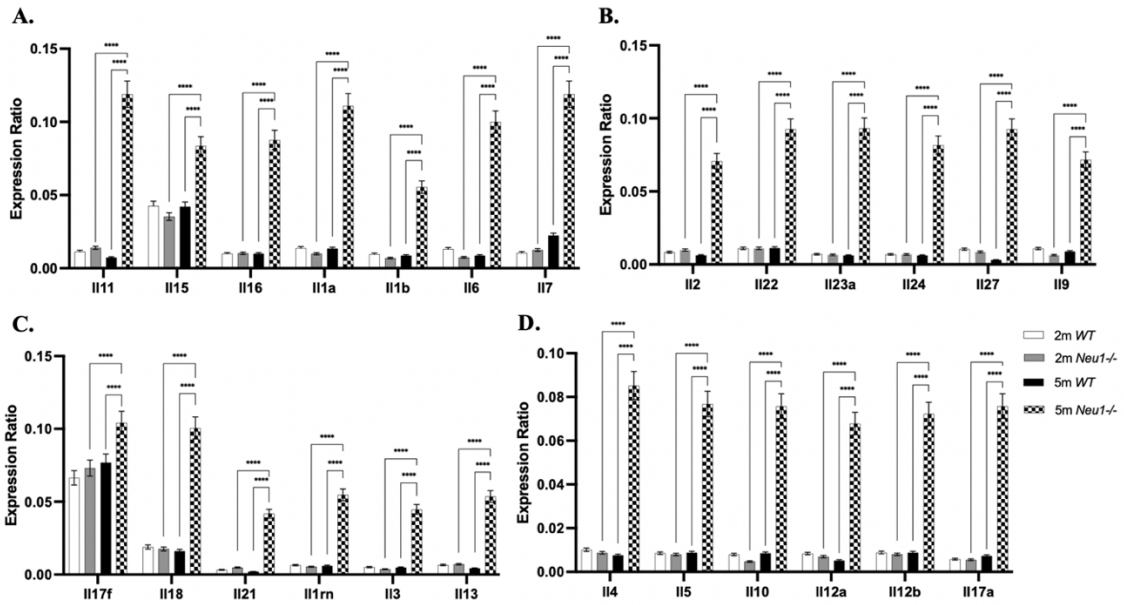

Figure 3.21. Gene expression ratio of interleukins (A-D) in 2 and 5-month-old *WT* and *Neu1-/-* mouse kidney. Orderly, 2-month-old *WT* and *Neu1-/-,* and 5-month-old *WT* and *Neu1-/-* kidney tissues. Expression ratios were calculated with ΔCT method and 2-way-ANOVA analysis was used to determine p-values by using GraphPad. Data were reported as means SEM (n=2, *p<0,05, **p<0,01, ***p<0,001).

In Figure 3.21A, gene expressions of Il11, Il15, Il16, Il1a, Il1b, Il6, and Il7 interleukins were significantly increased in 5-month-old *Neu1-/-* kidney compared to *WT*, and 2-month-old *Neu1-/-* kidney. In Figure 3.21B, interleukins including Il2, Il22, Il23a, Il24, Il27, and Il9 were remarkably increased in 5-month-old *Neu1-/-* kidney compared to *WT*, and 2-month-old *Neu1-/-* kidney. In Figure 3.21C, Il17f, Il18, Il21, Il1rn, Il3, and Il13 interleukins were highly expressed in 5-month-old *Neu1-/-* kidney in comparison to *WT*, and 2-month-old *Neu1-/-* kidney. In Figure 3.21D, Il4, Il5, Il10, Il12a, Il12b, and Il17a interleukin expressions were shown in elevated levels in 5-month-old *Neu1-/-* kidney compared to *WT*, and 2-month-old *Neu1-/-* kidney.

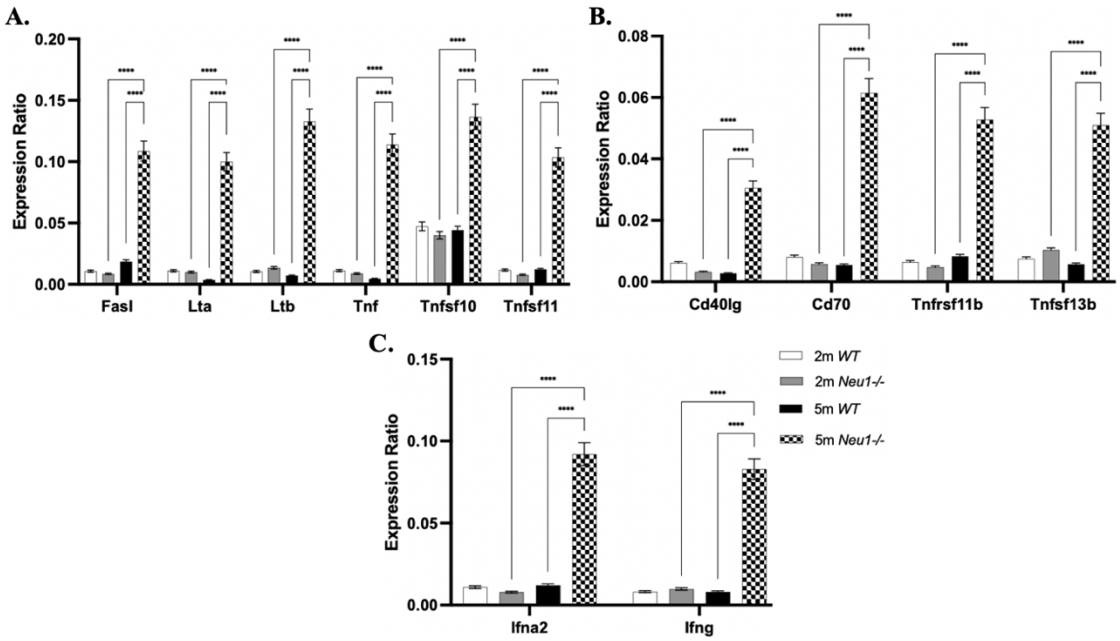

Figure 3.22. Gene expression ratio of TNF-receptor family members (A, B), and interferons in 2 and 5-month-old *WT* and *Neu1-/-* mouse kidney. Orderly, 2-month-old *WT* and *Neu1-/-,* and 5-month-old *WT* and *Neu1-/-* kidney tissues. Expression ratios were calculated with ΔCT method and 2-way-ANOVA analysis was used to determine p-values by using GraphPad. Data were reported as means SEM (n=2, *p<0,05, **p<0,01, ***p<0,001).

In Figure 3.22A, TNF-receptor family members including FasI, Lta, Ltb, Tnf, Tnfsf10, and Tnfsf11 gene expressions were increased in 5-month-old *Neu1-/-* mice kidney in comparison to *WT*, and younger *Neu1-/-* mice kidney. In Figure 3.22B, Cd40lg, Cd70, Tnfrsf11b, and Tnfsf13b levels were significantly higher in 5-month-old *Neu1-/-* mice kidney compared to *WT*, and 2-month-old *Neu1-/-* mice kidney. In Figure 3.22C, Ifna, and Ifng members' expression were remarkably elevated in 5-month-old *Neu1-/-* mice kidney when compared to younger *Neu1-/-* and 5-month-old *WT* kidney tissues.

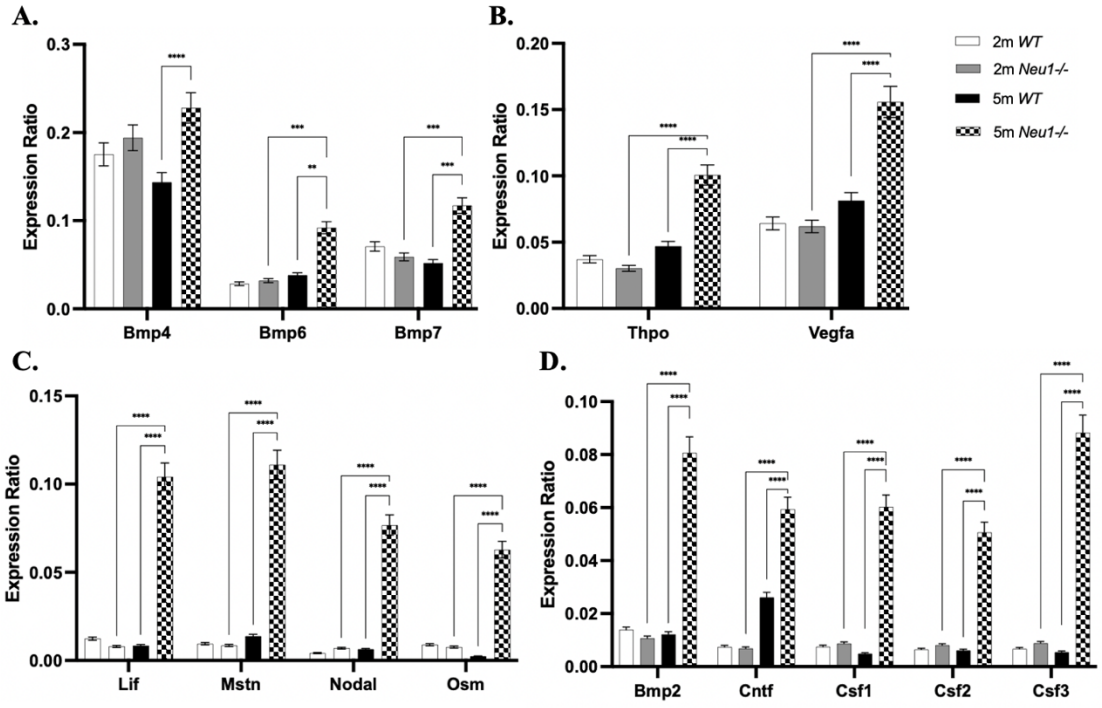

Figure 3.23. Gene expression ratio of growth factors (A-D) in 2 and 5-month-old *WT* and *Neu1-/-* mouse kidney. Orderly, 2-month-old *WT* and *Neu1-/-,* and 5-month-old *WT* and *Neu1-/-* kidney tissues. Expression ratios were calculated with ΔCT method and 2-way-ANOVA analysis was used to determine p-values by using GraphPad. Data were reported as means SEM (n=2, *p<0,05, **p<0,01, ***p<0,001).

In Figure 3.23A, Bmp4 growth factor was highly expressed in 5-month-old *Neu1-/-* mice kidney when compared to 5-month-old *WT*, while the Bmp6 and Bmp7 were increased in 5-month-old *Neu1-/-* mice when compared to *WT*, and younger *Neu1-/-* kidney tissues. In Figure 3.23B, Thpo and Vegfa growth factors expression were elevated in 5-month-old *Neu1-/-* mice in comparison to *WT*, and younger *Neu1-/-* mice kidney. In Figure 3.23C, Lif, Mstn, Nodal, and Osm growth factors were monitored in increasing levels in 5-month-old Neu1-/ mice according to *WT*, and younger *Neu1-/-* mice kidney. In Figure 3.23D, Bmp2, Cntf, Csf1, Csf2, and Csf3 growth factors were expressed in elevated levels in 5-month-old *Neu1-/-* mice kidney in comparison to *WT*, and younger *Neu1-/-* mice kidney.

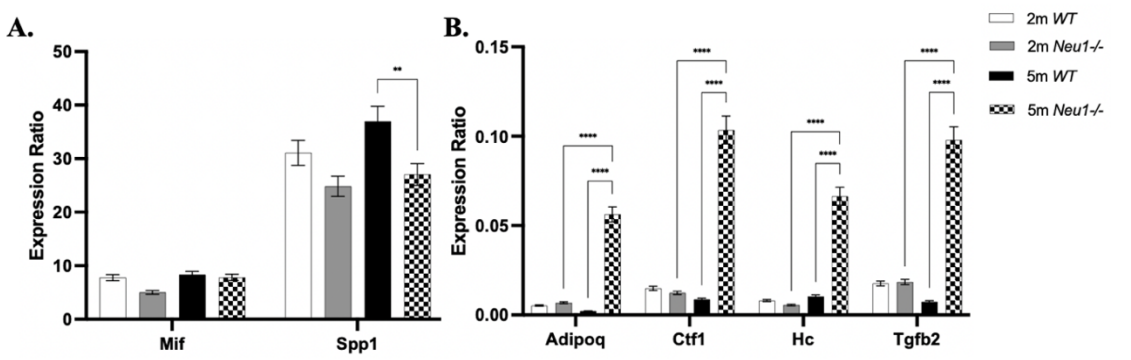

Figure 3.24. Gene expression ratio of other cytokines (A-D) in 2 and 5-month-old *WT* and *Neu1-/-* mouse kidney. Orderly, 2-month-old *WT* and *Neu1-/-,* and 5-month-old *WT* and *Neu1-/-* kidney tissues. Expression ratios were calculated with ΔCT method and 2-way-ANOVA analysis was used to determine p-values by using GraphPad. Data were reported as means SEM (n=2, *p<0,05, **p<0,01, ***p<0,001).

In Figure 3.24A, Spp1 cytokine was expressed in reduced levels in 5-month-old *Neu1-/-* mice kidney compared to 5-month-old *WT* kidney, even though there was no alteration in Mif cytokine expression levels of both 2 and 5-month-old *Neu1-/-* kidney tissues. In Figure 3.24B, Adipoq, Ctf1, Hc and Tgfb2 cytokines were expressed in remarkably increasing levels in 5-month-old *Neu1-/-* kidney tissues compared to *WT*, and younger *Neu1-/-* kidney tissues.

3.5. Western Blotting

Western Blot analyses were performed with primary antibodies: anti-IkB-α (9242, Cell Signalling), anti-NF-kB (ab32536, Abcam), and anti-B-actin (13E5, Cell Signalling) for detection of inflammatory response in cortex, cerebellum, kidney and spleen tissues of 2- and 5-month-old *Neu1-/-* mice in comparison to *WT*.

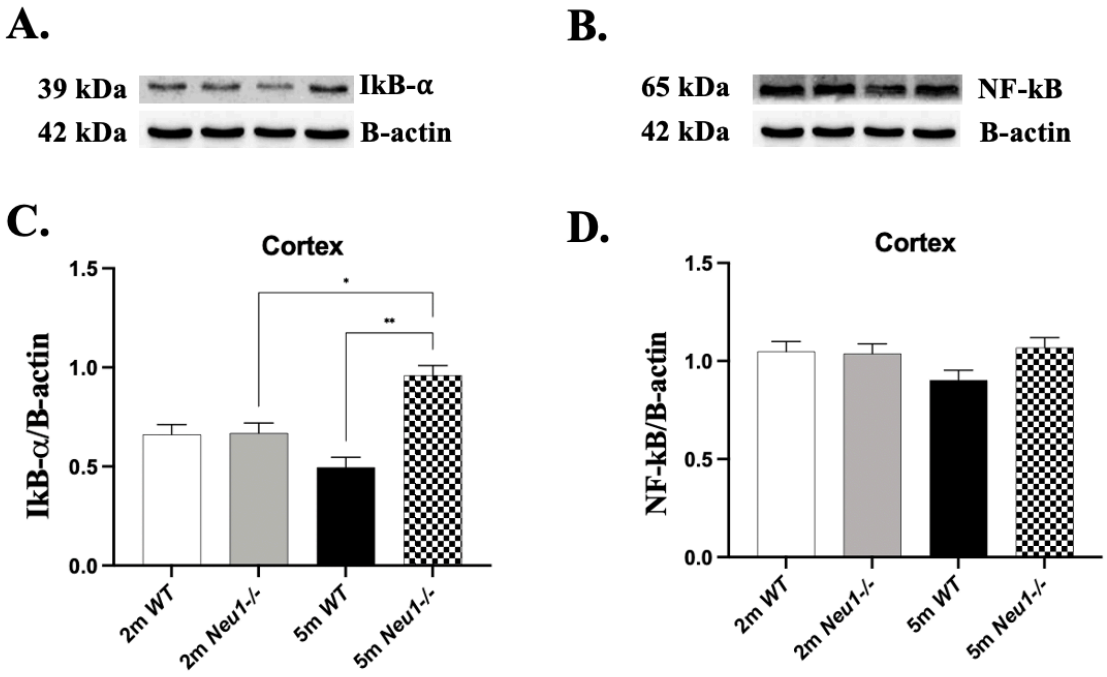

Figure 3.25. Western blot analysis of IkB-α (A) and NF-kB (B) in cortex tissue of 2 and 5-month-old *WT* and *Neu1-/-* mice. Intensity analysis of IkB-α and NF-kB for 2- and 5-month-old *WT*, and *Neu1-/-* mice (C and D). B-actin was used as control. Each band intensity was measured with ImageJ and normalized to β-actin intensity. One-way-Anova analysis was performed to determine p-values via GraphPad. Data were reported as means SE (n=3, *p<0,05).

In Figure 3.25C, significant increase was obtained in IkB-α expression levels in 5-month-old *Neu1-/-* mice cortex region compared to *WT*, and 2-month-old *Neu1-/-* groups. In Figure 3.25D, NF-kB expression levels were not significantly changed in both 2- and 5-month-old *Neu1-/-* mice cortex in comparison to *WT*.

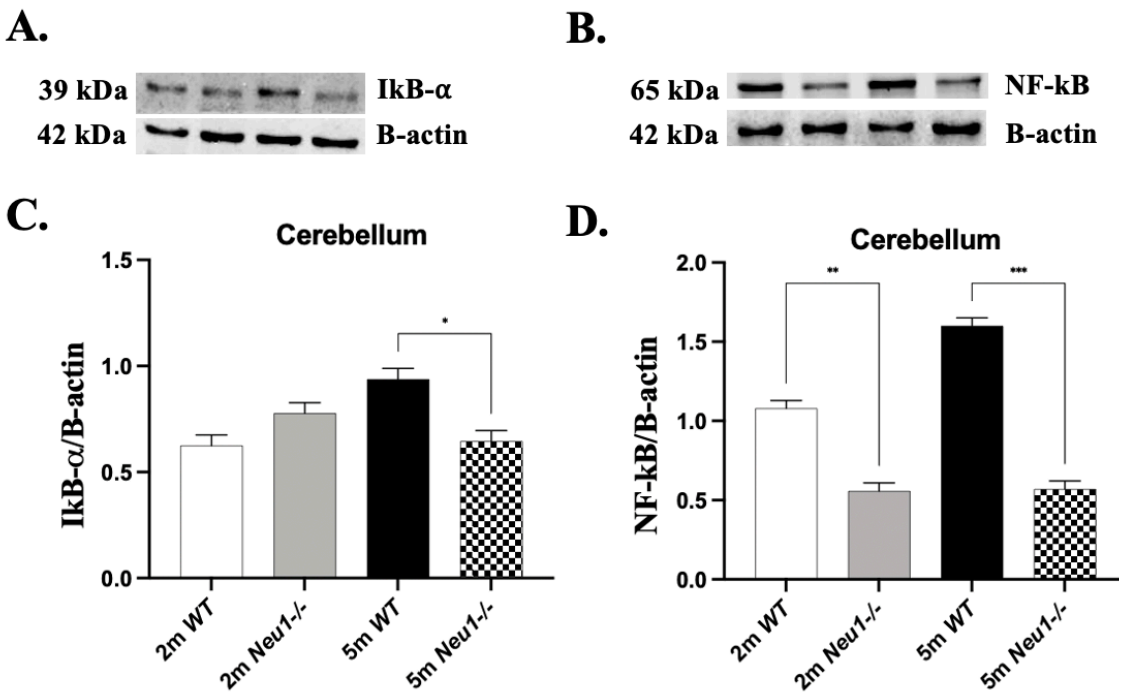

Figure 3.26. Western blot analysis of IkB-α (A) and NF-kB (B) in cerebellum tissue of 2 and 5-month-old *WT* and *Neu1-/-* mice. Intensity analysis of IkB-α and NF-kB for 2- and 5-month-old *WT*, and *Neu1-/-* mice (C and D). B-actin was used as control. Each band intensity was measured with ImageJ and normalized to β-actin intensity. One-way-Anova analysis was performed to determine p-values via GraphPad. Data were reported as means SE (n=3, *p<0,05).

In Figure 3.26C, remarkable reduction was monitored in IkB-α expression levels in only 5-month-old *Neu1-/-* mice cerebellar region compared to *WT*. In Figure 3.26D, NF-kB expression levels were significantly decreased in both 2- and 5-month-old *Neu1-/-* mice cerebellum in comparison to *WT*.

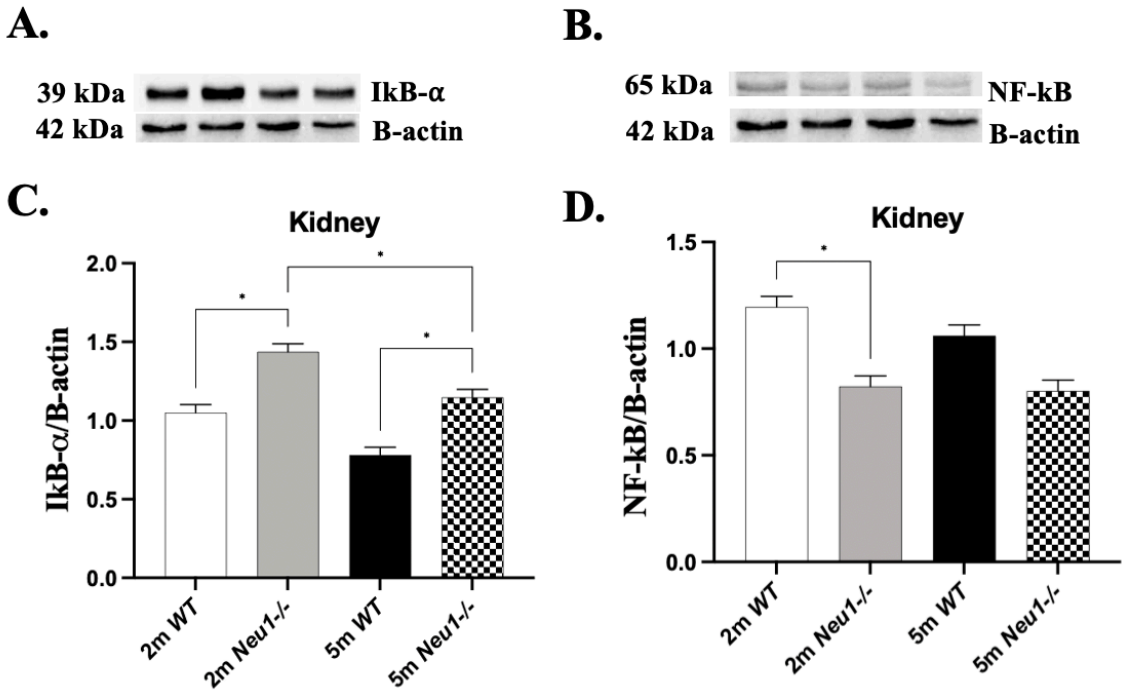

Figure 3.27. Western blot analysis of IkB-α (A) and NF-kB (B) in kidney tissue of 2 and 5-month-old *WT* and *Neu1-/-* mice. Intensity analysis of IkB-α and NF-kB for 2- and 5-month-old *WT*, and *Neu1-/-* mice (C and D). B-actin was used as control. Each band intensity was measured with ImageJ and normalized to β-actin intensity. One-way-Anova analysis was performed to determine p-values via GraphPad. Data were reported as means SE (n=3, *p<0,05).

In Figure 3.27C, apparent increase was monitored in IkB-α expression levels in both 2- and 5-month-old *Neu1-/-* mice kidney compared to *WT,* and IkB-α expression was decreased in 5-month-old Neu1-/- mice kidney in comparison to 2-month-old *Neu1-/-*. In Figure 3.27D, NF-kB expression levels were significantly decreased in only 2-month-old *Neu1-/-* mice kidney in comparison to *WT*.

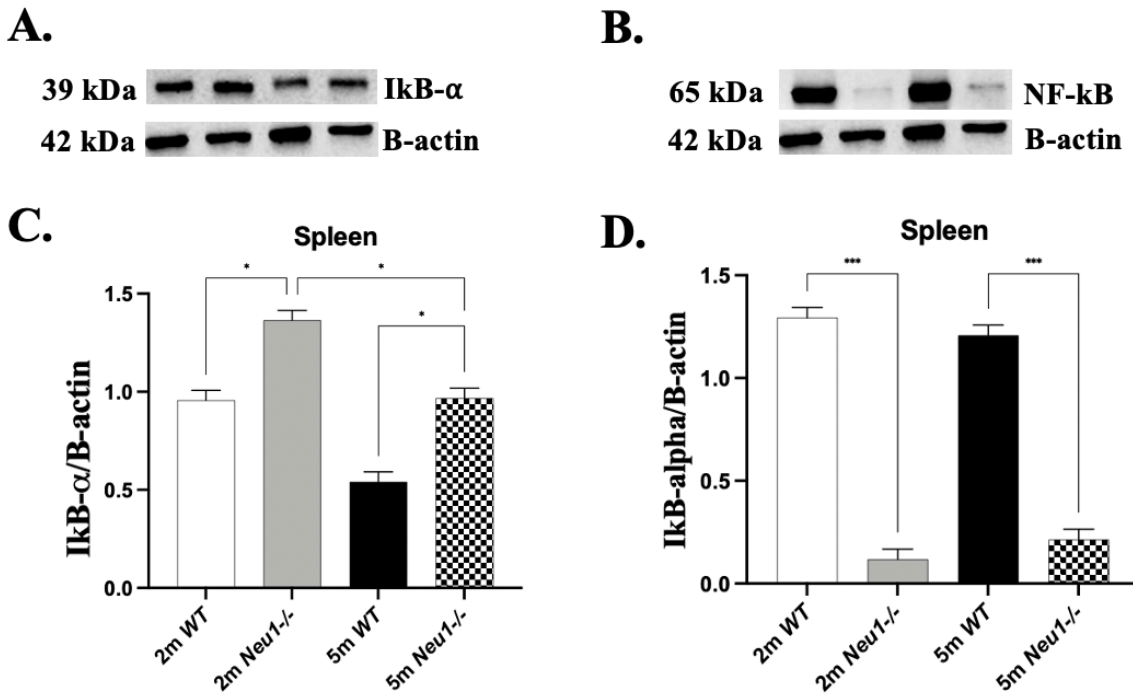

Figure 3.28. Western blot analysis of IkB-α (A) and NF-kB (B) in spleen tissue of 2 and 5-month-old *WT* and *Neu1-/-* mice. Intensity analysis of IkB-α and NF-kB for 2- and 5-month-old *WT*, and *Neu1-/-* mice (C and D). B-actin was used as control. Each band intensity was measured with ImageJ and normalized to β-actin intensity. One-way-Anova analysis was performed to determine p-values via GraphPad. Data were reported as means SE (n=3, *p<0,05).

In Figure 3.28C, significant increase was monitored in IkB-α expression levels in both 2- and 5-month-old *Neu1-/-* mice spleen compared to *WT,* and IkB-α expression was decreased in 5-month-old Neu1-/- mice spleen in comparison to 2-month-old *Neu1-/-*. In Figure 3.28D, NF-kB expression levels were significantly decreased in both 2- and 5-month-old *Neu1-/-* mice spleen in comparison to *WT*.

3.6. Histopathological Analysis

Histopathological staining was carried out in cortex, hippocampus, thalamus and cerebellum regions of brain, kidney and spleen tissues of 2 and 5-month-old *WT* and *Neu1-/-* mice for examination of morphological changes, and tissue degeneration by Hematoxylin-Eosin staining. Periodic Acid-Schiff staining was performed specifically to identify glycoconjugate accumulation. Toluidine-Blue staining was done to investigate mast cells, and axonal degeneration.

3.6.1. Hematoxylin-Eosin (H & E) Staining

Tissue degenerations, and abnormalities in tissue morphology was detected and analyzed with Hematoxylin-Eosin staining between the 2 and 5-month-old *WT* and *Neu1-/-* mice cortex, hippocampus, thalamus, cerebellum, spleen and kidney tissue sections.

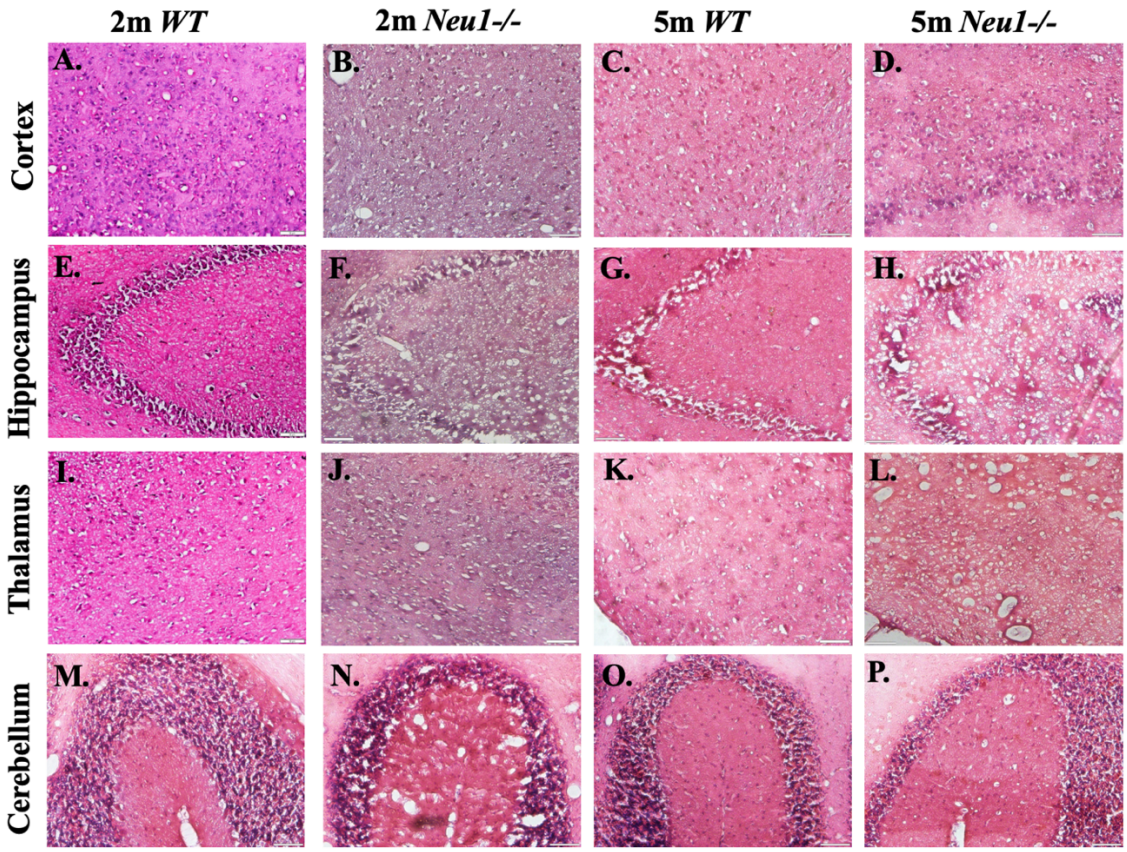

Figure 3.29. Hematoxylin- Eosin staining in 2- and 5-month-old *WT*, *Neu1-/-* mice brain coronal sections, cortex (A, B, C, D), hippocampus (E, F, G, H), thalamus (I, J, K, L) and cerebellum (M, N, O, P). Images were taken at 20X magnification by Olympus light microscope.

In Figure 3.29A, and Figure 3.29C, histological findings of 6 layers of cortex in 2- and 5-month-old *WT* mice was evaluated as normal, however; there were edema, and disorganization in younger and older *Neu1-/-* mice model, and additionally vessels with dilation were observed in 2 and 5-month-old *Neu1-/-* mice (Figure 3.29B, and Figure 3.29D). In hippocampal region of 2- and 5-month-old *WT* mice, any pathological conditions were not detected, and also CA1, CA2, CA3, and CA4 regions of hippocampus were developed normally in both age groups of *WT* (Figure 3.29E, and Figure 3.29G). In the 2- and 5-month-old *Neu1-/-* mice hippocampal region, vacuolization, edema, and vessels with dilation was identified, and cellular loss with degeneration was observed (Figure 3.29F, and Figure 3.29H). In the 2- and 5-month-old *WT* mice brain, appearance of thalamus histology was normal (Figure 3.29I, and Figure 3.29K), but there was dilation in vessels, edema, vacuolization, plaque-like structure and loss in thalamic cells in both

younger and elder group of *Neu1-/-* mice model (Figure 3.29J, and Figure 3.29L). In the cerebellar region of both 2- and 5-month-old *WT* mice, organization and histological conditions was detected as normal (Figure 3.29M, and Figure 3.29O). In the 2- and 5-month-old *Neu1-/-* mice cerebellum, vessels with dilation, edema, disorganization and deletions in Purkinje cell layer was detected (Figure 3.29N, and Figure 3.29P).

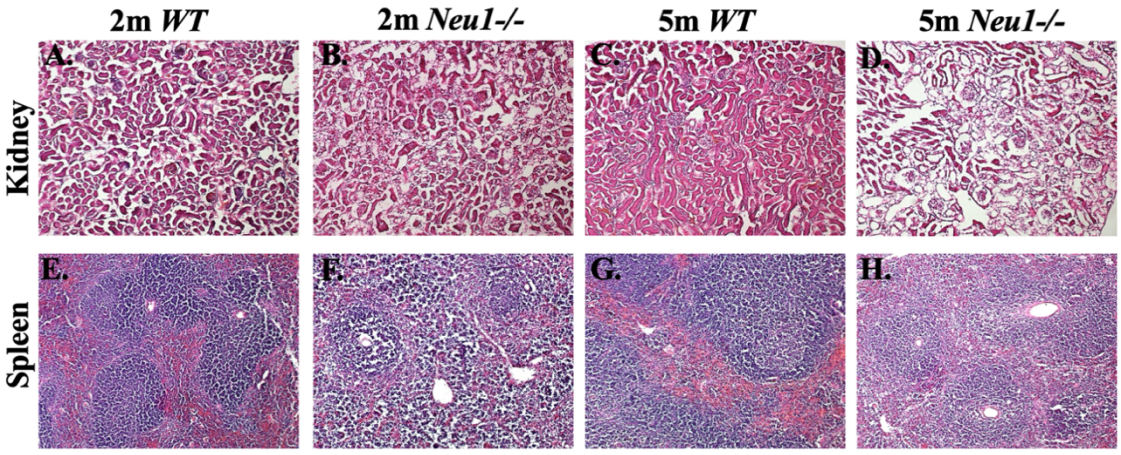

Figure 3.30. Hematoxylin – Eosin staining in 2- and 5-month-old *WT*, *Neu1-/-* mice kidney and spleen coronal sections, kidney (A, B, C, D), and spleen (E, F, G, H). Images were taken at 20X magnification by Olympus light microscope.

In Figure 3.30A, and Figure 3.30C, histology of 2- and 5-month-old *WT* mice was observed as normal in glomerular cells, and tubular cells, and any degeneration and vacuolated structure was not detected; however, there was vacuolized glomerular cells, and degenerated Bowman capsule in both 2- and 5-month-old *Neu1-/-* mice kidney, and additionally there was vacuolization and degeneration in tubular cells of kidney in younger, and elder group of *Neu1-/-* mice (Figure 3.30B, and Figure 3.30D). It was remarkably shown that degeneration and vacuolization of epithelial cells of kidney is increased in elder group of *Neu1-/-* mice. In Figure 3.30E, and Figure 3.30G, the red pulp and white pulp regions of 2- and 5-month-old *WT* mice spleen was defined without degeneration and vacuolization; however, there was vacuolization in the cells of both red and white pulp of spleen in younger and older group of *Neu1-/-* mice (Figure 3.30F, and Figure 3.30H).

3.6.2. Periodic Acid- Schiff (PAS) Staining

Glycoconjugate accumulation was determined and analyzed with Periodic Acid-Schiff staining among the 2 and 5-month-old *WT* and *Neu1-/-* mice cortex, hippocampus, thalamus, cerebellum, spleen and kidney tissue sections.

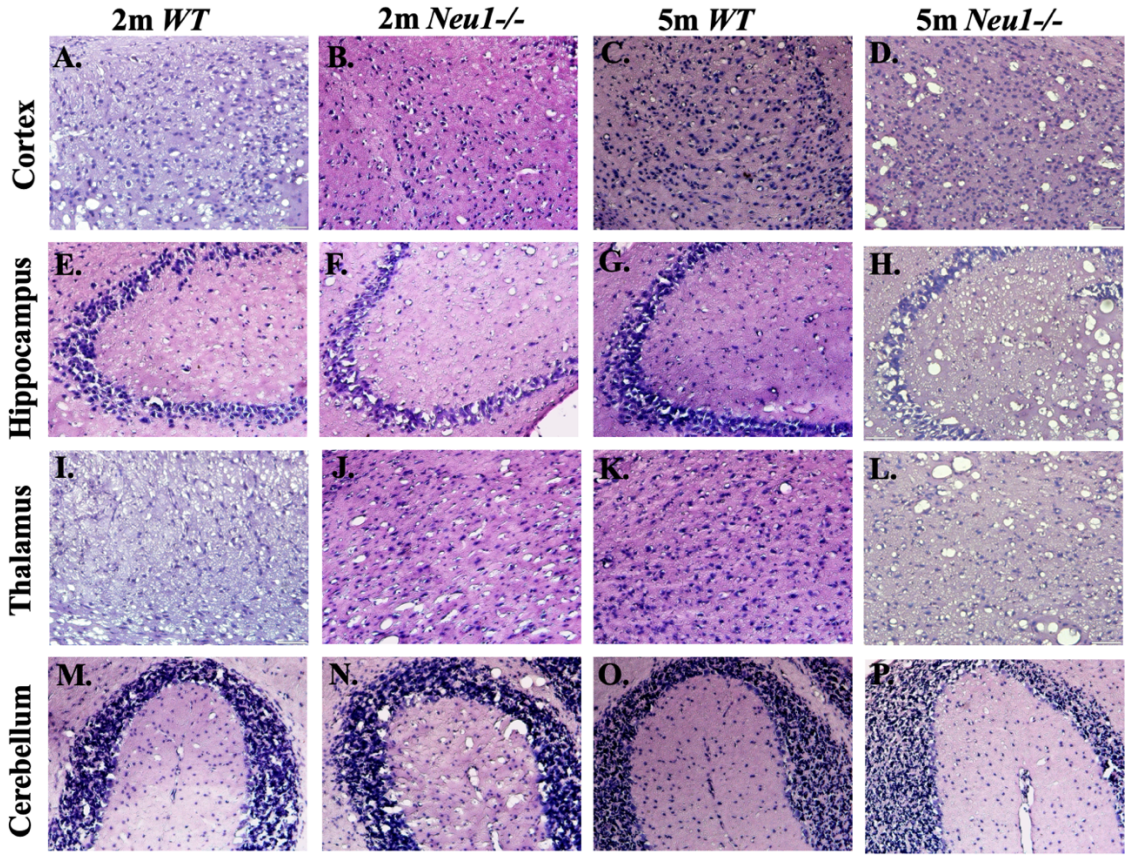

Figure 3.31. Periodic Acid- Schiff staining in 2- and 5-month-old *WT*, *Neu1-/-* mice brain coronal sections, cortex (A, B, C, D), hippocampus (E, F, G, H), thalamus (I, J, K, L) and cerebellum (M, N, O, P). Images were taken at 20X magnification by Olympus light microscope.

In Figure 3.31, glycoconjugate accumulation such as oligosaccharides, glycolipids, and glycoproteins were not observed, and identified in 2- and 5-month-old *WT* mice cortex, hippocampus, thalamus and cerebellum regions of brain. Although,

glycoconjugate accumulations were monitored in cortex, hippocampus, thalamus and cerebellum region of both 2- and 5-month-old *Neu1-/-* mice brain.

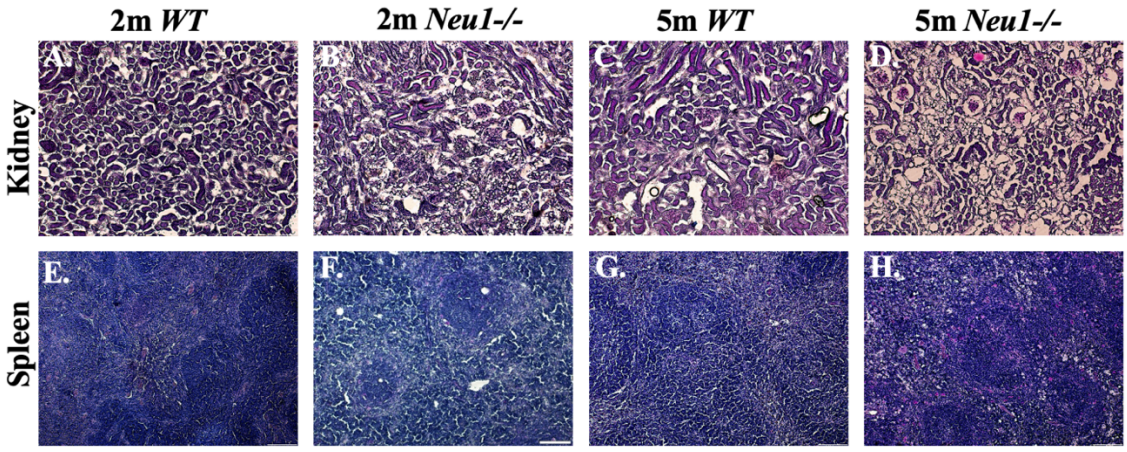

Figure 3.32. Periodic Acid-Schiff staining in 2- and 5-month-old *WT*, *Neu1- /-* mice kidney and spleen coronal sections, kidney (A, B, C, D), and spleen (E, F, G, H). Images were taken at 20X magnification by Olympus light microscope.

In Figure 3.32, there was no glycoconjugate accumulation in glomerular, and tubular cells of kidney was observed in 2 and 5-month-old *WT* mice; however, glycoconjugates were identified in both 2- and 5-month-old *Neu1-/-* mice kidney glomeruli and tubular cells. Additionally, any glycoconjugate accumulation in 2- and 5-month-old *WT* spleen white, and red pulp region of spleen was not identified, even though glycoconjugate accumulation was clearly seen in the 2- and 5-month-old *Neu1-/-* mice red and white pulp regions, especially elevated in increasing age groups, and there was no glycoconjugate accumulation in both younger, and elder *WT* groups.

3.6.3. Toluidine Blue Staining

Identification of mast cells, axonal degeneration, and identification of structural abnormalities was detected by Toluidine-Blue staining in the 2 and 5-month-old *WT* and *Neu1-/-* mice cortex, hippocampus, thalamus, cerebellum, spleen and kidney tissue sections.

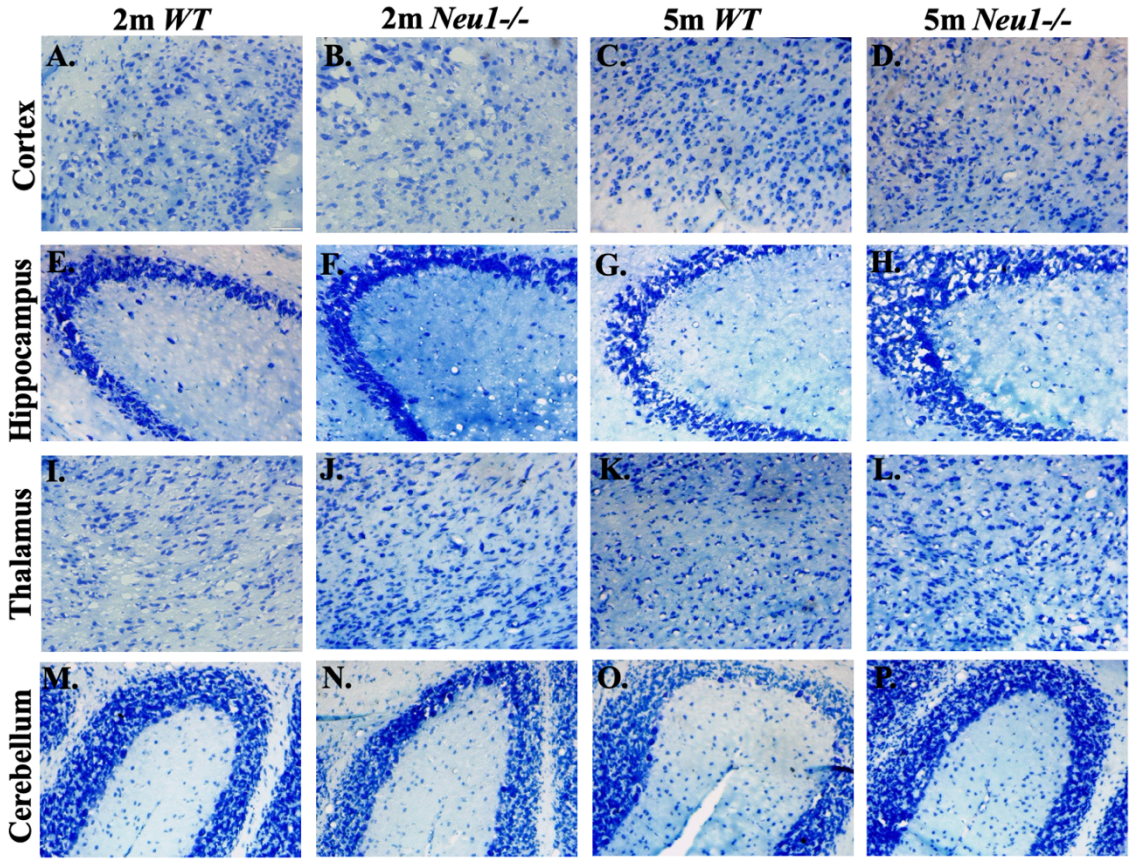

Figure 3.33. Toluidine Blue staining in 2- and 5-month-old *WT*, *Neu1-/-* mice brain coronal sections, cortex (A, B, C, D), hippocampus (E, F, G, H), thalamus (I, J, K, L) and cerebellum (M, N, O, P). Images were taken at 20X magnification by Olympus light microscope.

In Figure 3.33, axonal degeneration was investigated in 2- and 5-month-old *Neu1-/-* mice brain regions such as cortex, hippocampus, thalamus and cerebellum, and it was shown that vacuolated neurons were observable in cortical, hippocampal and thalamic regions of younger and elder *Neu1-/-* mice, however, they were more visible in 5-month-old *Neu1-/-* mice in comparison to younger and *WT* mice. There was less apparent axonal degeneration in the Purkinje cell layer of cerebellar region of both 2- and 5-month-old *Neu1-/-* mice.

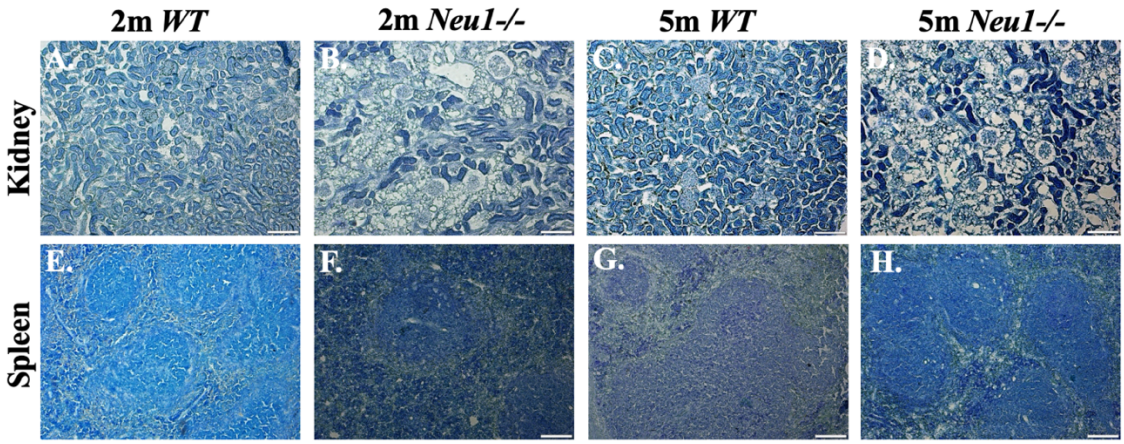

Figure 3.34. Toluidine blue staining in 2- and 5-month-old *WT*, *Neu1-/-* mice kidney and spleen coronal sections, kidney (A, B, C, D), and spleen (E, F, G, H). Images were taken at 20X magnification by Olympus light microscope.

In Figure 3.34, there was no detection of mast cells in both *WT*, and *Neu1-/-* mice of 2- and 5-month-old mice kidney tissues; however, highly vacuolated lysosomes in the epithelial cells of intraglomerular, and tubular regions with condensation of glomeruli, and deformed structure in tubuli was identified in both 2- and 5-month-old *Neu1-/-* mice kidney tissues; even though these were not observed in younger, and elder groups of *WT* kidney tissues. Besides the renal pathology, the mast cells were identified in the red and white pulp regions of both 2- and 5-month-old *Neu1-/-* mice spleen, while the younger and elder *WT* spleen tissues was observed less mast cells in their red and white pulp regions.

3.7. Immunohistochemical Analysis

Immunohistochemical analyses of fixed cortex, and cerebellum brain regions of 2- and 5-month-old *WT* and *Neu1-/-* mice were done for detection of active astrocytes with anti-GFAP staining (glial fibrillary acidic protein), anti-NeuN staining for neuron number, anti-CNPase staining for identification of oligodendrocytes and demyelination, and observation of microglial/macrophage activation by anti-MOMA2 staining.

3.7.1. Active Astrocyte Analysis

In this study, analysis of reactive astrocytes was carried out with specific anti-GFAP (Glial Fibrous Acidic Protein) antibody staining which is a standardized useful method to identify and visualize active astrocytes which is depending on the different genotypes, and age groups. Astrocytes are responsible for energy supplying for neurons, homeostasis of blood brain barrier and its integrity, removal of the excess neurotransmitters from synapses, and regulation of microglial cells, and neuroinflammatory responses (Jäkel & Dimou, 2017; Valles et al., 2023). Cortex, thalamus, hippocampus, and cerebellum regions of brain of 2-month-old *WT*, 2-month-old *Neu1-/-*, 5-month-old *WT* and 5-month-old *Neu1-/-* mice were performed anti-GFAP immunostaining, and comparison of active astrocyte intensity between various genotypes, and age groups was carried out.

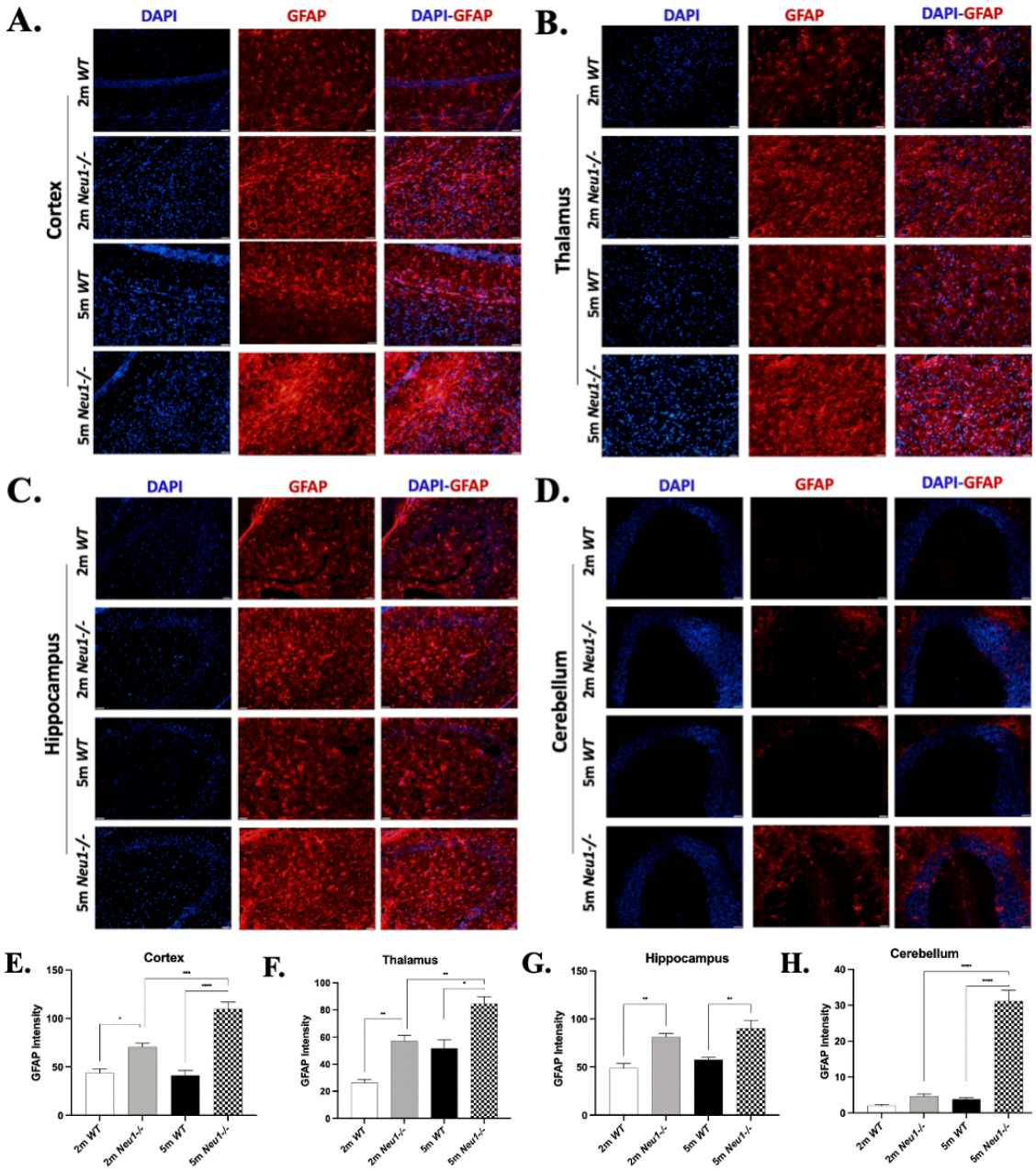

Figure 3.35. Immunohistochemical analysis for activated astrocytes in coronal sections of 2 and 5-month-old *WT*, and *Neu1−/−* mice brain. The cortex (A), thalamus (B), hippocampus (C), and cerebellum regions of brain (D) of 2 and 5-month-old *WT*, and *Neu1−/−* mice were stained with anti-GFAP antibody (red), and DAPI (blue). Activated astroglial cells are defined with red signal (GFAP;specific marker for astrocytes), and DAPI with blue signal for nucleus from the different brain regions. All images were taken under 20X magnification, and same light intensity. The GFAP intensity was measured with ImageJ, and activated microglial cells were shown in the cortex (E), thalamus (F), hippocampus (G), and cerebellum (H). Scale bar =

50 μm. The data are represented as the mean ± SEM. One-way ANOVA was used for statistical analysis (*p < 0.05, **p < 0.025, ***p < 0.01, and ****p < 0.001)

In the cortex, and thalamus regions, active astrocyte number was significantly increased in 2-month-old *Neu1-/-*, and 5-month-old *Neu1-/-* in comparison to 2- and 5-month-old *WT*, and also; 5-month-old *Neu1-/-* mice had more active astrocytes compared to 2-month-old *Neu1-/-* mice (Figure 3.35E, and Figure 3.35F). In the hippocampus regions, reactive astrocytes were apparantly elevated in both 2 and 5-month-old *Neu1-/-* mice when compared to 2- and 5-month-old *WT* mice (Figure 3.35G). Additionally, in cerebellum regions, 5-month-old *Neu1-/-* mice was shown in higher number of reactive astrocytes in comparison to 5-month-old *WT*, and younger *Neu1-/-* mice (Figure 3.35H).

3.7.2. Neuronal Density Analysis

In this study, neuronal density analysis was carried out with specific anti-NeuN antibody which is a functional immunostaining method for identification of mature neurons *in vitro*, and *in vivo* studies. NeuN immunostaining was helpful for determination of number of neuronal cells, and detection of neuronal cell death depending on the different genotypes, and age groups. In different brain regions containing cortex, thalamus, hippocampus, and cerebellum, anti-NeuN immunostaining were carried out in 2-month-old *WT*, 2-month-old *Neu1-/-*, 5-month-old *WT* and 5-month-old *Neu1-/-* mice, and comparison of neuronal density, and neuronal cell death between various genotypes, and age groups was performed.

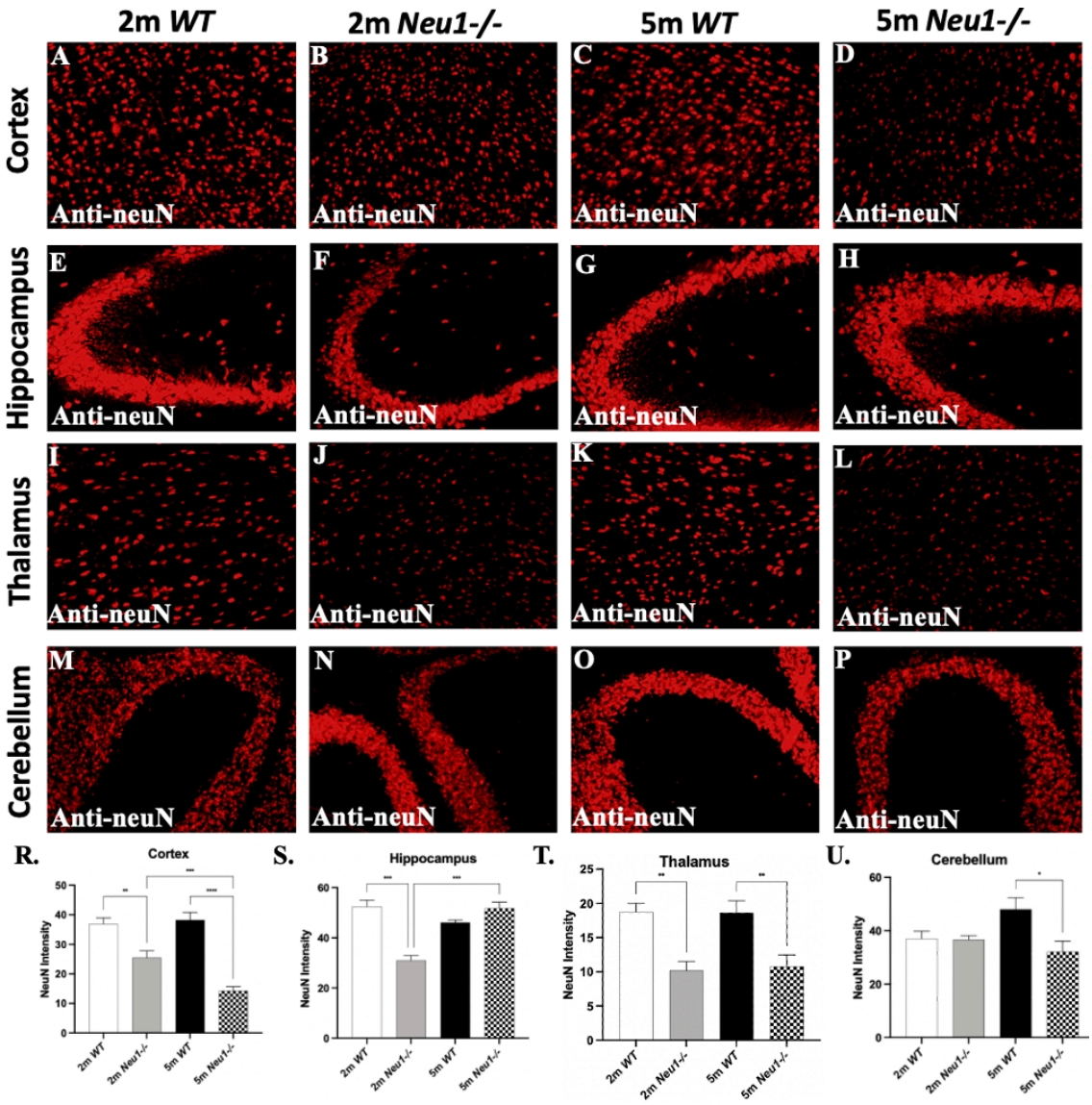

Figure 3.36. Immunohistochemical analysis for neuronal density in coronal sections of 2 and 5-month-old *WT*, and *Neu1−/−* mice brain. The cortex (A,B,C,D), hippocampus (E,F,G,H), thalamus (I,J,K,L), and cerebellum (M,N,O,P) regions of brain of 2 and 5-month-old *WT*, and *Neu1−/−* mice were stained with anti-NeuN antibody (red). Neuronal density are identified with red signal (NeuN;specific neuron marker) from the different brain regions. All images were taken under 20X magnification, and same light intensity. The NeuN intensity was measured with ImageJ, and density of neuronal cells were shown in the cortex (R), hippocampus (S), thalamus (T), and cerebellum (U). Scale bar = 50 µm. The data are represented as the mean ± SEM. One-way ANOVA was used for statistical analysis (*$p < 0.05$, **$p < 0.025$, ***$p < 0.01$, and ****$p < 0.001$)

In Figure 3.36R, neuronal density were reduced in 2- and 5-month-old *Neu1-/-* mice cortex regions in comparison to 2- and 5-month-old *WT* cortex regions; and also, neuronal cell death was increased in 5-month-old *Neu1-/-* mice cortex compared to 2-month-old *Neu1-/-* mice cortex. In Figure 3.36S, neuronal density was decreased in 2-month-old *Neu1-/-* mice hippocampus compared to *WT*, and neuronal cell death in 2-month-old *Neu1-/-* mice was less than 5-month-old *Neu1-/-* mice hippocampus. In thalamus region, neuronal cell death was significantly higher in both 2- and 5-month-old *Neu1-/-* mice thalamus in comparison to 2- and 5-month-old *WT* (Figure 3.36T). In the cerebellar region, neuronal density was reduced in only 5-month-old *Neu1-/-* mice compared to *WT*, and there was no remarkable change in 2-month-old *Neu1-/-* mice (Figure 3.36U).

3.7.3. Oligodendrocyte Analysis

In this study, oligodendrocyte analysis was performed with specific anti-CNPase antibody which is a convenient immunostaining technique for identification of oligodendrocyte number on the different genotypes, and age groups. Oligodendrocytes have an important role in myelination and myelin sheath formation in central nervous system. In different brain regions containing cortex, and cerebellum, anti-CNPase immunostaining were carried out in 2-month-old *WT*, 2-month-old *Neu1-/-*, 5-month-old *WT* and 5-month-old *Neu1-/-* mice, and comparison of oligodendrocyte density between various genotypes, and age groups was carried out.

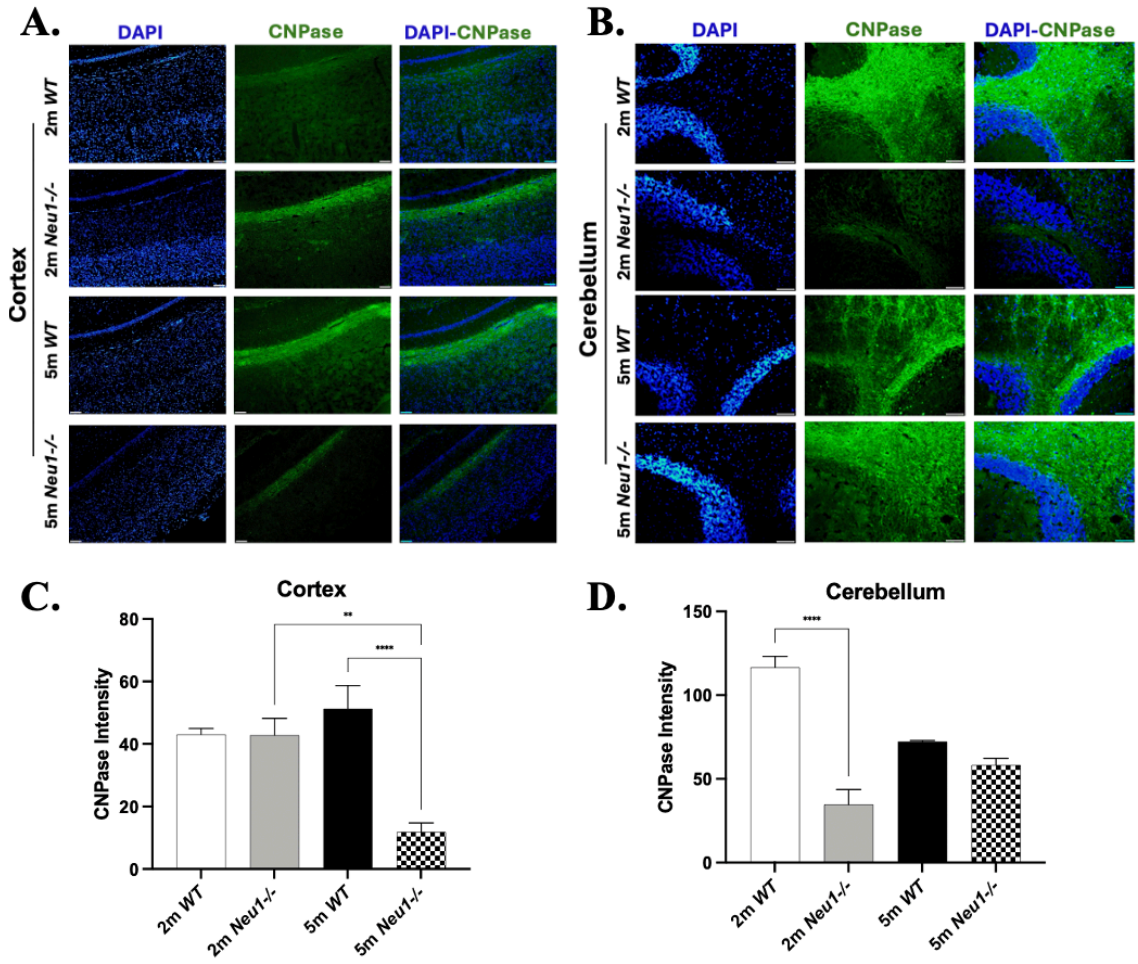

Figure 3.37. Immunohistochemical analysis for oligodentrocyte analysis in coronal sections of 2 and 5-month-old *WT*, and *Neu1−/−* mice brain. The cortex (A), and cerebellum (B) regions of brain of 2 and 5-month-old *WT*, and *Neu1−/−* mice were stained with anti-CNPase antibody (green). Oligodentrocyte number analysis are identified with green signal (CNPase; specific oligodentrocyte marker) and DAPI with blue signal for nucleus from the different brain regions. All images were taken under 20X magnification, and same light intensity. The CNPase intensity was measured with ImageJ, and density of oligodentrocytes were shown in the cortex (C), and cerebellum (D). Scale bar = 50 µm. The data are represented as the mean ± SEM. One-way ANOVA was used for statistical analysis (*$p < 0.05$, **$p < 0.025$, ***$p < 0.01$, and ****$p < 0.001$)

In Figure 3.37C, the number of oligodendrocyte cells were significantly decreased in 5-month-old *Neu1-/-* mice cortex in comparison to both 5-month-old *WT*, and 2-month-

old *Neu1-/-* mice cortex. In the cerebellum region of 2-month-old *Neu1-/-* mice, oligodendrocyte cell number were remarkably reduced in comparison to 2-month-old *WT*; although, there was no apparent alteration in CNPase density in 5-month-old *Neu1-/-* mice cerebellum when compared to 5-month-old *WT*, and different age groups of *Neu1-/-* mice cerebellum (Figure 3.37D).

3.7.4. Microglial Activation Analysis

In this study, analysis of activated microglial cells was performed with specific anti-MOMA-2 (Macrophage/Monocyte marker) antibody staining which is an important detection technique for identification and visualization active microglia which is depending on the different genotypes, and age groups. Microglial cells are the local immune cells in brain and spinal cord, and they are important for neurotropic and growth factor release, repairment of the CNS tissues by communicating with astrocytes and oligodendrocytes, cytokine/chemokine expression and release, and avoidance of neuronal death (Bachiller et al., 2018). Cortex, thalamus, hippocampus, and cerebellum regions of brain of 2-month-old *WT*, 2-month-old *Neu1-/-*, 5-month-old *WT* and 5-month-old *Neu1-/-* mice were carried out with anti-MOMA-2 immunostaining, and comparison of active microglia intensity between various genotypes, and age groups was performed.

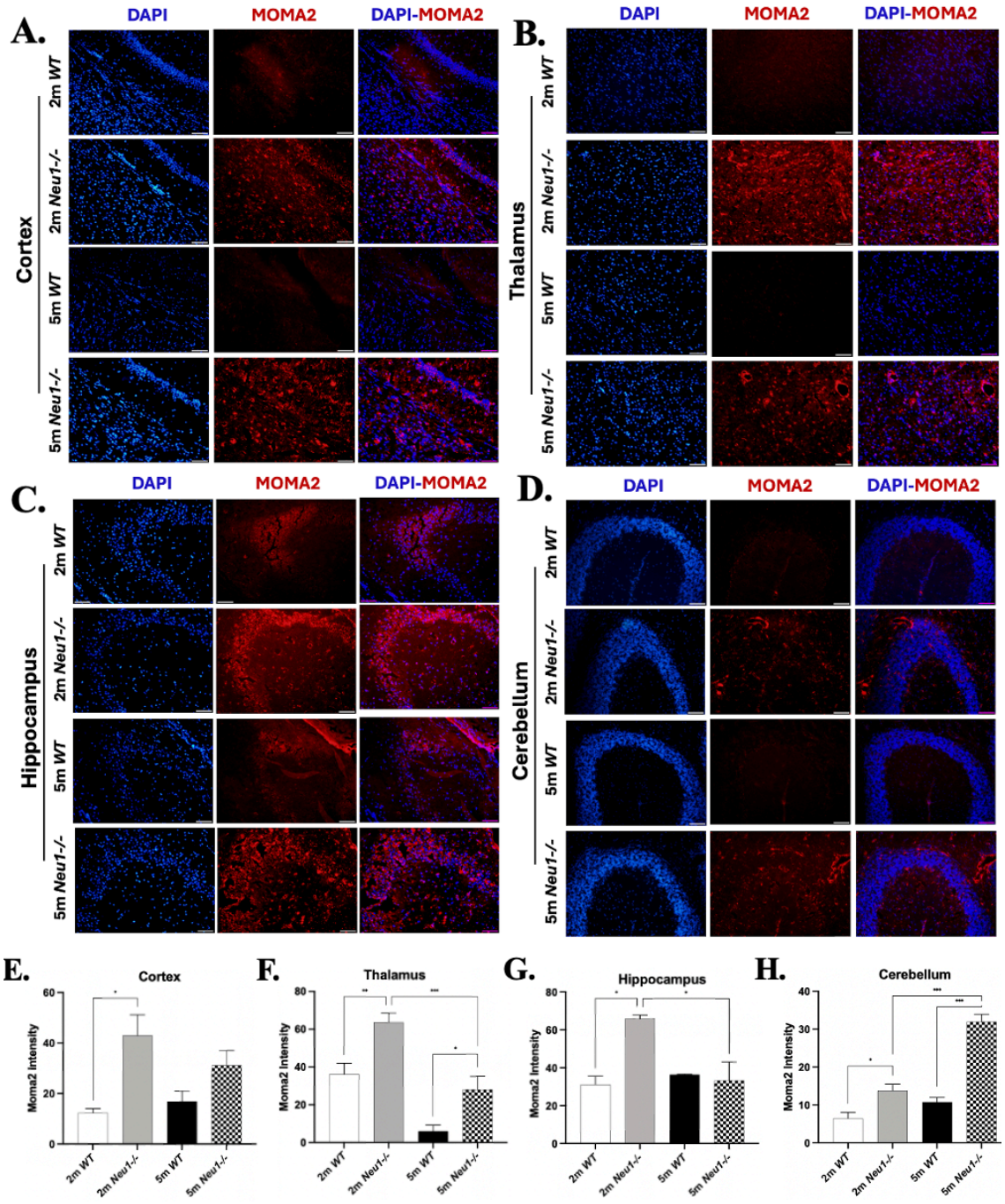

Figure 3.38. Immunohistochemical analysis for activation of microglial cells in coronal sections of 2 and 5-month-old *WT*, and *Neu1−/−* mice brain. The cortex (A), thalamus (B), hippocampus (C), and cerebellum regions of brain (D) of 2 and 5-month-old *WT*, and *Neu1−/−* mice were stained with anti-Moma2 antibody (red), and DAPI (blue). Activated microglial cells are defined with red signal (Moma2;microglial/macrophage marker), and DAPI with blue signal for nucleus from the different brain regions. All images were taken under 20X magnification, and same light intensity. The Moma2 intensity

was measured with ImageJ, and activated microglial cells were shown in the cortex (E), thalamus (F), hippocampus (G), and cerebellum (H). Scale bar = 50 μm. The data are represented as the mean ± SEM. One-way ANOVA was used for statistical analysis (*p < 0.05, **p < 0.025, ***p < 0.01, and ****p < 0.001)

In the cortex, active microglial cell number was increased in only 2-month-old *Neu1-/-* compared to *WT*; however; there was no significant alteration was detected in 5-month-old *Neu1-/-* , and different age groups (Figure 3.38E). In thalamus region, microglia cell density was increased in both 2- and 5-month-old *Neu1-/-* mice in comparison to 2- and 5-month-old *WT*; and additionally, microglial cell number was remarkably decreased in 5-month-old *Neu1-/-* compared to younger group (Figure 3.38F). In hippocampus region, activated microglia cell number were increased in 2-month-old *Neu1-/-* compared to 2-month-old *WT*, and 5-month-old *Neu1-/-* mice had less reactive microglial cells than 2-month-old *Neu1-/-* (Figure 3.38G). In the cerebellar region, reactive microglia number was significantly elevated in both 2 and 5-month-old *Neu1-/-* mice in comparison to 2- and 5 month-old *WT*, and also, increasing number of activated microglial cells were shown in 5-month-old *Neu1-/-* than younger group (Figure 38H).

CHAPTER 4

DISCUSSION

Sialidases are responsible for removal of alpha-glycosidically linked sialic acid residues from glycoproteins, glycolipids, oligosaccharides and gangliosides (Monti & Miyagi, 2012), and have an important role in intercellular communication, cellular growth, and neuronal plasticity (Minami et al., 2021; Miyagi & Yamaguchi, 2012). Neuraminidase 1 (Neu1 sialidase) has the highest expression level which is found in lysosomes and carry out the sialic acid removal from oligosaccharides and sialylated glycoconjugates degradation in lysosomes (Bonten et al., 1996; Magesh et al., 2006). Neuraminidase 1 enzyme is found in an active and stable protein complex with the glycosidase β-galactosidase (β-GAL) enzyme and lysosomal protective protein cathepsin A (PPCA) (Pshezhetsky & Ashmarina, 2001; Verheijen et al., 1982). The protective protein cathepsin A is one of the chaperone proteins, and PPCA interaction with β-galactosidase enzyme maintains the stabilization of β-GAL, and it is significantly important for Neu1 sialidase due to lysosomal localization, active state of catalyzation, and stability of Neu1 enzyme in lysosomes (D'Azzo et al., 1982). The deficiency of protective protein cathepsin A enzyme causes impairment in glycosidase β-galactosidase activity, and results with galactosialidosis that is one of the lysosomal storage diseases (D'Azzo et al., 1982; Zhou, 1996). Lysosomal storage disorders are rare and inheritable single-gene defects which belong to metabolic disorders due to accumulation of various molecules (oligosaccharides, glycoproteins, glycolipids) in lysosomes of visceral organs and central nervous systems because of mutations in enzyme encoding genes, and the deficient activator or transport proteins that are specifically necessary for functional enzyme activity (Platt et al., 2012, 2018). Sialidosis is a glycoprotein disease which belongs to LSDs, and caused by the deficiency in Neuraminidase 1 enzyme, and oligosaccharides with sialic acid residues, glycoconjugates such as glycosphingolipids, and glycoproteins accumulate gradually in lysosomes of the cells (Seyrantepe et al., 2003). Sialidosis patients are diagnosed with the accumulated biomarkers of the disease in urine and body fluid samples (Van Pelt et al., 1988). Sialidosis have two variant onsets in classification of severity of disease symptoms, onset of the age and residual enzyme activity; Type I Sialiodosis (late, mild, nonneuropathic form) and Type II Sialidosis (early,

dysmorphic) (Seyrantepe et al., 2003; Van Pelt et al., 1988). Neuraminidase 1 deficient mice model was firstly created in 2002 by d'Azzo et.al. with null knock out in Neu1 gene locus to highlight the importance of Neu1 enzyme in cellular pathways. Created Neu1 mice model represents the Type II sialidosis patient characteristics, and d'Azzo et.al. showed that Neu1 knock out mice model has enlarged visceral organs such as spleen and liver (hepatosplenomegaly), severe deformities in spinal cord, and defects in kidneys, impairments in neurological status, and oligosaccharides accumulation in urine samples (de Geest, 2002). In previous studies, gangliosides accumulation (GD3, GM3, GM4 and LM1) in sialidosis patients' visceral organs is defined, and *Neu1-/-* mice model was related with neuroinflammation due to examination of vacuolated microglial cells and macrophages are observed with the storage materials. However, identification of alterations in secondary lipid metabolism, and neuroinflammation in *Neu1-/-* mice model was not carried out previously. In the frame of this thesis study, biological importance of lysosomal sialidase Neu1 in secondary lipid alterations and neuroinflammation in different tissues such as brain, kidney, spleen and age groups of *Neu1-/-* mice models were investigated. For that purpose, molecular, histopathological, and immunohistochemical analyses of *Neu1-/-* mice model were performed and compared to the different age groups 2- and 5-month-old *Neu1-/-* mice models, and the wild type mice models in order to identify inflammatory conditions, and secondary lipid alterations.

In earlier studies, certain lipids glycerophospholipids and cholesterol are essential components of the cellular membrane of central nervous system, and have a role in the neuronal development, and proper functioning of neurons (Fuller & Futerman, 2018). In the lysosomal storage diseases, deficiency/mutation in enzymes/activator/transporter proteins causes certain lipid accumulation, and results with impaired lipid metabolism and secondary lipid alterations because of the impairment in lysosomal integrity (Samie & Xu, 2014). Dysfunctional lipid metabolism results with the primary disorder in lipidomics, and secondary lipids are altered in lysosomal storage diseases (primary disorders) (Samie & Xu, 2014; Vruchte et al., 2004). Besides the alterations in the lipid metabolism, neuroinflammation is clearly identified in lysosomal diseases with increased levels of neuroinflammatory markers, and reactive neuroglial cells such as microgliosis and astrogliosis because of the impairment in lysosomal degradation of specific biomolecules (Bosch & Kielian, 2015). Therefore, investigation of neuroinflammation, alterations in secondary lipid metabolism, and relationship of these pathways in sialidosis mice model is critical to enlighten the pathogenesis of sialidosis.

Lipidomic analyses were carried out to detect alterations in secondary lipid metabolism in 2- and 5-month-old *Neu1-/-* mice cortex and cerebellum tissues in comparison to *WT* tissues. According to the lipidomic analysis results, remarkable decrease was indicated in nearly 1.5-fold PC, 2-fold PE, and 2-fold PE O- major glycerophospholipid levels (Figure 3.2A), in 2.5-fold PA, 1.5-fold PC O- and PI intermediate glycerophospholipid amounts (Figure 3.2B), in LPE, and LPS minor glycerophospholipid levels (Figure 3.2C) of 2-month-old *Neu1-/-* mice cortex in comparison to age matched *WT* mice. Besides, PC, PA and PI glycerophospholipid levels were significantly increased in 5-month-old *Neu1-/-* mice cortex in comparison to the 2-month-old *Neu1-/-* mice cortex tissue; and only LPS glycerophospholipid levels were detected in reduced levels in 5-month-old *Neu1-/-* mice cortex according to the 2-month-old *Neu1-/-* mice cortex (Figure 3.2C).

In previous studies, anti-inflammatory effects of PC were shown; TNF-α levels were decreased, and inflammatory responses by NF-kB pathway were inhibited by PC by exogenous addition of PC, and it is defined that have a significant role in pro-inflammatory signaling pathway. In another study, it was demonstrated that PC is responsible for the regulation of the neurotropic factors, and synaptic protein expression, and reducing the damage in nerve cells, and dysfunctionality in synapses (Tan et al., 2020; Treede et al., 2007). Another earlier study showed that PC is responsible for macrophage polarization and regulation, and it has a role in reduction of inflammation; therefore, PC may be considered as potential therapy for treatment of inflammatory diseases (Ai et al., 2022). In this study, 1.5-fold decrease in phosphotidylcholine in 2-months-old *Neu1-/-* compared to *WT* can be related with the increasing pro-inflammatory cytokines, and their release in CNS.

PE glycerophospholipid is involved in different cellular pathways, and diseases such as neurodegeneration, and cancer which shows that PE may be positively effective in homeostasis. Previously, it was identified that PE is responsible for the attenuation of OX-LDL-induced inflammation with autophagy induction, and alleviation of inflammasome-mediated inflammation by reducing the pro and cleaved-IL-1β protein levels in kidney macrophages (Hao et al., 2023). In this study, previous studies reveal that phophotidylethanolamine is related with anti-inflammatory state, and decreased levels of PE can be correlated with elevated levels of cytokine production and neuroinflammation.

Phosphatidic acid is a significant glycerophospholipid, which is the main precursor for other glycerophospholipid molecules, one of the essential subunits of

cellular membrane, and secondary messenger molecules in many signaling pathways. In earlier studies, researches proposed that phosphatidic acid is the main regulatory biomolecules in inflammation, release of PA from the macrophages causes the expression and release of pro-inflammatory cytokines such as TNF-α, IL-6 and IL-1β with Akt-mTOR signaling cascade; due to these findings, PA glycerophospholipid may be targeted for further therapies of disease treatments with acute inflammation (Lim et al., 2003). In this research, decreasing levels of PA in 2-months-old *Neu1-/-* mice was surprising due to the role in activated inflammatory response; however, its increase in 5-month-old *Neu1-/-* mice cortex may be correlated with increased astrogliosis compared to 2-month-old *Neu1-/-* mice cortex.

Phosphatidyl inositol is an important signaling glycerophospholipid is an important constituent in cellular signaling, and physiology, insulin signaling, and membrane trafficking. In previous studies, it was concluded that phosphatidyl inositol is responsible for the inhibition of Il2, Il4, Il17, and IFN-gamma cytokine release from T helper cells in mice; so, it can be demonstrated that PI can have anti-inflammatory effect on inflammatory response (van Dieren et al., 2011). In this thesis study, reducing level of PC indicates increasing of neuroinflammation which may be related with increasing microgliosis, and neuronal cell death in the cortex of 2-month-old *Neu1-/-* mice.

Lysophospholipids are one of the bioactive molecules which can be part of the different pathological conditions in the reproductive system and can have a role in physical conditions. Previous studies showed that LPE, and LPC may regulate the anti-inflammatory response by increasing the IL-10 anti-inflammatory cytokine secretion by macrophages, and ensures inhibition of pro-inflammatory cytokine expression (TNF-α, IL-1β, MCP-1, MIP-1alpha, MIP-2, and IL-6), and leukocyte migration; additionally, IL-10 cytokine can be responsible for blocking of activation of NF-kB with IkB-α stabilization, and inhibition its degradation (Hung et al., 2011). According to the results of lipidome analysis, decrease in lyso-phosphatidylethanolamine which have anti-inflammatory role, may be one of the biomarkers of the increasing neuroinflammation that was revelated with microgliosis.

In Figure 3.3., remarkable reduction in HexCer levels in both 2 and 5-month-old *Neu1-/-* mice cortex tissues were monitored when compared to 2 and 5-month-old *WT* mice cortex, and HexCer were increased in 5-month-old *Neu1-/-* mice cortex compared to younger *Neu1-/-* mice cortex. Hexosylceramides are important to maintain structure of cellular membrane, and its fluidity, HexCer is the key precursor biomolecule for

production of more complex glycolipids gangliosides, and globosides. In different studies, reducing levels of CRP, TGF- beta, and IL-1β cytokines were related with the elevated levels of HexCer glycolipid; therefore, HexCer were considered as key biomolecules in lipid metabolism, and inflammatory pathways (A. Wang et al., 2023). By looking at these findings, reducing levels of HexCer in both younger, and elder group of *Neu1-/-* mice can be related as biomarker of neuroinflammation, and decreased number of oligodendrocyte cells.

In this study, surprisingly there were no significant increase or decrease in the levels of major, intermediate, and minor glycerophospholipids, and glycolipids of both 2 and 5-month-old *Neu1-/-* mice cerebellum when compared to 2 and 5-month-old *WT* cerebellum tissues; although increasing levels of pro, and anti-inflammatory cytokines, and microgliosis/astrogliosis were monitored. To minimize and obtain significant alteration levels in lipidomic analyses, further investigations with increasing n number of cerebellum tissues will be needed.

Gene expression analyses with real-time PCR and QPCR array was carried out to investigate alterations of inflammation-related gene expressions in younger and elder *Neu1-/-* mice in comparison to *WT*, and also, to find out the relation between inflammatory response and secondary lipid profile. Chemokines are the chemotactic cytokines that are responsible for the recruitment of immune cells such as neutrophils, monocytes and lymphocytes into the inflammation sites, and provides the cellular trafficking; and they have an active role in many disease progression and pathological conditions autoimmune diseases, vascular diseases and cancer (Bhavsar et al., 2015; Deshmane et al., 2009; Marques et al., 2013).

Increasing levels of Ccl2 in cortex (Figure 3.6A), cerebellum in only 5-month-old *Neu1-/-* (Figure 3.7A), kidney (Figure 3.8A), and spleen tissues (Figure 3.9A), of both 2- and 5-month-old *Neu1-/-* mice was detected as activated inflammatory response and correlated with literature. Ccl2, also named as MCP-1, is a monocyte chemoattractant protein, is responsible for the chemoattraction of monocytes, and oxidative stress conditions, many growth factors and cytokines induce the expression of Ccl2. Endothelial and epithelial cells, fibroblasts, astrocytes, monocytes, and microglia can produce Ccl2, and monocytes/macrophages expresses as major source of the Ccl2 where monocytes, and NK cells migrate and infiltrate by Ccl2 regulation (Deshmane et al., 2009).

Elevated levels of Ccl3 in cortex (Figure 3.6B), cerebellum (Figure 3.7B) and kidney tissues (Figure 3.8B) of in both 2- and 5-month-old *Neu1-/-* mice compared to *WT*

indicated inflammation and related with previous studies. Ccl3, other name is macrophage inflammatory protein (MIP-1alpha), is one the chemokines, which is expressed, and produced in response to inflammation by macrophages, and it supplies the recruitment of immune cells such as monocytes, dendritic cells, and neutrophils, and it specifically binds to Ccr1, and Ccr5 chemokine receptors to induce recruitment of macrophages, and lymphocytes into the inflammation sites, and Ccl3 is expressed in very low levels under normal conditions; however, in inflammatory state, elevated levels of pro-inflammatory cytokines such as IL-1β results with the increasing expression levels of Ccl3 (Ritter et al., 1995; Standiford et al., 1993).

Ccl5 gene expression was increased in cortex (Figure 3.6C), cerebellum (Figure 3.7C), and kidney tissues (Figure 3.8C) of 2- and 5-month-old *Neu1-/-* mice; however, unexpectedly Ccl5 gene expression was decreased in 5-month-old *Neu1-/-* cortex compared to younger *Neu1-/-* mice (Figure 3.6C), and besides that, Ccl5 gene expression was reduced in both 2- and 5-month-old *Neu1-/-* spleen tissues compared to *WT* spleen (Figure 3.9C). Ccl5 is one of the pro-inflammatory cytokines and it provides the recruitment and migration of dendritic cells, T cells, and mast cells (Marques et al., 2013). Elevated levels of pro-inflammatory chemokines such as Ccl2, Ccl3, and Ccl5 was monitored in various lysosomal storage diseases in Gaucher Disease, MPSIIIA, and MPSIIIB, and Tay-Sachs diseases (Demir et al., 2020b; Pandey et al., 2014; Reichel et al., 2009; Villani et al., 2007; Vitner et al., 2012). Additionally, decreasing levels of Ccl5 chemokines can be explained with the anti-inflammatory characteristic which was identified in previous research studies. It was suggested in earlier that Ccl5 chemokine may induce the expression of Il10 interleukins which have an anti-inflammatory role in inflammation, and decreasing levels of Ccl5 expression can be a marker of elevated inflammation (Dioszeghy et al., 2008; Kim et al., 2015). In this research, elevated levels of Ccl5 may be related with pro-inflammatory role in inflammatory response, while decreasing levels of Ccl5 can be responsible for alleviation of inflammation.

Cxcl10 chemokine expression was altered in cortex (Figure 3.6D), cerebellum (Figure 3.7D), kidney (Figure 3.8D) and spleen tissues (Figure 3.9D) of *Neu1-/-* mice. In 2-months-old *Neu1-/-* cortex, Cxcl10 expression were shown in elevated levels compared to *WT* (Figure 3.6D). In cerebellum tissue of *Neu1-/-* mice, Cxcl10 expression were decreased in 2-month-old *Neu1-/-* mice but increased in 5-month-old *Neu1-/-* mice in comparison to *WT* (Figure 3.7D). Remarkable increase in Cxcl10 chemokine expression was observed in both 2- and 5-month-old *Neu1-/-* kidney in comparison to *WT* (Figure

3.8D). Surprisingly, decreased expression levels of Cxcl10 chemokine were monitored in 5-month-old *Neu1-/-* mice spleen compared to *WT*, and younger *Neu1-/-* mice spleen (Figure 3.9D). Cxcl10 is one of the chemoattractant cytokines which is responsible for the production of chemotactic signals by binding to specific receptor Cxcr3 that is highly expressed in dendritic cells, macrophages, and T lymphocytes, and microglial cells and astrocytes in CNS. Cxcl10 gene expression levels were increased in inflammation, act as a proinflammatory cytokines, and its secretion occurs by the monocytes, leukocytes, and endothelial cells, and it is induced by IFN-γ. Cxcl10 chemokine is involved in pathogenesis of cancer, autoimmune diseases (Kanda et al., 2007; Loetscher et al., 1996; Luster & Ravetch, 1987). Increasing levels of Cxcl10 was correlated with literature which suggest Cxcl10 chemokine involves in the inflammatory response by recruiting the macrophages into the inflammation site, and in Tay-Sachs disease, increased levels of Cxcl10 was related to neuroinflammation in Tay-Sachs mice model cortex and cerebellum previously (Demir et al., 2020b; Mirones et al., 2013).

Higher expression of GFAP in cortex (Figure 3.6E), and cerebellum (Figure 3.7E) of 2- and 5-month-old *Neu1-/-* compared to *WT* was supported by the various studies. GFAP, glial fibrillary acidic protein, is an intermediate filament that is majorly located in astrocytes in central nervous system. Expression levels of GFAP is controlled with many growth factors, and LPS. Increased levels of GFAP expression, and protein production was related with the astrogliosis, reactive astrocytic cells, and specific biomarker of injuries in CNS, and degeneration in the nervous system, especially in neurological diseases (Laranjeira et al., 2011; Yang & Wang, 2015). In previous studies, reduced levels of GFAP are related to decreasing levels of neuroinflammation with also decreasing levels of pro-inflammatory cytokines in gene expression analyses (Y. Liu et al., 2018). In another study, immunostaining with GFAP antibodies showed that active astrocytes in different lysosomal storage diseases Sandhoff, Pompei and Niemann Pick A and C disease models (Clarke et al., 2021).

In QPCR analysis, pro-inflammatory cytokines Cxcl16, Cxcl5, Ccl3, Ccl4, and Xcl1 chemokines were shown in elevated levels remarkably in both 2 and 5-month-old *Neu1-/-* mice cortex in comparison to *WT* cortex tissues. Surprisingly, Ccl12, Ccl17, Ccl2, Cxcl12, Cxcl10, Ccl5, Ccl20, Cxcl3, and Xcl1 expression ratios were observed as increasing in 2-month-old *Neu1-/-* mice cortex compared to *WT* cortex tissues; but their expression levels were reduced in 5-month-old *Neu1-/-* mice cortex tissues in comparison to younger groups. Additionally, Ccl1, Ccl22, and Ccl24 chemokine gene expressions

were decreased in 2-month-old *Neu1-/-* mice cortex in comparison to *WT* cortex; but Ccl1, Ccl22, and Ccl24 levels were increased in elderly *Neu1-/-* mice cortex in Figure 3.10. Gene expression ratios of anti-inflammatory cytokines which are Ccl19, Ccl7, and Xcl1 were increased in 2-month-old *Neu1-/-* cortex compared to *WT*, but in 5-month-old *Neu1-/-* cortex, their expression levels were reduced compared to younger *Neu1-/-* mice. According to the results of QPCR array of cortex tissue, Ccl3, Ccl4, Ccl5, and Cxcl10 pro-inflammatory cytokine expression levels were correlated with RT-PCR results. Increasing levels of pro-inflammatory cytokines are correlated by previous studies which are related to inflammatory conditions in different diseases. Cxcl16 is pro-inflammatory cytokine expressions were carried out by various immune cells, macrophages, monocytes, and dendritic cells; and they have an active role in cell signaling such as NF-kB activation, expression of TNF-α, and results with proliferation and migration of cells in autoimmune diseases, and multiple sclerosis (Bao et al., 2023; Chandrasekar et al., 2004; Li et al., 2022). Cxcl5 is also one of the pro-inflammatory cytokines, and it contributes to infiltrations of immune cells acting as chemoattractant biomolecule, and previous research showed that Cxcl5-Cxcr2 interaction was related to neurogenic inflammation in gouty arthritis (Yin et al., 2024). Decreasing levels of anti-inflammatory cytokines are correlated by earlier studies. Ccl19 chemokine is able to chemoattract immune cells into inflammation site, but additionally; Ccl19 can block the immune response by suppressing the IL-10 expression and production, negatively regulating the dendritic cell movement, and programmed cell death of dendritic cells (Bosè et al., 2013; Ellingsen et al., 2014; N. Yamashita et al., 2006). Ccl7 chemokine is also one of the regulatory biomolecules of inflammation, and it is effective on regulation of innate and adaptive immunity by participating cell signaling though binding chemokine-specific receptor Ccr2, Ccr5 (Ben-Baruch et al., 1995). In another study, negative regulation of mediated cutaneous inflammation by Ccl7 chemokine was revealed (Ford et al., 2019).

Pro-inflammatory interleukins Il5, Il11, Il12b, and Il1beta expression levels were decreased in 5-month-old *Neu1-/-* mice compared to younger *Neu1-/-* mice cortex. Il1rn, and Il9 expression levels were elevated in 5-month-old *Neu1-/-* in comparison to 2-month-old *Neu1-/-* mice. Il4, Il6, and Il22 interleukins have a different characteristic which have both pro-inflammatory and anti-inflammatory roles in regulation of inflammation, and their expression levels were decreased in 5-month-old *Neu1-/-* mice cortex in comparison to younger *Neu1-/-* mice (Figure 3.11). Increasing levels of pro-inflammatory interleukins were correlated with activated immune response in various

studies. Il9 interleukin is a part of the allergic responses, and related with autoimmune diseases such as multiple sclerosis, and lupus erythematous. Il9 interleukin expression were shown with MS, and it is related with modulation of macrophage characteristics in central nervous system (Donninelli et al., 2020). Il6 interleukin is one of the pro-inflammatory cytokines which have crucial role in autoimmune diseases, and chronic inflammatory conditions, and also participates in T-cell differentiation (Tanaka et al., 2014). Another study showed that Il6 is a part of anti-inflammatory responses in local and systemic inflammation by regulation of pro-inflamamtory cytokines (Xing et al., 1998). Il4 interleukin, a cytokine, which provides both anti-, and pro-inflammatory properties by regulating the immune cells such as basophils, eosinophils, and mast cells (Gadani et al., 2012). According to environmental conditions, Il4 can be effective on progression and regression of inflammatory state Il4 can be effective on reduction of nitric oxide production, and release of TNF in astrocytes of mouse. Also, nitric oxide expression can be increased by Il4 with activation of Il1-beta and TNF (Brodie et al., 1998; Hu et al., 1995). Besides that, Il4 treatment in AD suggested that Il4 interleukin delivery into the CNS alleviated disease progression in AD mice model (Kiyota et al., 2010).

Tumor necrosis factor receptor family members were investigated in both 2, and 5-month-old *Neu1-/-* mice cortex compared to *WT*. TNF superfamily ligands (TNFSF) and receptors (TNFRSF) is responsible for the cellular communication among distinct cells in developmental processes of lymphoid organs, and initiation of tissue-specific responses, and maintenance of organ homeostasis. TNF superfamily members participate in costimulatory and coinhibitory signaling cascades in innate and adaptive immune systems with regulation of T-cells (Ward-Kavanagh et al., 2016). Figure 3.12, gene expression levels of TNF-receptor family members Tnfrsf11b, Tnfsf10, and Cd70 was observed in reduced levels in 2-month-old *Neu1-/-* mice cortex in comparison to *WT*; besides, Tnfsf10 expression levels were decreased in 5-month-old *Neu1-/-* mice cortex according to 5-month-old *WT*. Lta, and Tnfsf11 gene expression were increased in 2-month-old *Neu1-/-* mice cortex when compared to WT (Figure 3.12B). Gene expression levels of Cd70, Tnf, and Tnfsf11 were increased in 5-month-old *Neu1-/-* mice in comparison to *WT*. Tnf and Tnfsf13b levels were elevated in 5-month-old *Neu1-/-* mice when compared to younger *Neu1-/-* mice cortex. Lta and Tnfsf11 members' expression were reduced in 5-month-old *Neu1-/-* mice according to younger groups (Figure 3.12B). Based on these findings, increasing levels of Cd70, Tnf, Tnfsf11, and Tnfsf13b may be linked to inflammatory response because of their pro-inflammatory character, and they

can be considered as markers of inflammation in various disease pathogenesis (Dhaeze et al., 2019; Fan et al., 2021). Besides that, decreasing levels of Tnfrsf11b, Tnfsf10, and Cd70 was contradictory in this study due to their participation in inflammatory response progression; however, reduced levels of TNF-receptor family members' gene expression can be explained with a response to increasing levels of anti-inflammatory gene expressions (Burgaletto et al., 2021; Papadaki et al., 2019).

Reduced levels of gene expression of Gpi1 growth factor were obtained in both 2 and 5-month-old *Neu1-/-* mice cortex in comparison to *WT* cortex tissues, and Bmp4 and Thpo gene expressions were decreased in 5-month-old mice cortex when compared to younger Neu-/- cortex tissues, although Thpo expression was increased in 2-month-old *Neu1-/-* cortex tissues according to 2-month-old *WT*. Expression of Lif, Ifna2, and Ifng was increased in 2-month-old *Neu1-/-* cortex in comparison to *WT*, however; in 5-month-old *Neu1-/-* cortex, their expression levels were decreased when compared to younger *Neu1-/-* mice cortex. Mstn growth factor expression was decreased in 2-month-old *Neu1-/-* mice cortex in comparison to *WT*, but its expression was increased in 5-month-old *Neu1-/-* mice cortex when compared to *WT*, and younger *Neu1-/-* mice cortex (Figure 3.13C). Nodal, Osm, Csf2 and Csf3 growth factor expression levels were elevated in comparison to *WT* cortex, and additionally; Csf3 gene expression were reduced in 5-month-old *Neu1-/-* cortex according to *WT* cortex tissues (Figure 3.13C). In the light of these findings, decreasing levels of Bmp4 which is a protective growth factor, can be explained with alleviation of the pathogenesis of inflammatory disorder by reducing the production, and release of the pro-inflammatory cytokines (Baraban et al., 2016). Increased levels of Thpo that is responsible for the production of platelets, and migration of immune cells by cytokines, can be explained with increasing levels of Thpo provides the diagnosis of various critical diseases in acute inflammatory response (Lupia et al., 2022; Margraf & Zarbock, 2019). Ifna, and Ifng interferon expression were monitored as both increasing and decreasing levels, and these results may contribute the regulation of inflammatory state based on their dual characteristics in inflammation which maintains the expression of both pro-, and anti-inflammatory cytokine expression (Mühl & Pfeilschifter, 2003; Tilg & Peschel, 1996).

Remarkable elevation in the Spp1 cytokine expression in mice cortex was monitored in both 2 and 5-month-old *Neu1-/-* mice in comparison to *WT* (Figure 3.14A). Increasing levels of Spp1 cytokine can be explained with increasing inflammatory response. Spp1 cytokine, also named as osteopontin, is defined as both pro-, and anti-

inflammatory cytokine because osteopontin is involved in modulation, and recruitment of immune cells such as T cells, and macrophages by induction of many pro-inflammatory cytokines; furthermore, osteopontin is crucial for the inhibition of nitric oxide synthesis, and production of nitric oxide is decreased leading to reduction of oxidative stress. Inhibition of oxidative stress resulted with the reduction of inflammation which is shown in mice with OPN-deficiency (Lund et al., 2009; Trostel et al., 2018; Yim et al., 2022). Differently, Adipoq cytokine expression was significantly reduced in both 2 and 5-month-old *Neu1-/-* mice when compared to *WT* (Figure 3.14B). Decreased expression of Adipoq cytokine may be explained with participation in inflammatory response as an anti-inflammatory cytokine which is shown in previous research. Adipoq cytokine, or adiponectin is highly expressed in adipose tissues, muscle and brain, and it was demonstrated that adiponectin inhibits the NF-kB activation by reduced expression of TNF-α and IL-6 pro-inflammatory cytokines, and also induction of IL-10 anti-inflammatory cytokine expression (Ouchi & Walsh, 2007).

In PCR Array results of *Neu1-/-* mice cerebellum and kidney tissues compared to age-matched *WT*, expression levels of all of the pro- and anti-inflammatory cytokines, interleukins, TNF-receptor family members, growth factors and other cytokines were significantly elevated in 5-month-old mice in comparison to age-matched *WT*, and younger *Neu1-/-* mice. Increasing expression levels of pro-inflammatory cytokines, and interleukins can be correlated from the earlier studies which indicates the chronic state of inflammation. Increasing levels of anti-inflammatory chemokines, and cytokines were unexpected and contradictory in this thesis study, however; elevated levels of these anti-inflammatory biomolecules may be explained with response to dysregulated and perpetuated neuroinflammation cycle which needs to be further investigated.

Western blotting analyses were performed to indicate the alterations of regulatory proteins of inflammatory response NF-kB, and IkB-α in 2- and 5-month-old *Neu1-/-* mice cortical and cerebellar regions of brain, kidney and spleen tissues, and compared to *WT*. Significant increase was observed in IkB-α expression levels in 5-month-old *Neu1-/-* mice cortex region compared to *WT*, and 2-month-old *Neu1-/-* groups (Figure 3.25C). NF-kB expression levels were not remarkably changed in both 2- and 5-month-old *Neu1-/-* mice cortex in comparison to *WT* (Figure 3.25D). Apparent reduction was identified in IkB-α expression levels in only 5-month-old *Neu1-/-* mice cerebellar region compared to *WT* (Figure 3.26C). NF-kB expression levels were significantly decreased in both 2- and 5-month-old *Neu1-/-* mice cerebellum in comparison to *WT* (Figure 3.26D). Remarkable

increase was monitored in IkB-α expression levels in both 2- and 5-month-old *Neu1-/-* mice kidney compared to *WT,* and IkB-α expression was decreased in 5-month-old Neu1-/- mice kidney in comparison to 2-month-old *Neu1-/-* (Figure 3.27C). NF-kB expression levels were apparently reduced in only 2-month-old *Neu1-/-* mice kidney in comparison to *WT* (Figure 3.27D). In Figure 3.28C, remarkable elevated levels were monitored in IkB-α expression in both 2- and 5-month-old *Neu1-/-* mice spleen compared to *WT,* and IkB-α expression was decreased in 5-month-old Neu1-/- mice spleen in comparison to 2-month-old *Neu1-/-*. NF-kB expression levels were significantly reduced in both 2- and 5-month-old *Neu1-/-* mice spleen in comparison to *WT* (Figure 3.28D). NF-kB is one of the essential regulatory proteins of inflammatory response by activating expressions of pro-inflammatory genes and mediating the innate and adaptive immunity. NF-kB transcription factors consist of five different proteins; NF-kB1 (p50), NF-kB2 (p52), c-Rel, RelA (p65), and RelB; and they are acting as transcription factors by upregulating the various cytokines, chemokines, and interleukins (T. Liu et al., 2017; S.-C. Sun et al., 2013). IkB-α is responsible for the sequestration of NF-kB in the cytoplasm of the cells which have an important role in inhibition of inflammation by inhibiting the NF-kB activity. NF-kB can be activated by two different signaling cascades; canonical, and noncanonical cascades. Canonical activation occurs by response to various receptors such as TNF receptor superfamily members (TNFR), T-cell receptor, and cytokine receptors. IKK (IkB kinase) activation occurs with response to cytokines, growth factors, and microbial components, it results with the phosphorylation of IkB-α, and phosphorylated IkB-α is degraded by proteasomes, and NF-kB proteins (p50/RelA, and p50/c-Rel) can localize to nuclear region and enhances the transcription of inflammatory cytokines (Karin & Delhase, 2000; Vallabhapurapu & Karin, 2009). In noncanonical activation of NF-kB, distinct ligands such as TNFR superfamily members binds to TNF receptors; but degradation of IkB-α protein in this signaling cascade is not involved. NF-kB2 (p52) precursor protein is processed by NIK (NF-kB-inducing kinase) that provides the IKK activation, and phosphorylation of p100 which results with ubiquitination and processing of NF-kB2 protein (Xiao et al., 2001). Then, functional p52/RelB heterodimer structure localizes to nucleus, and activates the transcription of inflammatory genes. Many inflammatory responses are regulated with canonical NF-kB signaling, and adaptive immune system is carried out with both canonical, and noncanonical NF-kB signaling cascade (T. Liu et al., 2017; S.-C. Sun & Liu, 2011). According to findings of this study, no significant change in NF-kB levels in both 2- and 5-month-old *Neu1-/-* cortex

compared to *WT*, and this result can be related with inflammatory response may be regulated with different signaling pathways such as MAPK, and JAK-STAT. In cerebellar region, decreased levels of IkB-α and NF-kB was shown in both 2- and 5-month-old *Neu1-/-* mice; IkB-α levels can be reduced by the negative feedback mechanisms due to perpetuation of inflammatory cycle. Also, increased levels of IkB-α and decreased levels of NF-kB in the kidney of both 2- and 5-month-old *Neu1-/-* can correlate each other; because increased IkB-α can inhibits the NF-kB activation and alleviate the inflammatory response. Besides that, increased levels of IkB-α and reduced levels of NF-kB protein production in both 2- and 5-month-old *Neu1-/-* spleen tissues can be correlated with decreasing levels of pro-inflammatory cytokine Ccl5, and Cxcl10. Additionally, previous studies showed and concluded that increasing levels of produced NF-kB protein can be related with reduced levels of inflammation that suggests NF-kB can be anti-inflammatory by inhibition of pro-inflammatory gene expression, and activation of anti-inflammatory cytokines such as IL-10 (Lawrence, 2009).

Histopathological analyses were carried out to understand the pathology in cortex, cerebellum, hippocampus, cerebellum regions of brain, kidney and spleen tissues of 2 and 5-month-old Type II sialidosis mice models. Figure 3.29B, and Figure 3.29D, edema, and disorganization, and vessels with dilation was observed in 2 and 5-month-old *Neu1-/-* mice. In the 2 and 5-month-old *Neu1-/-* mice hippocampal region, vacuolization, edema, and vessels with dilation was identified, and cellular loss with degeneration was observed (Figure 3.29F, and Figure 3.29H). There was dilation in vessels, edema, vacuolization, plaque-like structure and loss in thalamic cells in both younger and elder group of *Neu1-/-* mice model (Figure 3.29J, and Figure 3.29L). In the 2- and 5-month-old *Neu1-/-* mice cerebellum, vessels with dilation, edema, disorganization and deletions in Purkinje cell layer was detected (Figure 3.29N, and Figure 3.29P). Previously, microglial cells, macrophages and neurons were excessively degenerated, and ballooned structure of macrophage-like cells in the 5-month-old *Neu1-/-* mice dentate gyrus region. A few degenerations in the Purkinje cell layer of 5-month-old *Neu1-/-* mice was shown (de Geest, 2002). In Figure 3.30B, and 3.30D, there was vacuolized glomerular cells, and degenerated Bowman capsule in both 2- and 5-month-old *Neu1-/-* mice kidney, and additionally there was vacuolization and degeneration in tubular cells of kidney in younger, and elder group of *Neu1-/-* mice, besides; degeneration and vacuolization of epithelial cells of kidney is increased in elder group of *Neu1-/-* mice. In earlier studies, vacuolization, ballooned structure due to storage of glycoconjugates, and cellular loss in

the glomeruli and tubuli regions was monitored in 5-month-old *Neu1-/-* kidney tissues (de Geest, 2002; Kho et al., 2023). In Figure 3.30F, and Figure 3.30H, there was vacuolization in the cells of both red and white pulp of spleen in younger and older group of *Neu1-/-* mice.

Periodic Acid-Schiff staining was performed in order to identify the glycoconjugate accumulation (glycolipids, and glycoproteins). In lysosomal diseases, neurodegenerative conditions in CNS resulted from the accumulation of undegraded biomolecules such as oligosaccharides and glycolipids. In Pompe disease, which caused by mutations in GAA enzyme, and defined with glycogen storage in the lysosomal compartments. In Pompe disease mice model brain, it was shown that accumulation of glycogen was highly visible (Turner et al., 2016). In Niemann-Pick Type C, GM2 accumulation was indicated in Purkinje cell layer (Sleat et al., 2004). In Niemann-Pick Type C, NPC1-deficient mice were monitored with cholesterol in late endosome/lysosome with damaged cells (Beltroy et al., 2007). Cholesterol accumulation was shown in MPS IIIA, Niemann-Pick Type C, and GM1 gangliosidosis in the neurons of disease mice models (Walkley & Vanier, 2009). In Tay-Sachs disease mice model, glycoconjugate accumulation was shown with PAS staining in cortex, hippocampus, and corpus callosum (Can et al., 2022). In Figure 3.31, glycoconjugate accumulation such as oligosaccharides, glycolipids, and glycoproteins in cortex, hippocampus, thalamus and cerebellum region of both younger and elder age groups of *Neu1-/-* mice brain, but not indicated in any *WT* brain regions. In Figure 3.32, glycoconjugates were identified in both 2- and 5-month-old *Neu1-/-* mice kidney glomeruli and tubular cells. Additionally, accumulated glycoconjugates was clearly seen in the 2- and 5-month-old *Neu1-/-* mice red and white pulp regions, especially elevated in increasing age groups, and any glycoconjugate accumulation in both younger, and elder *WT* groups was monitored.

Toluidine staining was done to define and monitor the axonal degeneration, and presence of mast cells in cortex, hippocampus, thalamus, cerebellum of brain regions, kidney and spleen tissues of both 2- and 5-month-old *WT*, and *Neu1-/-* mice. In Figure 3.33, it was monitored that vacuolated neurons were observable in cortical, hippocampal and thalamic regions of younger and elder *Neu1-/-* mice, but they were more apparent in 5-month-old *Neu1-/-* mice in comparison to younger and *WT* mice. Less visible axonal degeneration in the Purkinje cell layer of cerebellar region of both 2- and 5-month-old *Neu1-/-* mice. In previous studies, axonal degeneration was demonstrated with toluidine blue staining in the cortex regions of brain in 5-month-old Tay-Sachs mice model (Can et

al., 2022). In another study, degeneration and recovery of the myelin sheath in Schwann cells were investigated with Toluidine Blue in rats with brain injury, and after treatment with tacrolimus (He et al., 2017). In Figure 3.34, mast cells in both *WT*, and *Neu1-/-* mice of 2- and 5-month-old mice kidney tissues was observed; however, highly vacuolated lysosomes in the epithelial cells of intraglomerular, and tubular regions with condensation of glomeruli, and deformed structure in tubuli was identified in both 2- and 5-month-old *Neu1-/-* mice kidney tissues. Additionally, the renal pathology, the mast cells were identified in the red and white pulp regions of both 2- and 5-month-old *Neu1-/-* mice spleen. These findings were correlated with the previous studies, mast cell infiltration was investigated, and low numbers of mast cells were monitored in kidney tissues with toluidine blue staining in the diabetic nephropathy in rat models (Hafez et al., 2020).

Immunohistochemical analyses of fixed cortex, hippocampus, and thalamus and cerebellum brain regions of 2- and 5-month-old *WT* and *Neu1-/-* mice were carried out to detect reactive astrocytes with anti-GFAP staining (glial fibrillary acidic protein). GFAP is one of the standardized techniques for activated astrocyte visualization (Schmidt-Kastner et al., 1993). In Figure 3.35, cortex, and thalamus regions, active astrocyte number was significantly increased in 2- and 5-month-old *Neu1-/-* in comparison to *WT*, and 5-month-old *Neu1-/-* mice had more active astrocytes compared to younger *Neu1-/-* mice. In the hippocampus regions of the brain, reactive astrocytes were apparantly elevated in both 2 and 5-month-old *Neu1-/-* mice when compared to *WT* mice (Figure 3.35G). In cerebellum regions of the brain, 5-month-old *Neu1-/-* mice was shown in higher number of reactive astrocytes in comparison to *WT*, and younger *Neu1-/-* mice (Figure 3.35H). Activated numbers of astrocytes can be related with the neuroinflammatory conditions in both ages of *Neu1-/-* mice, and increasing numbers of proinflammatory cytokines in cortex, and cerebellum regions can be related with active state of infammation. Besides these findings, active astrocytes were identified in previous researches of lysosomal storage diseases; increasing GFAP intensity was shown in the cortex region of brain in Sandhoff mice model (Sango et al., 1995), Niemann Pick A mice model was also monitored with astrogliosis in the cebellar region, Niemann-Pick C mice model was indicated with elevated levels of GFAP intensity in their cerebellar region, and Pompe mice models was monitored in astrogliosis in their hippocampal and cerebellar region of brains (Clarke et al., 2021).

In immunohistochemical analyses of neuronal density of 2- and 5-month-old *Neu1-/-* mice models, anti-NeuN staining was performed in cortex, hippocampus,

thalamus, and cerebellum regions of the brain (Figure 3.36). In 2- and 5-month-old *Neu1-/-* mice cortex regions in comparison to *WT* cortex regions. Neuronal cell death was increased in 5-month-old *Neu1-/-* mice cortex compared to younger *Neu1-/-* mice cortex, and neuronal density was decreased in 2-month-old *Neu1-/-* mice hippocampus compared to *WT*, and neuronal cell death in 2-month-old *Neu1-/-* mice was less than elder gorup of *Neu1-/-* mice hippocampus. Neuronal cell death was significantly higher in both 2- and 5-month-old *Neu1-/-* mice thalamus in comparison to *WT* (Figure 3.36T). In the cerebellar region, neuronal density was reduced in only 5-month-old *Neu1-/-* mice compared to *WT*, and, there was no remarkable change in younger *Neu1-/-* mice (Figure 3.36U). NeuN protein is specifically found in the neuronal cells' nuclei, and their cytoplasm in the mammal CNS, and therefore; neuronal density, and differentiation was identified with the NeuN staining (Gusel'nikova & Korzhevskiy, 2015). According to findings of NeuN immunohistochemistry, increasing number of neuronal death in all regions of the brain in 2- and 5-month-old *Neu1-/-* mice compared to *WT* brain may be correlated with increasing number of astrogliosis, and microgliosis with elevated levels of pro-inflammatory cytokine expressions, significant increase in GFAP, and Moma-2 intensity, and neurodegeneration in the specific brain regions due to accumulation of glycoconjugates. Earlier studies are correlated with these results in 2- and 5-month-old group of *Neu1-/-* mice brain, because neurodegenrative conditions were strongly linked to neuronal cell death, and decreasing neuron numbers. In Tay-Sachs mice model, decreasing neuronal density was shown in cortex, thalamus, and pons regions of the 5-month-old Hexa-/-Neu3-/- mice brain with NeuN staining (Demir et al., 2020).

In immunohistochemical analysis of cortex,thalamus, hippocampus and cerebellum regions of brain in 2- and 5-month-old *Neu1-/-* was immunostained with anti-CNPase in order to investigate demyelination. In Figure 3.37C, oligodendrocyte cell number were significantly decreased in 5-month-old *Neu1-/-* mice cortex in comparison to *WT*, and younger *Neu1-/-* mice cortex. In cerebellum region of only 2-month-old *Neu1-/-* mice, oligodendrocyte cell number were remarkably reduced in comparison to *WT*. In this study, decreasing number of oligodendrocytes is identified with decreasing intensity of CNPase which is one of the major proteins of myelin, the myelin maintenance and integrity of axons (Olga et al., 2020). Decreasing number of oligodendrocytes was monitored and linked to decreasing myelin sheath in various studies. In Tay-Sachs disease mice model, it was shown that decreasing intensity of anti-CNPase immunohistostaining in cortex, thalamus, cerebellum and pons regions of brain (Demir et al., 2020). In another

study, reduced expression of myelin basic protein was detected in Tay-Sachs and Sandhoff disease mice model cerebellar region of brain (Myerowitz, 2002). According to these findings, decreased number of oligodendrocytes can be correlated with increasing neurodegeneration, and neuronal cell death.

Immunohistochemical staining of 2- and 5-month-old *Neu1-/-* mice cortex, thalamus, hippocampus and cerebellum regions of brain was performed with anti-Moma-2. In the Figure 3.38E, active microglial cell number was increased in only 2-month-old *Neu1-/-* cortex, compared to *WT*. In thalamus region, microglia cell density was increased in both 2- and 5-month-old *Neu1-/-* mice in comparison to *WT*; and microglial cell number was remarkably decreased in 5-month-old *Neu1-/-* compared to younger group (Figure 3.38F). In hippocampus region, activated microglia cell number were increased in 2-month-old *Neu1-/-* compared to *WT*, and 5-month-old *Neu1-/-* mice had reduced number of reactive microglial cells than younger *Neu1-/-* (Figure 3.38G). In the cerebellum region of both 2 and 5-month-old *Neu1-/-* mice, reactive microglia number was significantly elevated in comparison to *WT*, and increasing number of activated microglial cells were shown in 5-month-old *Neu1-/-* than younger group (Figure 38H). Moma-2 immunohistochemistry is one of the most useful methods for identification of monocytes, and macrophages in specific tissues, and microglial cells are the resident macrophages which can be monitored in anti-Moma-2 antibody. Previously, it was shown that increasing intensity of Moma-2 in the cortex of the 14-month-old MPS I, and 3-months-old MPS IIIB mouse models supported the presence of active inflammatory response (Ohmi et al., 2003). Another study concluded that increasing number of Moma-2-positive cells in 5-month-old Tay-Sachs mice model cortex, hippocampus, thalamus, cerebellum, and pons regions of the brain (Demir et al., 2020). In this study, increasing number of Moma-2 intensity can be linked to increasing expression of pro-inflammatory cytokines, and accumulated glycoconjugates in the different sections of brain, besides these findings, neuronal cell death can be resulted from the elevated numbers of reactive astrocytes, and microglial cells.

In this day, deficiency/mutation in certain enzymes or their activator/transporter proteins result in the accumulation of specific biomolecules which are the targets of these defined enzymes and leading to impairment in the lipid metabolism and accumulation of the secondary lipids due to the breakdown of the lysosomal integrity, and results with lysosomal storage diseases (Samie & Xu, 2014). Impaired degradation of lipid molecules results with the primary disorder in lipidomics, and additionally alterations in secondary

lipids is defined in several lysosomal storage diseases (primary disorders) (Samie & Xu, 2014; Vruchte et al., 2004). Sialidosis is a glycoprotein disease is one of the lysosomal storage diseases, and inheritance occurs with autosomal recessive manner. Sialidosis is caused from the Neuraminiadase 1 enzyme deficiency, and oligosaccharides with sialic acid residues, glycosphingolipids, and glycoproteins accumulates gradually in lysosomes of the cells (Seyrantepe et al., 2003). Sialidosis patients are diagnosed with the accumulated biomarkers of the disease in urine and body fluid samples (Van Pelt et al., 1988). Sialidosis separated to two onsets; based on severity of disease symptoms, and onset of the age; Type I Sialiodosis (late, mild, nonneuropathic form) and Type II (early, dysmorphic) Sialidosis (Seyrantepe et al., 2003; Van Pelt et al., 1988). Accumulated gangliosides (GD3, GM3, GM4 and LM1) in patients' visceral organs is identified (Breiden & Sandhoff, 2020). Many lysosomal diseases demonstrated elevated levels of neuroinflammatory markers and activated microgliosis and astrogliosis due to the impairment of lysosomal degradation (Bosch & Kielian, 2015). In this study, remarkable decrease was indicated in nearly PC, PE, PE O-, PA, PC O-, PI, LPE, and LPS glycerophospholipid levels (Figure 3.2C) of 2-month-old *Neu1-/-* mice cortex in comparison to age matched *WT* mice. Besides, PC, PA and PI glycerophospholipid levels were significantly increased in 5-month-old *Neu1-/-* mice cortex in comparison to younger mice cortex tissue, and any significant alterations in secondary lipid metabolism is not detected in cerebellum tissues of both 2- and 5-month-old *Neu1-/-*. Increasing levels of pro-inflammatory cytokines in cortex, cerebellum, kidney and spleen tissues of 2- and 5-month-old *Neu1-/-* mice, and decreased expression levels of anti-inflammatory chemokines were shown in cortex, cerebellum, kidney, and spleen tissues by gene expression analyses; these findings indicate the presence of inflammation. Morphological changes in cortex, hippocampus, thalamus, and cerebellum regions of brain, glomeruli and tubuli regions of kidney, and white and red pulp regions of spleen tissues were identified with edema, dilation of vessels, and vacuolization in 2- and 5-month-old *Neu1-/-* mice with H&E staining. Glycoconjugate accumulations in cortex, hippocampus, thalamus, and cerebellum regions of brain, glomeruli and tubuli regions of kidney, and white and red pulp regions of spleen tissues 2- and 5-month-old *Neu1-/-* mice were monitored by PAS staining. Toluidine Blue staining indicated axonal degeneration, and presence of mast cells in cortex, hippocampus, thalamus, and cerebellum regions of brain, glomeruli and tubuli regions of kidney, and white and red pulp regions of spleen tissues 2- and 5-month-old *Neu1-/-* mice. Increasing levels of astrogliosis and microgliosis were

monitored in cortex, hippocampus, thalamus, and cerebellum regions of brain, while decreasing levels of neuronal cells, and oligodendrocytes was obtained in 2- and 5-month-old *Neu1-/-* mice. Decreased levels of anti-inflammatory glycerophospholipids may be indicative of inflammatory response in all age groups of *Neu1-/-* mice models.

CHAPTER 5

CONCLUSION

Sialidase 1 is found in lysosomes of the cell, and its gene expression is identified in all tissues throughout the humans, but expression levels are different from each other; highest expression is shown in pancreas, and low expression is seen in the brain. Neu1 expression differ in tissue-specific manner, highest levels of Neu1 expression are defined in kidney and pancreas tissues, and less expression is observed in brain, and spinal cord, and lowest expression is in liver, spleen and lung tissues of mice. Previously created Neu1 mice model mimics the Type II sialidosis patient characteristics. This Neu1 deficient mice model has hepatosplenomegaly, severe degeneration in kidneys, impairments in neurological status, defects in spinal cord, and accumulation of oligosaccharides in urine samples. In this study, lipidomic, gene expression analyses, histopathological, and immunohistochemical analyses were performed to find out the altered secondary lipid metabolism and regulation of inflammatory response in 2- and 5-month-old *Neu1-/-* mice brain, kidney and spleen tissues. Decreasing levels of anti-inflammatory glycerophospholipids, phosphatidylcholine, phosphatidylethanolamine, and phosphatidylinositol can be related with elevated levels of pro-inflammatory chemokines such as Ccl2, Ccl3, Cxcl10. Glycoconjugate accumulation, presence of mast cells, degeneration and vacuolization were obtained in the brain, spleen and kidney tissues of 2- and 5-month-old *Neu1-/-* mice. Astrogliosis and microgliosis were defined in cortex, thalamus, hippocampus and cerebellum regions of the 2- and 5-month-old *Neu1-/-* mice model and because of the neuroinflammation, neurodegeneration, neuronal and oligodendrocyte cell death were shown.

Based on these findings, Neu1 deficiency showed altered levels of glycerophospholipid, and expression of inflammatory mediator biomolecules in 2- and 5-month-old mice tissues. Changes in secondary lipid metabolism and inflammatory response may be linked and is crucial to understand the pathogenesis of sialidosis.

5.1. Future Directions

In this thesis study, pathogenesis, altered lipid metabolism, and presence of inflammatory response was shown. Besides that, for understanding and finding out the association of the role of Neu1 in secondary lipid alteration, and inflammatory response *in vitro* studies may be performed. In previous research papers, reduced expression levels of Neu1 were shown, correspondingly elevated levels of GM3 ganglioside were monitored in decreased Neu1 sialidase activity in highly metastatic mice cancer cells (Sawada et al., 2002). In another study, it was proposed that GM3 ganglioside is one of the substrates of lysosomal sialidase in vitro, but later studies demonstrated that all Neu1 deficient cells are not observed with accumulation of GM3 ganglioside (Aerts et al., 2019; Fingerhut et al., 1992). Additionally, in Neu1-/- mice model brain, degenerated microglial cells, and macrophages were monitored. Based on these earlier studies, investigation of lipid profile, and inflammation in vitro studies such as neuroglial and fibroblast cell cultures of *Neu1-/-* mice can be crucial for comprehending the correlation of in vivo studies. Furthermore, exploration of changes in secondary lipid metabolism, and inflammatory response in vivo and in vitro studies can be providing insights for further therapeutic approaches for patients who suffers from the sialidosis. In the results of this study, remarkable reduction was shown in glycerophospholipids, and glycolipids in 2-month-old cortex region of *Neu1-/-* brain in comparison to age-matched *WT*. Decreasing levels of these lipid molecules were linked to elevated levels of cytokine/chemokine production, and presence of inflammation. Based on this relationship, altered glycerophospholipids, and glycolipids can be targeted by using lipid activators or inhibitors of specific enzymes for elimination of lipidomic content alterations and alleviation of inflammatory response.

As a brief summary, all of the findings of this thesis study present that secondary lipid alterations, and inflammatory response relationship in the deficiency of Neu1, and this link may be considered as new therapeutic strategy for lessening of Sialidosis pathogenesis by using inhibitor/activators of altered lipidomic profile.

REFERENCES

Abdulkhalek, S., Amith, S. R., Franchuk, S. L., Jayanth, P., Guo, M., Finlay, T., Gilmour, A., Guzzo, C., Gee, K., Beyaert, R., & Szewczuk, M. R. (2011). Neu1 Sialidase and Matrix Metalloproteinase-9 Cross-talk Is Essential for Toll-like Receptor Activation and Cellular Signaling. *Journal of Biological Chemistry*, *286*(42), 36532–36549. https://doi.org/10.1074/jbc.M111.237578

Aerts, J. M. F. G., Kuo, C.-L., Lelieveld, L. T., Boer, D. E. C., van der Lienden, M. J. C., Overkleeft, H. S., & Artola, M. (2019). Glycosphingolipids and lysosomal storage disorders as illustrated by gaucher disease. *Current Opinion in Chemical Biology*, *53*, 204–215. https://doi.org/10.1016/j.cbpa.2019.10.006

Ai, R., Xu, J., Ji, G., & Cui, B. (2022). Exploring the Phosphatidylcholine in Inflammatory Bowel Disease: Potential Mechanisms and Therapeutic Interventions. *Current Pharmaceutical Design*, *28*(43), 3486–3491. https://doi.org/10.2174/1381612829666221124112803

Amith, S. R., Jayanth, P., Franchuk, S., Finlay, T., Seyrantepe, V., Beyaert, R., Pshezhetsky, A. V., & Szewczuk, M. R. (2010). Neu1 desialylation of sialyl α-2,3-linked β-galactosyl residues of TOLL-like receptor 4 is essential for receptor activation and cellular signaling. *Cellular Signalling*, *22*(2), 314–324. https://doi.org/10.1016/j.cellsig.2009.09.038

Annunziata, I., Patterson, A., Helton, D., Hu, H., Moshiach, S., Gomero, E., Nixon, R., & d'Azzo, A. (2013). Lysosomal NEU1 deficiency affects amyloid precursor protein levels and amyloid-β secretion via deregulated lysosomal exocytosis. *Nature Communications*, *4*(1), 2734. https://doi.org/10.1038/ncomms3734

Bachiller, S., Jiménez-Ferrer, I., Paulus, A., Yang, Y., Swanberg, M., Deierborg, T., & Boza-Serrano, A. (2018). Microglia in Neurological Diseases: A Road Map to Brain-Disease Dependent-Inflammatory Response. *Frontiers in Cellular Neuroscience*, *12*. https://doi.org/10.3389/fncel.2018.00488

Ballabio, A., & Bonifacino, J. S. (2020). Lysosomes as dynamic regulators of cell and organismal homeostasis. *Nature Reviews Molecular Cell Biology*, *21*(2), 101–118. https://doi.org/10.1038/s41580-019-0185-4

Bao, N., Fu, B., Zhong, X., Jia, S., Ren, Z., Wang, H., Wang, W., Shi, H., Li, J., Ge, F., Chang, Q., Gong, Y., Liu, W., Qiu, F., Xu, S., & Li, T. (2023). Role of the CXCR6/CXCL16 axis in autoimmune diseases. *International Immunopharmacology*, *121*, 110530. https://doi.org/10.1016/j.intimp.2023.110530

Baraban, E., Chavakis, T., Hamilton, B. S., Sales, S., Wabitsch, M., Bornstein, S. R., & Ehrhart-Bornstein, M. (2016). Anti-inflammatory properties of bone morphogenetic protein 4 in human adipocytes. *International Journal of Obesity*, *40*(2), 319–327. https://doi.org/10.1038/ijo.2015.141

Bellettato, C. M., & Scarpa, M. (2010). Pathophysiology of neuropathic lysosomal storage disorders. *Journal of Inherited Metabolic Disease*, *33*(4), 347–362. https://doi.org/10.1007/s10545-010-9075-9

Beltroy, E. P., Liu, B., Dietschy, J. M., & Turley, S. D. (2007). Lysosomal unesterified cholesterol content correlates with liver cell death in murine Niemann-Pick type C disease. *Journal of Lipid Research*, *48*(4), 869–881. https://doi.org/10.1194/jlr.M600488-JLR200

Ben-Baruch, A., Xu, L., Young, P. R., Bengali, K., Oppenheim, J. J., & Wang, J. M. (1995). Monocyte Chemotactic Protein-3 (MCP3) Interacts with Multiple Leukocyte Receptors. *Journal of Biological Chemistry*, *270*(38), 22123–22128. https://doi.org/10.1074/jbc.270.38.22123

Bhavsar, I., Miller, C. S., & Al-Sabbagh, M. (2015). *Macrophage Inflammatory Protein-1 Alpha (MIP-1 alpha)/CCL3: As a Biomarker* (pp. 223–249). https://doi.org/10.1007/978-94-007-7696-8_27

Bobillo Lobato, J., Jiménez Hidalgo, M., & Jiménez Jiménez, L. (2016). Biomarkers in Lysosomal Storage Diseases. *Diseases*, *4*(4), 40. https://doi.org/10.3390/diseases4040040

Bonten, E., van der Spoel, A., Fornerod, M., Grosveld, G., & d'Azzo, A. (1996). Characterization of human lysosomal neuraminidase defines the molecular basis of the metabolic storage disorder sialidosis. *Genes & Development*, *10*(24), 3156–3169. https://doi.org/10.1101/gad.10.24.3156

Borodzicz, S., Czarzasta, K., Kuch, M., & Cudnoch-Jedrzejewska, A. (2015). Sphingolipids in cardiovascular diseases and metabolic disorders. *Lipids in Health and Disease*, *14*(1), 55. https://doi.org/10.1186/s12944-015-0053-y

Bosch, M. E., & Kielian, T. (2015). Neuroinflammatory paradigms in lysosomal storage diseases. *Frontiers in Neuroscience*, *9*. https://doi.org/10.3389/fnins.2015.00417

Bosè, F., Petti, L., Diani, M., Moscheni, C., Molteni, S., Altomare, A., Rossi, R. L., Talarico, D., Fontana, R., Russo, V., Altomare, G., & Reali, E. (2013). Inhibition of CCR7/CCL19 Axis in Lesional Skin Is a Critical Event for Clinical Remission Induced by TNF Blockade in Patients with Psoriasis. *The American Journal of Pathology*, *183*(2), 413–421. https://doi.org/10.1016/j.ajpath.2013.04.021

Boustany, R.-M. N. (2013). Lysosomal storage diseases—the horizon expands. *Nature Reviews Neurology*, *9*(10), 583–598. https://doi.org/10.1038/nrneurol.2013.163

Breiden, B., & Sandhoff, K. (2020a). Mechanism of Secondary Ganglioside and Lipid Accumulation in Lysosomal Disease. *International Journal of Molecular Sciences*, *21*(7), 2566. https://doi.org/10.3390/ijms21072566

Breiden, B., & Sandhoff, K. (2020b). Mechanism of Secondary Ganglioside and Lipid Accumulation in Lysosomal Disease. *International Journal of Molecular Sciences*, *21*(7), 2566. https://doi.org/10.3390/ijms21072566

Breiden, B., & Sandhoff, K. (2020c). Mechanism of Secondary Ganglioside and Lipid Accumulation in Lysosomal Disease. *International Journal of Molecular Sciences*, *21*(7), 2566. https://doi.org/10.3390/ijms21072566

Brodie, C., Goldreich, N., Haiman, T., & Kazimirsky, G. (1998). Functional IL-4 receptors on mouse astrocytes: IL-4 inhibits astrocyte activation and induces NGF secretion. *Journal of Neuroimmunology*, *81*(1–2), 20–30. https://doi.org/10.1016/S0165-5728(97)00154-9

Burgaletto, C., Platania, C. B. M., Di Benedetto, G., Munafò, A., Giurdanella, G., Federico, C., Caltabiano, R., Saccone, S., Conti, F., Bernardini, R., Bucolo, C., & Cantarella, G. (2021). Targeting the miRNA-155/TNFSF10 network restrains inflammatory response in the retina in a mouse model of Alzheimer's disease. *Cell Death & Disease*, *12*(10), 905. https://doi.org/10.1038/s41419-021-04165-x

Caciotti, A., Melani, F., Tonin, R., Cellai, L., Catarzi, S., Procopio, E., Chilleri, C., Mavridou, I., Michelakakis, H., Fioravanti, A., d'Azzo, A., Guerrini, R., & Morrone, A. (2020). Type I sialidosis, a normosomatic lysosomal disease, in the differential diagnosis of late-onset ataxia and myoclonus: An overview. *Molecular Genetics and Metabolism*, *129*(2), 47–58. https://doi.org/10.1016/j.ymgme.2019.09.005

Can, M., Sengül, T., Demir, S. A., İnci, O. K., Basırlı, H., & Seyrantepe, V. (2022). Analysis of Brain Lipids in the Early-Onset Tay–Sachs Disease Mouse Model With the Combined Deficiency of β-Hexosaminidase A and Neuraminidase 3. *Frontiers in Molecular Biosciences*, *9*. https://doi.org/10.3389/fmolb.2022.892248

Cermenati, G., Mitro, N., Audano, M., Melcangi, R. C., Crestani, M., De Fabiani, E., & Caruso, D. (2015). Lipids in the nervous system: From biochemistry and molecular biology to patho-physiology. *Biochimica et Biophysica Acta (BBA) - Molecular and Cell Biology of Lipids*, *1851*(1), 51–60. https://doi.org/10.1016/j.bbalip.2014.08.011

Chandrasekar, B., Bysani, S., & Mummidi, S. (2004). CXCL16 Signals via Gi, Phosphatidylinositol 3-Kinase, Akt, IκB Kinase, and Nuclear Factor-κB and Induces Cell-Cell Adhesion and Aortic Smooth Muscle Cell Proliferation. *Journal of Biological Chemistry*, *279*(5), 3188–3196. https://doi.org/10.1074/jbc.M311660200

Chen, G.-Y., Brown, N. K., Wu, W., Khedri, Z., Yu, H., Chen, X., van de Vlekkert, D., D'Azzo, A., Zheng, P., & Liu, Y. (2014). Broad and direct interaction between TLR and Siglec families of pattern recognition receptors and its regulation by Neu1. *ELife*, *3*. https://doi.org/10.7554/eLife.04066

Chen, X. P., Enioutina, E. Y., & Daynes, R. A. (1997). The control of IL-4 gene expression in activated murine T lymphocytes: a novel role for neu-1 sialidase. *Journal of Immunology (Baltimore, Md. : 1950)*, *158*(7), 3070–3080.

Chen, Y., Qin, C., Huang, J., Tang, X., Liu, C., Huang, K., Xu, J., Guo, G., Tong, A., & Zhou, L. (2020). The role of astrocytes in oxidative stress of central nervous system: A mixed blessing. *Cell Proliferation*, *53*(3). https://doi.org/10.1111/cpr.12781

Cheng-Sánchez, I., & Sarabia, F. (2018). Chemistry and Biology of Bioactive Glycolipids of Marine Origin. *Marine Drugs*, *16*(9), 294. https://doi.org/10.3390/md16090294

Clarke, J., Kayatekin, C., Viel, C., Shihabuddin, L., & Sardi, S. P. (2021). Murine Models of Lysosomal Storage Diseases Exhibit Differences in Brain Protein Aggregation and Neuroinflammation. *Biomedicines*, *9*(5), 446. https://doi.org/10.3390/biomedicines9050446

Coet, T., Suzuki, K., Popko, B., Suzuki, K., Popko, B., Suzuki, K., & Popko, B. (1998). New perspectives on the function of myelin galactolipids. *Trends in Neurosciences*, *21*(3), 126–130. https://doi.org/10.1016/S0166-2236(97)01178-8

Colonna, M., & Butovsky, O. (2017). Microglia Function in the Central Nervous System During Health and Neurodegeneration. *Annual Review of Immunology*, *35*(1), 441–468. https://doi.org/10.1146/annurev-immunol-051116-052358

Conzelmann, E., & Sandhoff, K. (1983). Partial Enzyme Deficiencies: Residual Activities and the Development of Neurological Disorders. *Developmental Neuroscience*, *6*(1), 58–71. https://doi.org/10.1159/000112332

Cross, A. S., Sakarya, S., Rifat, S., Held, T. K., Drysdale, B.-E., Grange, P. A., Cassels, F. J., Wang, L.-X., Stamatos, N., Farese, A., Casey, D., Powell, J., Bhattacharjee, A. K., Kleinberg, M., & Goldblum, S. E. (2003). Recruitment of Murine Neutrophils in Vivothrough Endogenous Sialidase Activity. *Journal of Biological Chemistry*, *278*(6), 4112–4120. https://doi.org/10.1074/jbc.M207591200

D'Angelo, G., Capasso, S., Sticco, L., & Russo, D. (2013). Glycosphingolipids: synthesis and functions. *FEBS Journal*, *280*(24), 6338–6353. https://doi.org/10.1111/febs.12559

D'Azzo, A., Hoogeveen, A., Reuser, A. J., Robinson, D., & Galjaard, H. (1982). Molecular defect in combined beta-galactosidase and neuraminidase deficiency in man. *Proceedings of the National Academy of Sciences*, *79*(15), 4535–4539. https://doi.org/10.1073/pnas.79.15.4535

D'Azzo, A., Machado, E., & Annunziata, I. (2015). Pathogenesis, emerging therapeutic targets and treatment in sialidosis. *Expert Opinion on Orphan Drugs*, *3*(5), 491–504. https://doi.org/10.1517/21678707.2015.1025746

de Geest, N. (2002). Systemic and neurologic abnormalities distinguish the lysosomal disorders sialidosis and galactosialidosis in mice. *Human Molecular Genetics*, *11*(12), 1455–1464. https://doi.org/10.1093/hmg/11.12.1455

Demir, S. A., Timur, Z. K., Ateş, N., Martínez, L. A., & Seyrantepe, V. (2020a). GM2 ganglioside accumulation causes neuroinflammation and behavioral alterations in a mouse model of early onset Tay-Sachs disease. *Journal of Neuroinflammation*, *17*(1), 277. https://doi.org/10.1186/s12974-020-01947-6

Demir, S. A., Timur, Z. K., Ateş, N., Martínez, L. A., & Seyrantepe, V. (2020b). GM2 ganglioside accumulation causes neuroinflammation and behavioral alterations in a mouse model of early onset Tay-Sachs disease. *Journal of Neuroinflammation*, *17*(1), 277. https://doi.org/10.1186/s12974-020-01947-6

Deshmane, S. L., Kremlev, S., Amini, S., & Sawaya, B. E. (2009). Monocyte Chemoattractant Protein-1 (MCP-1): An Overview. *Journal of Interferon & Cytokine Research*, *29*(6), 313–326. https://doi.org/10.1089/jir.2008.0027

Dhaeze, T., Tremblay, L., Lachance, C., Peelen, E., Zandee, S., Grasmuck, C., Bourbonnière, L., Larouche, S., Ayrignac, X., Rébillard, R.-M., Poirier, J., Lahav, B., Duquette, P., Girard, M., Moumdjian, R., Bouthillier, A., Larochelle, C., & Prat, A. (2019). CD70 defines a subset of proinflammatory and CNS-pathogenic TH1/TH17 lymphocytes and is overexpressed in multiple sclerosis. *Cellular & Molecular Immunology*, *16*(7), 652–665. https://doi.org/10.1038/s41423-018-0198-5

Ding, Z.-B., Song, L.-J., Wang, Q., Kumar, G., Yan, Y.-Q., & Ma, C.-G. (2021). Astrocytes: a double-edged sword in neurodegenerative diseases. *Neural Regeneration Research*, *16*(9), 1702. https://doi.org/10.4103/1673-5374.306064

Dioszeghy, V., Rosas, M., Maskrey, B. H., Colmont, C., Topley, N., Chaitidis, P., Kühn, H., Jones, S. A., Taylor, P. R., & O'Donnell, V. B. (2008). 12/15-Lipoxygenase Regulates the Inflammatory Response to Bacterial Products In Vivo. *The Journal of Immunology*, *181*(9), 6514–6524. https://doi.org/10.4049/jimmunol.181.9.6514

DiSabato, D. J., Quan, N., & Godbout, J. P. (2016). Neuroinflammation: the devil is in the details. *Journal of Neurochemistry*, *139*(S2), 136–153. https://doi.org/10.1111/jnc.13607

Donninelli, G., Saraf-Sinik, I., Mazziotti, V., Capone, A., Grasso, M. G., Battistini, L., Reynolds, R., Magliozzi, R., & Volpe, E. (2020). Interleukin-9 regulates macrophage activation in the progressive multiple sclerosis brain. *Journal of Neuroinflammation*, *17*(1), 149. https://doi.org/10.1186/s12974-020-01770-z

Dridi, L., Seyrantepe, V., Fougerat, A., Pan, X., Bonneil, É., Thibault, P., Moreau, A., Mitchell, G. A., Heveker, N., Cairo, C. W., Issad, T., Hinek, A., & Pshezhetsky, A. V. (2013). Positive Regulation of Insulin Signaling by Neuraminidase 1. *Diabetes*, *62*(7), 2338–2346. https://doi.org/10.2337/db12-1825

Ellingsen, T., Hansen, I., Thorsen, J., Møller, B., Tarp, U., Lottenburger, T., Andersen, L., Skjødt, H., Pedersen, J., Lauridsen, U., Svendsen, A., Lindegaard, H., Jacobsen, S., Østergaard, M., Vestergaard, A., Jurik, A., Junker, P., Christensen, A., Hetland, M., … Stengaard-Pedersen, K. (2014). Upregulated baseline plasma CCL19 and CCR7 cell-surface expression on monocytes in early rheumatoid arthritis normalized during treatment and CCL19 correlated with radiographic progression. *Scandinavian Journal of Rheumatology*, *43*(2), 91–100. https://doi.org/10.3109/03009742.2013.803149

Elmore, M. R. P., Hohsfield, L. A., Kramár, E. A., Soreq, L., Lee, R. J., Pham, S. T., Najafi, A. R., Spangenberg, E. E., Wood, M. A., West, B. L., & Green, K. N. (2018). Replacement of microglia in the aged brain reverses cognitive, synaptic, and neuronal deficits in mice. *Aging Cell*, *17*(6). https://doi.org/10.1111/acel.12832

Fan, H., Lu, B., Cao, C., Li, H., Yang, D., Huang, L., Ding, T., Wu, M., & Lu, G. (2021). Plasma TNFSF13B and TNFSF14 Function as Inflammatory Indicators of Severe

Adenovirus Pneumonia in Pediatric Patients. *Frontiers in Immunology*, *11*. https://doi.org/10.3389/fimmu.2020.614781

Farfel-Becker, T., Vitner, E. B., Kelly, S. L., Bame, J. R., Duan, J., Shinder, V., Merrill, A. H., Dobrenis, K., & Futerman, A. H. (2014). Neuronal accumulation of glucosylceramide in a mouse model of neuronopathic Gaucher disease leads to neurodegeneration. *Human Molecular Genetics*, *23*(4), 843–854. https://doi.org/10.1093/hmg/ddt468

Ferreira, C. R., & Gahl, W. A. (2017). Lysosomal storage diseases. *Translational Science of Rare Diseases*, *2*(1–2), 1–71. https://doi.org/10.3233/TRD-160005

Ford, J., Hughson, A., Lim, K., Bardina, S. V., Lu, W., Charo, I. F., Lim, J. K., & Fowell, D. J. (2019). CCL7 Is a Negative Regulator of Cutaneous Inflammation Following Leishmania major Infection. *Frontiers in Immunology*, *9*. https://doi.org/10.3389/fimmu.2018.03063

Frisch, A., & Neufeld, E. F. (1979). A rapid and sensitive assay for neuraminidase: Application to cultured flbroblasts. *Analytical Biochemistry*, *95*(1), 222–227. https://doi.org/10.1016/0003-2697(79)90209-4

Fu, L., Inui, K., Nishigaki, T., Tatsumi, N., Tsukamoto, H., Kokubu, C., Muramatsu, T., & Okada, S. (1999). Molecular heterogeneity of Krabbe disease. *Journal of Inherited Metabolic Disease*, *22*(2), 155–162. https://doi.org/10.1023/A:1005449919660

Fuller, M., & Futerman, A. H. (2018a). The brain lipidome in neurodegenerative lysosomal storage disorders. *Biochemical and Biophysical Research Communications*, *504*(3), 623–628. https://doi.org/10.1016/j.bbrc.2018.03.042

Fuller, M., & Futerman, A. H. (2018b). The brain lipidome in neurodegenerative lysosomal storage disorders. *Biochemical and Biophysical Research Communications*, *504*(3), 623–628. https://doi.org/10.1016/j.bbrc.2018.03.042

Funakoshi, Y., & Suzuki, T. (2009). Glycobiology in the cytosol: The bitter side of a sweet world. *Biochimica et Biophysica Acta (BBA) - General Subjects*, *1790*(2), 81–94. https://doi.org/10.1016/j.bbagen.2008.09.009

Futerman, A. H., & van Meer, G. (2004). The cell biology of lysosomal storage disorders. *Nature Reviews Molecular Cell Biology*, *5*(7), 554–565. https://doi.org/10.1038/nrm1423

Gadani, S. P., Cronk, J. C., Norris, G. T., & Kipnis, J. (2012). IL-4 in the Brain: A Cytokine To Remember. *The Journal of Immunology*, *189*(9), 4213–4219. https://doi.org/10.4049/jimmunol.1202246

Gros, F., & Muller, S. (2023). The role of lysosomes in metabolic and autoimmune diseases. *Nature Reviews Nephrology*, *19*(6), 366–383. https://doi.org/10.1038/s41581-023-00692-2

Guo, S., Wang, H., & Yin, Y. (2022). Microglia Polarization From M1 to M2 in Neurodegenerative Diseases. *Frontiers in Aging Neuroscience*, *14*. https://doi.org/10.3389/fnagi.2022.815347

Gusel'nikova, V. V., & Korzhevskiy, D. E. (2015). NeuN As a Neuronal Nuclear Antigen and Neuron Differentiation Marker. *Acta Naturae*, *7*(2), 42–47. https://doi.org/10.32607/20758251-2015-7-2-42-47

Hafez, H. M., Abdel-Hakeem, E. A., & Hassanein, H. (2020). Rupatadine, a dual antagonist of histamine and platelet-activating factor (PAF), attenuates experimentally induced diabetic nephropathy in rats. *Naunyn-Schmiedeberg's Archives of Pharmacology*, *393*(8), 1487–1500. https://doi.org/10.1007/s00210-020-01856-8

Hao, T., Fang, W., Xu, D., Chen, Q., Liu, Q., Cui, K., Cao, X., Li, Y., Mai, K., & Ai, Q. (2023). Phosphatidylethanolamine alleviates OX-LDL-induced macrophage inflammation by upregulating autophagy and inhibiting NLRP1 inflammasome activation. *Free Radical Biology and Medicine*, *208*, 402–417. https://doi.org/10.1016/j.freeradbiomed.2023.08.031

He, X., Ma, J., Wang, H., Hu, T., Sun, B., Gao, Y., Liu, S., Wang, W., & Wang, P. (2017). Brain injury in combination with tacrolimus promotes the regeneration of injured peripheral nerves. *Neural Regeneration Research*, *12*(6), 987. https://doi.org/10.4103/1673-5374.208595

Hinek, A., Pshezhetsky, A. V., von Itzstein, M., & Starcher, B. (2006). Lysosomal Sialidase (Neuraminidase-1) Is Targeted to the Cell Surface in a Multiprotein Complex That Facilitates Elastic Fiber Assembly. *Journal of Biological Chemistry*, *281*(6), 3698–3710. https://doi.org/10.1074/jbc.M508736200

Hishikawa, D., Hashidate, T., Shimizu, T., & Shindou, H. (2014). Diversity and function of membrane glycerophospholipids generated by the remodeling pathway in mammalian cells. *Journal of Lipid Research*, *55*(5), 799–807. https://doi.org/10.1194/jlr.R046094

Holt, O. J., Gallo, F., & Griffiths, G. M. (2006). Regulating Secretory Lysosomes. *The Journal of Biochemistry*, *140*(1), 7–12. https://doi.org/10.1093/jb/mvj126

Hu, S., Sheng, W. S., Peterson, P. K., & Chao, C. C. (1995). Differential regulation by cytokines of human astrocyte nitric oxide production. *Glia*, *15*(4), 491–494. https://doi.org/10.1002/glia.440150412

Hung, N. D., Kim, M. R., & Sok, D. (2011). 2-Polyunsaturated Acyl Lysophosphatidylethanolamine Attenuates Inflammatory Response in Zymosan A-Induced Peritonitis in Mice. *Lipids*, *46*(10). https://doi.org/10.1007/s11745-011-3589-2

Igdoura, S. A., Gafuik, C., Mertineit, C., Saberi, F., Pshezhetsky, A. V., Potier, M., Trasler, J. M., & Gravel, R. A. (1998). Cloning of the cDNA and Gene Encoding Mouse Lysosomal Sialidase and Correction of Sialidase Deficiency in Human Sialidosis and Mouse SM/J Fibroblasts. *Human Molecular Genetics*, *7*(1), 115–120. https://doi.org/10.1093/hmg/7.1.115

Iqbal, J., Walsh, M. T., Hammad, S. M., & Hussain, M. M. (2017). Sphingolipids and Lipoproteins in Health and Metabolic Disorders. *Trends in Endocrinology & Metabolism*, *28*(7), 506–518. https://doi.org/10.1016/j.tem.2017.03.005

Jäkel, S., & Dimou, L. (2017). Glial Cells and Their Function in the Adult Brain: A Journey through the History of Their Ablation. *Frontiers in Cellular Neuroscience*, *11*. https://doi.org/10.3389/fncel.2017.00024

Jala, R. C. R., Vudhgiri, S., & Kumar, C. G. (2022). A comprehensive review on natural occurrence, synthesis and biological activities of glycolipids. *Carbohydrate Research*, *516*, 108556. https://doi.org/10.1016/j.carres.2022.108556

Kanda, N., Shimizu, T., Tada, Y., & Watanabe, S. (2007). IL-18 enhances IFN-γ-induced production of CXCL9, CXCL10, and CXCL11 in human keratinocytes. *European Journal of Immunology*, *37*(2), 338–350. https://doi.org/10.1002/eji.200636420

Karin, M., & Delhase, M. (2000). The IκB kinase (IKK) and NF-κB: key elements of proinflammatory signalling. *Seminars in Immunology*, *12*(1), 85–98. https://doi.org/10.1006/smim.2000.0210

Kho, I., Demina, E. P., Pan, X., Londono, I., Cairo, C. W., Sturiale, L., Palmigiano, A., Messina, A., Garozzo, D., Ung, R.-V., Mac-Way, F., Bonneil, É., Thibault, P., Lemaire, M., Morales, C. R., & Pshezhetsky, A. V. (2023). Severe kidney dysfunction in sialidosis mice reveals an essential role for neuraminidase 1 in reabsorption. *JCI Insight*, *8*(20). https://doi.org/10.1172/jci.insight.166470

Khodadadei, F., Arshad, R., Morales, D. M., Gluski, J., Marupudi, N. I., McAllister, J. P., Limbrick, D. D., & Harris, C. A. (2022). The effect of A1 and A2 reactive astrocyte expression on hydrocephalus shunt failure. *Fluids and Barriers of the CNS*, *19*(1), 78. https://doi.org/10.1186/s12987-022-00367-3

Kim, H. Y., Cha, H. J., & Kim, H. S. (2015). CCL5 upregulates IL-10 expression and partially mediates the antihypertensive effects of IL-10 in the vascular smooth muscle cells of spontaneously hypertensive rats. *Hypertension Research*, *38*(10), 666–674. https://doi.org/10.1038/hr.2015.62

Kima, P. E., Burleigh, B., & Andrews, N. W. (2000). Surface-targeted lysosomal membrane glycoprotein-1 (Lamp-1) enhances lysosome exocytosis and cell invasion by Trypanosoma cruzi. *Cellular Microbiology*, *2*(6), 477–486. https://doi.org/10.1046/j.1462-5822.2000.00071.x

Kiyota, T., Okuyama, S., Swan, R. J., Jacobsen, M. T., Gendelman, H. E., & Ikezu, T. (2010). CNS expression of anti-inflammatory cytokine interleukin-4 attenuates Alzheimer's disease-like pathogenesis in APP+PS1 bigenic mice. *The FASEB Journal*, *24*(8), 3093–3102. https://doi.org/10.1096/fj.10-155317

Laranjeira, C., Sandgren, K., Kessaris, N., Richardson, W., Potocnik, A., Vanden Berghe, P., & Pachnis, V. (2011). Glial cells in the mouse enteric nervous system can undergo neurogenesis in response to injury. *Journal of Clinical Investigation*, *121*(9), 3412–3424. https://doi.org/10.1172/JCI58200

Lawrence, T. (2009). The Nuclear Factor NF- B Pathway in Inflammation. *Cold Spring Harbor Perspectives in Biology*, *1*(6), a001651–a001651. https://doi.org/10.1101/cshperspect.a001651

Li, T., Pan, J., Chen, H., Fang, Y., & Sun, Y. (2022). CXCR6-based immunotherapy in autoimmune, cancer and inflammatory infliction. *Acta Pharmaceutica Sinica B*, *12*(8), 3255–3262. https://doi.org/10.1016/j.apsb.2022.03.012

Liang, F., Seyrantepe, V., Landry, K., Ahmad, R., Ahmad, A., Stamatos, N. M., & Pshezhetsky, A. V. (2006). Monocyte Differentiation Up-regulates the Expression of the Lysosomal Sialidase, Neu1, and Triggers Its Targeting to the Plasma Membrane via Major Histocompatibility Complex Class II-positive Compartments. *Journal of Biological Chemistry*, *281*(37), 27526–27538. https://doi.org/10.1074/jbc.M605633200

Lim, H.-K., Choi, Y.-A., Park, W., Lee, T., Ryu, S. H., Kim, S.-Y., Kim, J.-R., Kim, J.-H., & Baek, S.-H. (2003). Phosphatidic Acid Regulates Systemic Inflammatory Responses by Modulating the Akt-Mammalian Target of Rapamycin-p70 S6 Kinase 1 Pathway. *Journal of Biological Chemistry*, *278*(46), 45117–45127. https://doi.org/10.1074/jbc.M303789200

Liu, T., Zhang, L., Joo, D., & Sun, S.-C. (2017). NF-κB signaling in inflammation. *Signal Transduction and Targeted Therapy*, *2*(1), 17023. https://doi.org/10.1038/sigtrans.2017.23

Liu, Y., Thalamuthu, A., Mather, K. A., Crawford, J., Ulanova, M., Wong, M. W. K., Pickford, R., Sachdev, P. S., & Braidy, N. (2021). Plasma lipidome is dysregulated in Alzheimer's disease and is associated with disease risk genes. *Translational Psychiatry*, *11*(1), 344. https://doi.org/10.1038/s41398-021-01362-2

Liu, Y., Zhang, Y., Zheng, X., Fang, T., Yang, X., Luo, X., Guo, A., Newell, K. A., Huang, X.-F., & Yu, Y. (2018). Galantamine improves cognition, hippocampal inflammation, and synaptic plasticity impairments induced by lipopolysaccharide in mice. *Journal of Neuroinflammation*, *15*(1), 112. https://doi.org/10.1186/s12974-018-1141-5

Lloyd-Evans, E., Morgan, A. J., He, X., Smith, D. A., Elliot-Smith, E., Sillence, D. J., Churchill, G. C., Schuchman, E. H., Galione, A., & Platt, F. M. (2008). Niemann-Pick disease type C1 is a sphingosine storage disease that causes deregulation of lysosomal calcium. *Nature Medicine*, *14*(11), 1247–1255. https://doi.org/10.1038/nm.1876

Loetscher, M., Gerber, B., Loetscher, P., Jones, S. A., Piali, L., Clark-Lewis, I., Baggiolini, M., & Moser, B. (1996). Chemokine receptor specific for IP10 and mig: structure, function, and expression in activated T-lymphocytes. *The Journal of Experimental Medicine*, *184*(3), 963–969. https://doi.org/10.1084/jem.184.3.963

Lukong, K. E., Seyrantepe, V., Landry, K., Trudel, S., Ahmad, A., Gahl, W. A., Lefrancois, S., Morales, C. R., & Pshezhetsky, A. V. (2001). Intracellular Distribution of Lysosomal Sialidase Is Controlled by the Internalization Signal in Its Cytoplasmic

Tail. *Journal of Biological Chemistry*, *276*(49), 46172–46181. https://doi.org/10.1074/jbc.M104547200

Lund, S. A., Giachelli, C. M., & Scatena, M. (2009). The role of osteopontin in inflammatory processes. *Journal of Cell Communication and Signaling*, *3*(3–4), 311–322. https://doi.org/10.1007/s12079-009-0068-0

Lupia, E., Capuano, M., Vizio, B., Schiavello, M., Bosco, O., Gelardi, M., Favale, E., Pivetta, E., Morello, F., Husain, S., Keshavjee, S., Del Sorbo, L., & Montrucchio, G. (2022). Thrombopoietin participates in platelet activation in COVID-19 patients. *EBioMedicine*, *85*, 104305. https://doi.org/10.1016/j.ebiom.2022.104305

Luster, A. D., & Ravetch, J. V. (1987). Biochemical characterization of a gamma interferon-inducible cytokine (IP-10). *The Journal of Experimental Medicine*, *166*(4), 1084–1097. https://doi.org/10.1084/jem.166.4.1084

Ma, W., Liu, A., Wu, X., Gao, L., Chen, J., Wu, H., Liu, M., Fan, Y., Peng, L., Yang, J., Kong, J., Li, B., Ji, Z., Dong, Y., Luo, S., Song, J., & Bao, F. (2023). The intricate role of CCL5/CCR5 axis in Alzheimer disease. *Journal of Neuropathology & Experimental Neurology*, *82*(11), 894–900. https://doi.org/10.1093/jnen/nlad071

Magesh, S., Suzuki, T., Miyagi, T., Ishida, H., & Kiso, M. (2006). Homology modeling of human sialidase enzymes NEU1, NEU3 and NEU4 based on the crystal structure of NEU2: Hints for the design of selective NEU3 inhibitors. *Journal of Molecular Graphics and Modelling*, *25*(2), 196–207. https://doi.org/10.1016/j.jmgm.2005.12.006

Mahadevan, S., Nduaguba, J. C., & Tappel, A. L. (1967). Sialidase of Rat Liver and Kidney. *Journal of Biological Chemistry*, *242*(19), 4409–4413. https://doi.org/10.1016/S0021-9258(18)99554-2

Margraf, A., & Zarbock, A. (2019). Platelets in Inflammation and Resolution. *The Journal of Immunology*, *203*(9), 2357–2367. https://doi.org/10.4049/jimmunol.1900899

Marques, R. E., Guabiraba, R., Russo, R. C., & Teixeira, M. M. (2013). Targeting CCL5 in inflammation. *Expert Opinion on Therapeutic Targets*, *17*(12), 1439–1460. https://doi.org/10.1517/14728222.2013.837886

Minami, A., Kurebayashi, Y., Takahashi, T., Otsubo, T., Ikeda, K., & Suzuki, T. (2021). The Function of Sialidase Revealed by Sialidase Activity Imaging Probe. *International Journal of Molecular Sciences*, *22*(6), 3187. https://doi.org/10.3390/ijms22063187

Mirones, I., de Prada, I., Gómez, A. M., Luque, A., Martín, R., Pérez-Jiménez, M. Á., Madero, L., García-Castro, J., & Ramírez, M. (2013). A Role for the CXCR3/CXCL10 Axis in Rasmussen Encephalitis. *Pediatric Neurology*, *49*(6), 451-457.e1. https://doi.org/10.1016/j.pediatrneurol.2013.07.019

Miyagi, T., Sagawa, J., Konno, K., Handa, S., & Tsuiki, S. (1990). Biochemical and Immunological Studies on Two Distinct Ganglioside-Hydrolyzing Sialidases from the Particulate Fraction of Rat Brain1. *The Journal of Biochemistry*, *107*(5), 787–793. https://doi.org/10.1093/oxfordjournals.jbchem.a123126

Miyagi, T., Sato, K., Hata, K., & Taniguchi, S. (1994). Metastatic potential of transformed rat 3Y1 cell lines is inversely correlated with lysosomal-type sialidase activity. *FEBS Letters*, *349*(2), 255–259. https://doi.org/10.1016/0014-5793(94)00682-2

Miyagi, T., & Tsuiki, S. (1984). Rat-liver lysosomal sialidase. *European Journal of Biochemistry*, *141*(1), 75–81. https://doi.org/10.1111/j.1432-1033.1984.tb08159.x

Miyagi, T., & Tsuiki, S. (1985). Purification and characterization of cytosolic sialidase from rat liver. *Journal of Biological Chemistry*, *260*(11), 6710–6716. https://doi.org/10.1016/S0021-9258(18)88837-8

Miyagi, T., & Yamaguchi, K. (2012). Mammalian sialidases: Physiological and pathological roles in cellular functions. *Glycobiology*, *22*(7), 880–896. https://doi.org/10.1093/glycob/cws057

Mohammad, A. N., Bruno, K. A., Hines, S., & Atwal, P. S. (2018). Type 1 sialidosis presenting with ataxia, seizures and myoclonus with no visual involvement. *Molecular Genetics and Metabolism Reports*, *15*, 11–14. https://doi.org/10.1016/j.ymgmr.2017.12.005

Monti, E., & Miyagi, T. (2012). *Structure and Function of Mammalian Sialidases* (pp. 183–208). https://doi.org/10.1007/128_2012_328

Monti, E., Preti, A., Nesti, C., & Ballabio, A. (1999). Expression of a novel human sialidase encoded by the NEU2 gene. *Glycobiology*, *9*(12), 1313–1321. https://doi.org/10.1093/glycob/9.12.1313

Mühl, H., & Pfeilschifter, J. (2003). Anti-inflammatory properties of pro-inflammatory interferon-γ. *International Immunopharmacology*, *3*(9), 1247–1255. https://doi.org/10.1016/S1567-5769(03)00131-0

Murakami, M., Taketomi, Y., Miki, Y., Sato, H., Hirabayashi, T., & Yamamoto, K. (2011). Recent progress in phospholipase A2 research: From cells to animals to humans. *Progress in Lipid Research*, *50*(2), 152–192. https://doi.org/10.1016/j.plipres.2010.12.001

Myerowitz, R. (2002). Molecular pathophysiology in Tay-Sachs and Sandhoff diseases as revealed by gene expression profiling. *Human Molecular Genetics*, *11*(11), 1343–1351. https://doi.org/10.1093/hmg/11.11.1343

Nan, X., Carubelli, I., & Stamatos, N. M. (2007). Sialidase expression in activated human T lymphocytes influences production of IFN-γ. *Journal of Leukocyte Biology*, *81*(1), 284–296. https://doi.org/10.1189/jlb.1105692

Neufeld, E. F. (1991). LYSOSOMAL STORAGE DISEASES. *Annual Review of Biochemistry*, *60*(1), 257–280. https://doi.org/10.1146/annurev.bi.60.070191.001353

Nilsson, O., & Svennerholm, L. (1982). Accumulation of Glucosylceramide and Glucosylsphingosine (Psychosine) in Cerebrum and Cerebellum in Infantile and Juvenile Gaucher Disease. *Journal of Neurochemistry*, *39*(3), 709–718. https://doi.org/10.1111/j.1471-4159.1982.tb07950.x

Ohmi, K., Greenberg, D. S., Rajavel, K. S., Ryazantsev, S., Li, H. H., & Neufeld, E. F. (2003). Activated microglia in cortex of mouse models of mucopolysaccharidoses I and IIIB. *Proceedings of the National Academy of Sciences*, *100*(4), 1902–1907. https://doi.org/10.1073/pnas.252784899

Ohmi, K., Kudo, L. C., Ryazantsev, S., Zhao, H.-Z., Karsten, S. L., & Neufeld, E. F. (2009). Sanfilippo syndrome type B, a lysosomal storage disease, is also a tauopathy. *Proceedings of the National Academy of Sciences*, *106*(20), 8332–8337. https://doi.org/10.1073/pnas.0903223106

Olga, K., Yulia, B., & Vassilios, P. (2020). The Functions of Mitochondrial 2′,3′-Cyclic Nucleotide-3′-Phosphodiesterase and Prospects for Its Future. *International Journal of Molecular Sciences*, *21*(9), 3217. https://doi.org/10.3390/ijms21093217

Olsen, A. S. B., & Færgeman, N. J. (2017). Sphingolipids: membrane microdomains in brain development, function and neurological diseases. *Open Biology*, *7*(5), 170069. https://doi.org/10.1098/rsob.170069

Oohira, T., Nagata, N., Akaboshi, I., Matsuda, I., & Naito, S. (1985). The infantile form of sialidosis type II associated with congenital adrenal hyperplasia: Possible linkage between HLA and the neuraminidase deficiency gene. *Human Genetics*, *70*(4), 341–343. https://doi.org/10.1007/BF00295374

Ouchi, N., & Walsh, K. (2007). Adiponectin as an anti-inflammatory factor. *Clinica Chimica Acta*, *380*(1–2), 24–30. https://doi.org/10.1016/j.cca.2007.01.026

Pandey, M. K., Jabre, N. A., Xu, Y.-H., Zhang, W., Setchell, K. D. R., & Grabowski, G. A. (2014). Gaucher disease: Chemotactic factors and immunological cell invasion in a mouse model. *Molecular Genetics and Metabolism*, *111*(2), 163–171. https://doi.org/10.1016/j.ymgme.2013.09.002

Papadaki, M., Rinotas, V., Violitzi, F., Thireou, T., Panayotou, G., Samiotaki, M., & Douni, E. (2019). New Insights for RANKL as a Proinflammatory Modulator in Modeled Inflammatory Arthritis. *Frontiers in Immunology*, *10*. https://doi.org/10.3389/fimmu.2019.00097

Pekny, M., & Pekna, M. (2014). Astrocyte Reactivity and Reactive Astrogliosis: Costs and Benefits. *Physiological Reviews*, *94*(4), 1077–1098. https://doi.org/10.1152/physrev.00041.2013

Pietzner, M., Kaul, A., Henning, A.-K., Kastenmüller, G., Artati, A., Lerch, M. M., Adamski, J., Nauck, M., & Friedrich, N. (2017). Comprehensive metabolic profiling of chronic low-grade inflammation among generally healthy individuals. *BMC Medicine*, *15*(1), 210. https://doi.org/10.1186/s12916-017-0974-6

Platt, F. M., Boland, B., & van der Spoel, A. C. (2012). Lysosomal storage disorders: The cellular impact of lysosomal dysfunction. *Journal of Cell Biology*, *199*(5), 723–734. https://doi.org/10.1083/jcb.201208152

Platt, F. M., d'Azzo, A., Davidson, B. L., Neufeld, E. F., & Tifft, C. J. (2018a). Lysosomal storage diseases. *Nature Reviews Disease Primers*, *4*(1), 27. https://doi.org/10.1038/s41572-018-0025-4

Platt, F. M., d'Azzo, A., Davidson, B. L., Neufeld, E. F., & Tifft, C. J. (2018b). Lysosomal storage diseases. *Nature Reviews Disease Primers*, *4*(1), 27. https://doi.org/10.1038/s41572-018-0025-4

Poswar, F. de O., Vairo, F., Burin, M., Michelin-Tirelli, K., Brusius-Facchin, A. C., Kubaski, F., Souza, C. F. M. de, Baldo, G., & Giugliani, R. (2019). Lysosomal diseases: Overview on current diagnosis and treatment. *Genetics and Molecular Biology*, *42*(1 suppl 1), 165–177. https://doi.org/10.1590/1678-4685-gmb-2018-0159

Pshezhetsky, A. V, & Ashmarina, M. (2001). *Lysosomal multienzyme complex: Biochemistry, genetics, and molecular pathophysiology* (pp. 81–114). https://doi.org/10.1016/S0079-6603(01)69045-7

Pshezhetsky, A. V., & Hinek, A. (2011). Where catabolism meets signalling: neuraminidase 1 as a modulator of cell receptors. *Glycoconjugate Journal*, *28*(7), 441–452. https://doi.org/10.1007/s10719-011-9350-5

Pshezhetsky, A. V., Richard, C., Michaud, L., Igdoura, S., Wang, S., Elsliger, M.-A., Qu, J., Leclerc, D., Gravel, R., Dallaire, L., & Potier, M. (1997). Cloning, expression and chromosomal mapping of human lysosomal sialidase and characterization of mutations in sialidosis. *Nature Genetics*, *15*(3), 316–320. https://doi.org/10.1038/ng0397-316

Reichel, C. A., Rehberg, M., Lerchenberger, M., Berberich, N., Bihari, P., Khandoga, A. G., Zahler, S., & Krombach, F. (2009). Ccl2 and Ccl3 Mediate Neutrophil Recruitment via Induction of Protein Synthesis and Generation of Lipid Mediators. *Arteriosclerosis, Thrombosis, and Vascular Biology*, *29*(11), 1787–1793. https://doi.org/10.1161/ATVBAHA.109.193268

Ritter, L. M., Bryans, M., Abdo, O., Sharma, V., & Wilkie, N. M. (1995). *MIP1* α Nuclear Protein (MNP), a Novel Transcription Factor Expressed in Hematopoietic Cells That Is Crucial for Transcription of the Human *MIP-1* α Gene. *Molecular and Cellular Biology*, *15*(6), 3110–3118. https://doi.org/10.1128/MCB.15.6.3110

Rodríguez, A., Webster, P., Ortego, J., & Andrews, N. W. (1997). Lysosomes Behave as Ca2+-regulated Exocytic Vesicles in Fibroblasts and Epithelial Cells. *The Journal of Cell Biology*, *137*(1), 93–104. https://doi.org/10.1083/jcb.137.1.93

Roy, D., & Tedeschi, A. (2021). The Role of Lipids, Lipid Metabolism and Ectopic Lipid Accumulation in Axon Growth, Regeneration and Repair after CNS Injury and Disease. *Cells*, *10*(5), 1078. https://doi.org/10.3390/cells10051078

Saito, M., Fronda, C. L., & Yu, R. K. (1996). Sialidase Activity in Nuclear Membranes of Rat Brain. *Journal of Neurochemistry*, *66*(5), 2205–2208. https://doi.org/10.1046/j.1471-4159.1996.66052205.x

Samie, M. A., & Xu, H. (2014). Lysosomal exocytosis and lipid storage disorders. *Journal of Lipid Research*, *55*(6), 995–1009. https://doi.org/10.1194/jlr.R046896

Sango, K., Yamanaka, S., Hoffmann, A., Okuda, Y., Grinberg, A., Westphal, H., McDonald, M. P., Crawley, J. N., Sandhoff, K., Suzuki, K., & Proia, R. L. (1995).

Mouse models of Tay–Sachs and Sandhoff diseases differ in neurologic phenotype and ganglioside metabolism. *Nature Genetics*, *11*(2), 170–176. https://doi.org/10.1038/ng1095-170

Sawada, M., Moriya, S., Saito, S., Shineha, R., Satomi, S., Yamori, T., Tsuruo, T., Kannagi, R., & Miyagi, T. (2002). Reduced sialidase expression in highly metastatic variants of mouse colon adenocarcinoma 26 and retardation of their metastatic ability by sialidase overexpression. *International Journal of Cancer*, *97*(2), 180–185. https://doi.org/10.1002/ijc.1598

Schmidt-Kastner, R., Wietasch, K., Weigel, H., & Eysel, U. T. (1993). Immunohistochemical staining for glial fibrillary acidic protein (GFAP) after deafferentation or ischemic infarction in rat visual system: Features of reactive and damaged astrocytes. *International Journal of Developmental Neuroscience*, *11*(2), 157–174. https://doi.org/10.1016/0736-5748(93)90076-P

Schwake, M., Schröder, B., & Saftig, P. (2013). Lysosomal Membrane Proteins and Their Central Role in Physiology. *Traffic*, *14*(7), 739–748. https://doi.org/10.1111/tra.12056

Sekijima, Y., Nakamura, K., Kishida, D., Narita, A., Adachi, K., Ohno, K., Nanba, E., & Ikeda, S. (2013). Clinical and Serial MRI Findings of a Sialidosis Type I Patient with a Novel Missense Mutation in the <i>NEU1</i> Gene. *Internal Medicine*, *52*(1), 119–124. https://doi.org/10.2169/internalmedicine.52.8901

Seyrantepe, V., Canuel, M., Carpentier, S., Landry, K., Durand, S., Liang, F., Zeng, J., Caqueret, A., Gravel, R. A., Marchesini, S., Zwingmann, C., Michaud, J., Morales, C. R., Levade, T., & Pshezhetsky, A. V. (2008). Mice deficient in Neu4 sialidase exhibit abnormal ganglioside catabolism and lysosomal storage. *Human Molecular Genetics*, *17*(11), 1556–1568. https://doi.org/10.1093/hmg/ddn043

Seyrantepe, V., Iannello, A., Liang, F., Kanshin, E., Jayanth, P., Samarani, S., Szewczuk, M. R., Ahmad, A., & Pshezhetsky, A. V. (2010a). Regulation of Phagocytosis in Macrophages by Neuraminidase 1. *Journal of Biological Chemistry*, *285*(1), 206–215. https://doi.org/10.1074/jbc.M109.055475

Seyrantepe, V., Iannello, A., Liang, F., Kanshin, E., Jayanth, P., Samarani, S., Szewczuk, M. R., Ahmad, A., & Pshezhetsky, A. V. (2010b). Regulation of Phagocytosis in Macrophages by Neuraminidase 1. *Journal of Biological Chemistry*, *285*(1), 206–215. https://doi.org/10.1074/jbc.M109.055475

Seyrantepe, V., Landry, K., Trudel, S., Hassan, J. A., Morales, C. R., & Pshezhetsky, A. V. (2004). Neu4, a Novel Human Lysosomal Lumen Sialidase, Confers Normal Phenotype to Sialidosis and Galactosialidosis Cells. *Journal of Biological Chemistry*, *279*(35), 37021–37029. https://doi.org/10.1074/jbc.M404531200

Seyrantepe, V., Poupetova, H., Froissart, R., Zabot, M.-T., Maire, I., & Pshezhetsky, A. V. (2003). Molecular pathology of NEU1 gene in sialidosis. *Human Mutation*, *22*(5), 343–352. https://doi.org/10.1002/humu.10268

Shimizu, T. (2009). Lipid Mediators in Health and Disease: Enzymes and Receptors as Therapeutic Targets for the Regulation of Immunity and Inflammation. *Annual*

Review of Pharmacology and Toxicology, *49*(1), 123–150. https://doi.org/10.1146/annurev.pharmtox.011008.145616

Shindou, H., Hishikawa, D., Harayama, T., Yuki, K., & Shimizu, T. (2009). Recent progress on acyl CoA: lysophospholipid acyltransferase research. *Journal of Lipid Research*, *50*, S46–S51. https://doi.org/10.1194/jlr.R800035-JLR200

Sidransky, E., & Lopez, G. (2012). The link between the GBA gene and parkinsonism. *The Lancet Neurology*, *11*(11), 986–998. https://doi.org/10.1016/S1474-4422(12)70190-4

Sleat, D. E., Wiseman, J. A., El-Banna, M., Price, S. M., Verot, L., Shen, M. M., Tint, G. S., Vanier, M. T., Walkley, S. U., & Lobel, P. (2004). Genetic evidence for nonredundant functional cooperativity between NPC1 and NPC2 in lipid transport. *Proceedings of the National Academy of Sciences*, *101*(16), 5886–5891. https://doi.org/10.1073/pnas.0308456101

Slotte, J. P. (2013). Biological functions of sphingomyelins. *Progress in Lipid Research*, *52*(4), 424–437. https://doi.org/10.1016/j.plipres.2013.05.001

Standiford, T. J., Kunkel, S. L., Liebler, J. M., Bur dick, M. D., Gilbert, A. R., & Strieter, R. M. (1993). Gene Expression of Macrophage Inflammatory Protein-1 *α* from Human Blood Monocytes and Alveolar Macrophages Is Inhibited by Interleukin-4. *American Journal of Respiratory Cell and Molecular Biology*, *9*(2), 192–198. https://doi.org/10.1165/ajrcmb/9.2.192

Stephenson, D. J., Hoeferlin, L. A., & Chalfant, C. E. (2017a). Lipidomics in translational research and the clinical significance of lipid-based biomarkers. *Translational Research*, *189*, 13–29. https://doi.org/10.1016/j.trsl.2017.06.006

Stephenson, D. J., Hoeferlin, L. A., & Chalfant, C. E. (2017b). Lipidomics in translational research and the clinical significance of lipid-based biomarkers. *Translational Research*, *189*, 13–29. https://doi.org/10.1016/j.trsl.2017.06.006

Sun, S.-C. (2011). Non-canonical NF-κB signaling pathway. *Cell Research*, *21*(1), 71–85. https://doi.org/10.1038/cr.2010.177

Sun, S.-C., Chang, J.-H., & Jin, J. (2013). Regulation of nuclear factor-κB in autoimmunity. *Trends in Immunology*, *34*(6), 282–289. https://doi.org/10.1016/j.it.2013.01.004

Sun, S.-C., & Liu, Z.-G. (2011). A special issue on NF-κB signaling and function. *Cell Research*, *21*(1), 1–2. https://doi.org/10.1038/cr.2011.1

Sun, Y., Koyama, Y., & Shimada, S. (2022). Inflammation From Peripheral Organs to the Brain: How Does Systemic Inflammation Cause Neuroinflammation? In *Frontiers in Aging Neuroscience* (Vol. 14). https://doi.org/10.3389/fnagi.2022.903455

Tan, W., Zhang, Q., Dong, Z., Yan, Y., Fu, Y., Liu, X., Zhao, B., & Duan, X. (2020). Phosphatidylcholine Ameliorates LPS-Induced Systemic Inflammation and Cognitive Impairments via Mediating the Gut–Brain Axis Balance. *Journal of*

Agricultural and Food Chemistry, *68*(50), 14884–14895. https://doi.org/10.1021/acs.jafc.0c06383

Tanaka, T., Narazaki, M., & Kishimoto, T. (2014). IL-6 in Inflammation, Immunity, and Disease. *Cold Spring Harbor Perspectives in Biology*, *6*(10), a016295–a016295. https://doi.org/10.1101/cshperspect.a016295

Tang, Y., & Le, W. (2016). Differential Roles of M1 and M2 Microglia in Neurodegenerative Diseases. *Molecular Neurobiology*, *53*(2), 1181–1194. https://doi.org/10.1007/s12035-014-9070-5

Tardy, C., Andrieu-Abadie, N., Salvayre, R., & Levade, T. (2004). Lysosomal Storage Diseases: Is Impaired Apoptosis a Pathogenic Mechanism? *Neurochemical Research*, *29*(5), 871–880. https://doi.org/10.1023/B:NERE.0000021232.05175.38

Tichauer, J. E., Flores, B., Soler, B., Eugenín-von Bernhardi, L., Ramírez, G., & von Bernhardi, R. (2014). Age-dependent changes on TGFβ1 Smad3 pathway modify the pattern of microglial cell activation. *Brain, Behavior, and Immunity*, *37*, 187–196. https://doi.org/10.1016/j.bbi.2013.12.018

Tilg, H., & Peschel, C. (1996). Interferon-Alpha and its Effects on the Cytokine Cascade: A Pro- and Anti-Inflammatory Cytokine. *Leukemia & Lymphoma*, *23*(1–2), 55–60. https://doi.org/10.3109/10428199609054802

Tokuyama, S., Moriya, S., Taniguchi, S., Yasui, A., Miyazaki, J., Orikasa, S., & Miyagi, T. (1997). Suppression of pulmonary metastasis in murine B16 melanoma cells by transfection of a sialidase cDNA. *International Journal of Cancer*, *73*(3), 410–415. https://doi.org/10.1002/(SICI)1097-0215(19971104)73:3<410::AID-IJC16>3.0.CO;2-G

TOURTELLOTTE, W. W., ALLEN, R. J., HAERER, A. F., & BRYAN, E. R. (1965). Study of Lipids in Cerebrospinal Fluid and Serum. *Archives of Neurology*, *12*(3), 300–310. https://doi.org/10.1001/archneur.1965.00460270076010

Treede, I., Braun, A., Sparla, R., Kühnel, M., Giese, T., Turner, J. R., Anes, E., Kulaksiz, H., Füllekrug, J., Stremmel, W., Griffiths, G., & Ehehalt, R. (2007). Anti-inflammatory Effects of Phosphatidylcholine. *Journal of Biological Chemistry*, *282*(37), 27155–27164. https://doi.org/10.1074/jbc.M704408200

Trostel, J., Truong, L. D., Roncal-Jimenez, C., Miyazaki, M., Miyazaki-Anzai, S., Kuwabara, M., McMahan, R., Andres-Hernando, A., Sato, Y., Jensen, T., Lanaspa, M. A., Johnson, R. J., & Garcia, G. E. (2018). Different effects of global osteopontin and macrophage osteopontin in glomerular injury. *American Journal of Physiology-Renal Physiology*, *315*(4), F759–F768. https://doi.org/10.1152/ajprenal.00458.2017

Turner, S. M. F., Hoyt, A. K., ElMallah, M. K., Falk, D. J., Byrne, B. J., & Fuller, D. D. (2016). Neuropathology in respiratory-related motoneurons in young Pompe (Gaa) mice. *Respiratory Physiology & Neurobiology*, *227*, 48–55. https://doi.org/10.1016/j.resp.2016.02.007

Uemura, T., Shiozaki, K., Yamaguchi, K., Miyazaki, S., Satomi, S., Kato, K., Sakuraba, H., & Miyagi, T. (2009). Contribution of sialidase NEU1 to suppression of

metastasis of human colon cancer cells through desialylation of integrin β4. *Oncogene*, *28*(9), 1218–1229. https://doi.org/10.1038/onc.2008.471

Ulrich-Bott, B., Klem, B., Kaiser, R., Spranger, J., & Cantz, M. (1987). Lysosomal Sialidase Deficiency: Increased Ganglioside Content in Autopsy Tissues of a Sialidosis Patient. *Enzyme*, *38*(1–4), 262–266. https://doi.org/10.1159/000469214

Vallabhapurapu, S., & Karin, M. (2009). Regulation and Function of NF-κB Transcription Factors in the Immune System. *Annual Review of Immunology*, *27*(1), 693–733. https://doi.org/10.1146/annurev.immunol.021908.132641

Valles, S. L., Singh, S. K., Campos-Campos, J., Colmena, C., Campo-Palacio, I., Alvarez-Gamez, K., Caballero, O., & Jorda, A. (2023). Functions of Astrocytes under Normal Conditions and after a Brain Disease. *International Journal of Molecular Sciences*, *24*(9), 8434. https://doi.org/10.3390/ijms24098434

van Dieren, J. M., Simons-Oosterhuis, Y., Raatgeep, H. C. (Rolien), Lindenbergh-Kortleve, D. J., Lambers, M. E. H., van der Woude, C. J., Kuipers, E. J., Snoek, G. T., Potman, R., Hammad, H., Lambrecht, B. N., Samsom, J. N., & Nieuwenhuis, E. E. S. (2011). Anti-inflammatory actions of phosphatidylinositol. *European Journal of Immunology*, *41*(4), 1047–1057. https://doi.org/10.1002/eji.201040899

van Meer, G., Voelker, D. R., & Feigenson, G. W. (2008). Membrane lipids: where they are and how they behave. *Nature Reviews Molecular Cell Biology*, *9*(2), 112–124. https://doi.org/10.1038/nrm2330

Van Pelt, J., Kamerling, J. P., Vliegenthart, J. F. G., Hoogeveen, AndréT., & Galjaard, H. (1988). A comparative study of the accumulated sialic acid-containing oligosaccharides from cultured human galactosialidosis and sialidosis fibroblasts. *Clinica Chimica Acta*, *174*(3), 325–335. https://doi.org/10.1016/0009-8981(88)90059-9

Vargiami, E., Papathanasiou, E., Batzios, S., Kyriazi, M., Dimitriou, E., Anastasiou, A., Michelakakis, H., Giese, A.-K., & Zafeiriou, D. (2016). Neuroradiological, neurophysiological and molecular findings in infantile Krabbe disease: two case reports. *Balkan Journal of Medical Genetics*, *19*(1), 85–90. https://doi.org/10.1515/bjmg-2016-0011

Verheijen, F., Brossmer, R., & Galjaard, H. (1982). Purification of acid β-galactosidase and acid neuraminidase from bovine testis: Evidence for an enzyme complex. *Biochemical and Biophysical Research Communications*, *108*(2), 868–875. https://doi.org/10.1016/0006-291X(82)90911-1

Verkhratsky, A., Rodríguez, J. J., & Steardo, L. (2014). Astrogliopathology. *The Neuroscientist*, *20*(6), 576–588. https://doi.org/10.1177/1073858413510208

Villani, G. R. D., Gargiulo, N., Faraonio, R., Castaldo, S., Gonzalez y Reyero, E., & Di Natale, P. (2007). Cytokines, neurotrophins, and oxidative stress in brain disease from mucopolysaccharidosis IIIB. *Journal of Neuroscience Research*, *85*(3), 612–622. https://doi.org/10.1002/jnr.21134

Vitner, E. B., Farfel-Becker, T., Eilam, R., Biton, I., & Futerman, A. H. (2012). Contribution of brain inflammation to neuronal cell death in neuronopathic forms of Gaucher's disease. *Brain*, *135*(6), 1724–1735. https://doi.org/10.1093/brain/aws095

Vruchte, D. te, Lloyd-Evans, E., Veldman, R. J., Neville, D. C. A., Dwek, R. A., Platt, F. M., van Blitterswijk, W. J., & Sillence, D. J. (2004). Accumulation of Glycosphingolipids in Niemann-Pick C Disease Disrupts Endosomal Transport. *Journal of Biological Chemistry*, *279*(25), 26167–26175. https://doi.org/10.1074/jbc.M311591200

Walkley, S. U., & Vanier, M. T. (2009a). Secondary lipid accumulation in lysosomal disease. *Biochimica et Biophysica Acta (BBA) - Molecular Cell Research*, *1793*(4), 726–736. https://doi.org/10.1016/j.bbamcr.2008.11.014

Walkley, S. U., & Vanier, M. T. (2009b). Secondary lipid accumulation in lysosomal disease. *Biochimica et Biophysica Acta (BBA) - Molecular Cell Research*, *1793*(4), 726–736. https://doi.org/10.1016/j.bbamcr.2008.11.014

Wang, A., Zhang, H., Liu, J., Yan, Z., Sun, Y., Su, W., Yu, J.-G., Mi, J., & Zhao, L. (2023). Targeted Lipidomics and Inflammation Response to Six Weeks of Sprint Interval Training in Male Adolescents. *International Journal of Environmental Research and Public Health*, *20*(4), 3329. https://doi.org/10.3390/ijerph20043329

Wang, J., Wu, G., Miyagi, T., Lu, Z., & Ledeen, R. W. (2009). Sialidase occurs in both membranes of the nuclear envelope and hydrolyzes endogenous GD1a. *Journal of Neurochemistry*, *111*(2), 547–554. https://doi.org/10.1111/j.1471-4159.2009.06339.x

Ward-Kavanagh, L. K., Lin, W. W., Šedý, J. R., & Ware, C. F. (2016). The TNF Receptor Superfamily in Co-stimulating and Co-inhibitory Responses. *Immunity*, *44*(5), 1005–1019. https://doi.org/10.1016/j.immuni.2016.04.019

White, A. B., Givogri, M. I., Lopez-Rosas, A., Cao, H., van Breemen, R., Thinakaran, G., & Bongarzone, E. R. (2009). Psychosine Accumulates in Membrane Microdomains in the Brain of Krabbe Patients, Disrupting the Raft Architecture. *The Journal of Neuroscience*, *29*(19), 6068–6077. https://doi.org/10.1523/JNEUROSCI.5597-08.2009

Womack, J. E., Yan, D. L. S., & Potier, M. (1981). Gene for Neuraminidase Activity on Mouse Chromosome 17 Near H-2: Pleiotropic Effects on Multiple Hydrolases. *Science*, *212*(4490), 63–65. https://doi.org/10.1126/science.7209520

Wong, K., Sidransky, E., Verma, A., Mixon, T., Sandberg, G. D., Wakefield, L. K., Morrison, A., Lwin, A., Colegial, C., Allman, J. M., & Schiffmann, R. (2004). Neuropathology provides clues to the pathophysiology of Gaucher disease. *Molecular Genetics and Metabolism*, *82*(3), 192–207. https://doi.org/10.1016/j.ymgme.2004.04.011

Woods, A. S., Colsch, B., Jackson, S. N., Post, J., Baldwin, K., Roux, A., Hoffer, B., Cox, B. M., Hoffer, M., Rubovitch, V., Pick, C. G., Schultz, J. A., & Balaban, C. (2013). Gangliosides and Ceramides Change in a Mouse Model of Blast Induced Traumatic

Brain Injury. *ACS Chemical Neuroscience*, *4*(4), 594–600. https://doi.org/10.1021/cn300216h

Wu, X., Steigelman, K. A., Bonten, E., Hu, H., He, W., Ren, T., Zuo, J., & d'Azzo, A. (2010a). Vacuolization and alterations of lysosomal membrane proteins in cochlear marginal cells contribute to hearing loss in neuraminidase 1-deficient mice. *Biochimica et Biophysica Acta (BBA) - Molecular Basis of Disease*, *1802*(2), 259–268. https://doi.org/10.1016/j.bbadis.2009.10.008

Wu, X., Steigelman, K. A., Bonten, E., Hu, H., He, W., Ren, T., Zuo, J., & d'Azzo, A. (2010b). Vacuolization and alterations of lysosomal membrane proteins in cochlear marginal cells contribute to hearing loss in neuraminidase 1-deficient mice. *Biochimica et Biophysica Acta (BBA) - Molecular Basis of Disease*, *1802*(2), 259–268. https://doi.org/10.1016/j.bbadis.2009.10.008

Xiao, G., Harhaj, E. W., & Sun, S.-C. (2001). NF-κB-Inducing Kinase Regulates the Processing of NF-κB2 p100. *Molecular Cell*, *7*(2), 401–409. https://doi.org/10.1016/S1097-2765(01)00187-3

Xing, Z., Gauldie, J., Cox, G., Baumann, H., Jordana, M., Lei, X. F., & Achong, M. K. (1998). IL-6 is an antiinflammatory cytokine required for controlling local or systemic acute inflammatory responses. *Journal of Clinical Investigation*, *101*(2), 311–320. https://doi.org/10.1172/JCI1368

Yamaguchi, K., Hata, K., Koseki, K., Shiozaki, K., Akita, H., Wada, T., Moriya, S., & Miyagi, T. (2005). Evidence for mitochondrial localization of a novel human sialidase (NEU4). *Biochemical Journal*, *390*(1), 85–93. https://doi.org/10.1042/BJ20050017

Yamaguchi, K., Hata, K., Wada, T., Moriya, S., & Miyagi, T. (2006). Epidermal growth factor-induced mobilization of a ganglioside-specific sialidase (NEU3) to membrane ruffles. *Biochemical and Biophysical Research Communications*, *346*(2), 484–490. https://doi.org/10.1016/j.bbrc.2006.05.136

Yamanaka, S., Johnson, M. D., Grinberg, A., Westphal, H., Crawley, J. N., Taniike, M., Suzuki, K., & Proia, R. L. (1994). Targeted disruption of the Hexa gene results in mice with biochemical and pathologic features of Tay-Sachs disease. *Proceedings of the National Academy of Sciences*, *91*(21), 9975–9979. https://doi.org/10.1073/pnas.91.21.9975

Yamashita, A., Hayashi, Y., Nemoto-Sasaki, Y., Ito, M., Oka, S., Tanikawa, T., Waku, K., & Sugiura, T. (2014). Acyltransferases and transacylases that determine the fatty acid composition of glycerolipids and the metabolism of bioactive lipid mediators in mammalian cells and model organisms. *Progress in Lipid Research*, *53*, 18–81. https://doi.org/10.1016/j.plipres.2013.10.001

Yamashita, N., Tashimo, H., Matsuo, Y., Ishida, H., Yoshiura, K., Sato, K., Yamashita, N., Kakiuchi, T., & Ohta, K. (2006). Role of CCL21 and CCL19 in allergic inflammation in the ovalbumin-specific murine asthmatic model. *Journal of Allergy and Clinical Immunology*, *117*(5), 1040–1046. https://doi.org/10.1016/j.jaci.2006.01.009

Yang, Z., & Wang, K. K. W. (2015). Glial fibrillary acidic protein: from intermediate filament assembly and gliosis to neurobiomarker. *Trends in Neurosciences*, *38*(6), 364–374. https://doi.org/10.1016/j.tins.2015.04.003

Yim, A., Smith, C., & Brown, A. M. (2022). Osteopontin/secreted phosphoprotein-1 harnesses glial-, immune-, and neuronal cell ligand-receptor interactions to sense and regulate acute and chronic neuroinflammation. *Immunological Reviews*, *311*(1), 224–233. https://doi.org/10.1111/imr.13081

Yin, C., Liu, B., Dong, Z., Shi, S., Peng, C., Pan, Y., Bi, X., Nie, H., Zhang, Y., Tai, Y., Hu, Q., Wang, X., Shao, X., An, H., Fang, J., Wang, C., & Liu, B. (2024). CXCL5 activates CXCR2 in nociceptive sensory neurons to drive joint pain and inflammation in experimental gouty arthritis. *Nature Communications*, *15*(1), 3263. https://doi.org/10.1038/s41467-024-47640-7

Yogalingam, G., Bonten, E. J., van de Vlekkert, D., Hu, H., Moshiach, S., Connell, S. A., & d'Azzo, A. (2008). Neuraminidase 1 Is a Negative Regulator of Lysosomal Exocytosis. *Developmental Cell*, *15*(1), 74–86. https://doi.org/10.1016/j.devcel.2008.05.005

Yu, E. A., He, S., Jones, D. P., Sun, Y. V, Ramirez-Zea, M., & Stein, A. D. (2021). Metabolomic Profiling Demonstrates Postprandial Changes in Fatty Acids and Glycerophospholipids Are Associated with Fasting Inflammation in Guatemalan Adults. *The Journal of Nutrition*, *151*(9), 2564–2573. https://doi.org/10.1093/jn/nxab183

Zanoteli, E., de Vlekkert, D. van, Bonten, E. J., Hu, H., Mann, L., Gomero, E. M., Harris, A. J., Ghersi, G., & d'Azzo, A. (2010). Muscle degeneration in neuraminidase 1-deficient mice results from infiltration of the muscle fibers by expanded connective tissue. *Biochimica et Biophysica Acta (BBA) - Molecular Basis of Disease*, *1802*(7–8), 659–672. https://doi.org/10.1016/j.bbadis.2010.04.002

Zhang, Z., Yue, P., Lu, T., Wang, Y., Wei, Y., & Wei, X. (2021). Role of lysosomes in physiological activities, diseases, and therapy. *Journal of Hematology & Oncology*, *14*(1), 79. https://doi.org/10.1186/s13045-021-01087-1

Zhou, X. (1996). Molecular and biochemical analysis of protective protein/cathepsin A mutations: correlation with clinical severity in galactosialidosis [published erratum appears in Hum Mol Genet 1997 Jan;6(1):146]. *Human Molecular Genetics*, *5*(12), 1977–1987. https://doi.org/10.1093/hmg/5.12.1977

Zhu, Q., Wu, Y., Mai, J., Guo, G., Meng, J., Fang, X., Chen, X., Liu, C., & Zhong, S. (2022). Comprehensive Metabolic Profiling of Inflammation Indicated Key Roles of Glycerophospholipid and Arginine Metabolism in Coronary Artery Disease. *Frontiers in Immunology*, *13*. https://doi.org/10.3389/fimmu.2022.829425

Zöller, T., Schneider, A., Kleimeyer, C., Masuda, T., Potru, P. S., Pfeifer, D., Blank, T., Prinz, M., & Spittau, B. (2018). Silencing of TGFβ signalling in microglia results in impaired homeostasis. *Nature Communications*, *9*(1), 4011. https://doi.org/10.1038/s41467-018-06224-y